Synthesis and characterization of hybrid drugs based on ruthenium complex moiety and biologically active organic compounds

Michal Pawel Łomzik

Faculty of Chemistry *Ecole Doctorale SESAMES*

PhD thesis

Michał Łomzik

Synthesis and characterization of hybrid drugs based on ruthenium complex moiety and biologically active organic compounds

Reviewers

Pr. Gilles Lemercier	Professor, Université de Reims
Dr. hab. Iwona Łakomska, prof. UMK	Professor, Nicolaus Copernicus University in Toruń

Examiners

Prof. dr. hab. Janusz Szklarzewicz	Professor, Jagiellonian University
Dr. hab. Małgorzata Brindell	Associate Professor, Jagiellonian University
Dr. Philippe Pierrat	Assistant Professor, Université de Lorraine
Pr. Marc Beley	Emeritus Professor, Université de Lorraine

Supervisors

Dr. Philippe C. Gros	CNRS-Research Director, Université de Lorraine, PhD Director
Prof. dr. hab. Grażyna Stochel	Professor, Jagiellonian University, PhD Co-Director

Kraków 2016

"I have not failed. I have just found 10,000 ways that won't work!"

by Thomas Alva Edison

Acknowledgements

I would like to express my sincere thanks and gratitude to prof. dr. hab. Grażyna Stochel and dr. Philippe C. Gros for their constant guidance, help, suggestions, motivation and interest throughout this work.

I would especially like to thank dr. hab. Małgorzata Brindell for her support and supervision. Dr. hab. Dorota Rutkowska-Żbik for her help with computational studies interpretation and dr. Fabien Lachaud for his help with HRMS studies.

I am very grateful to whole Coordination and Bioinorganic Physicochemistry Group and Team Photosens for their kindness and help.

Finally, I would like to thanks my parents for their constant support on my way to complete this thesis.

I would also like to thanks for financial support to Polish Ministry of Science and Higher Education for providing "Diamentowy Grant" and French Embassy in Poland for providing "BGF Doctorat en cotutelle" program.

Abbreviations

A	- adenine
Ar	- argon
ACN	- acetonitryle
bpy	- 2,2′-bipirydyne
CuI	- copper(I) iodine
dip	- 4,7′-diphenyl-1,10-phenantroline
DiPA	- diisopropylamine
DMAE	- dimethylaminoethanol
DMF	- N,N-dimethylformamide
dmso	- Dimethyl sulfoxide
dsDNA	- double stranded deoxyribonucleic acid
DSSC	- dye-sensitized solar cells
EtOH	- ethanol
G	- guanine
Ha	- Hartree
HMG	- high mobility groups
HOMO	- Highest Occupied Molecular Orbital
iPrMgCl	- isopropylmagnesium chloride
LDA	- Lithium diisopropylamide
LiTMP	- Lithium 2,2,6,6-tetramethylpiperidine
LUMO	- Lowest Unoccupied Molecular Orbital
MAO	- monoamine oxidase
Mebpy	- 4,4′-dimethyl-2,2′bipirydyne
MeOH	- methanol
MRI	- magnetic resonance imaging
MW	- microwave
NBO	- Natural bond orbital
nBuLi	- n-butyllithium
NDP	- nucleoside diphosphate
NTP	- nucleoside triphosphate
Phbpy	- 4,4′-diphenyl-2,2′bipirydyne

$Pd(PPh)_4$ - tetrakis(triphenylphosphine)palladium(0)
PDT - photodynamic therapy
pTSA - p-toluenesulfonic acid monohydrate
QY - quantum yield
RNR - ribonucleotide reductase
rt - room temperature
tBbpy - 4,4′-di-*tert*-butyl-2,2′bipirydyne
THF - tetrahydrofuran

Abstract

The main goal of this thesis was synthesis and preliminary characterization of novel ruthenium(II) polypyridyl complexes bearing biologically active molecules as potential theranostic agents. Luminescence for the diagnostic applications, and cytotoxicity for the anticancer, therapeutic applications are cosidered as the theranostic properties. Four new ligands containing biologically active moieties - 5-(4-4′-methyl-[2,2′-bipyridine]-4-ylbut-1-yn-1-yl)pyridine-2-carbaldehyde semicarbazone (**L1**), 3-(5-4′-methyl-[2,2′-bipyridine]-4-ylpentyl)imidazolidine-2,4-dione (**L2**), 5,5-dimethyl-3-(5-4′-methyl-[2,2′-bipyridine]-4-ylpentyl)imidazolidine-2,4-dione (**L3**) and [1-(5-4′-methyl-[2,2′-bipyridine]-4-ylpentyl)-2,5-dioxoimidazolidin-4-yl]urea (**L4**) were synthesized and characterized. The ligands were used to obtain nine novel ruthenium(II) polypyridyl complexes. Six complexes were synthesized with ligand **L1** ($[Ru(bpy)_2(L1)]^{2+}$, $[Ru(Mebpy)_2(L1)]^{2+}$, $[Ru(tBubpy)_2(L1)]^{2+}$, $[Ru(Phbpy)_2(L1)]^{2+}$, $[Ru(dip)_2(L1)]^{2+}$, $[Ru(SO_3dip)_2(L1)]^{2-}$) and three with ligands **L2**, **L3** and **L4** ($[Ru(bpy)_2(L2)]^{2+}$, $[Ru(bpy)_2(L3)]^{2+}$, $[Ru(bpy)_2(L4)]^{2+}$) (bpy = 2,2′-bipyridine, Mebpy = 4,4′-dimethyl-2,2-bipyridine, tBubpy = 4,4′-tert-butyl-2,2′-bipyridine, Phbpy = 4,4′-diphenyl-2,2-bipyridine, dip = 4,7-diphenyl-1,10-phenantroline and SO_3dip = 4,7-di-(4-sulfonatophenyl)-1,10-phenantroline).

The spectroscopic and photophysical properties of those complexes were determined. The presence of ligands **L1-L4** in the structure of the complex decreased luminescence quantum yield and luminescence lifetime in comparison with unmodified $[Ru(bpy)_3]^{2+}$ complex. The theoretical calculations have shown that ligands **L1-L4** do not have influence on ruthenium core geometry. However, they increased the energy of the HOMO that resulted in a shorter band gap. The simulated electronic absorption spectra were in a good agreement with the experimental data.

The interactions between the studied ruthenium complexes and human serum albumin (HSA) were investigated. All studied Ru(II) complexes exhibited strong affinity to HSA with the association constant 10^5 $M^{-1}s^{-1}$, which suggests formation of Ru complex-HSA adducts. It was also determined that ruthenium complexes most likely bind to the hydrophobic pocket of protein, located in Sudlow's site I in the subdomain II A. Preliminary cytotoxicity evaluation for the studied ruthenium complexes showed their cytotoxic activity towards cancer cell lines. Those results, together with good luminescence properties of the studied ruthenium complexes (luminescence lifetimes and luminescence quantum yield) make them interesting candidates for potential theranostic applications.

Streszczenie

Głównym celem rozprawy doktorskiej była synteza i wstępna charakterystyka nowych polipirydylowych kompleksów rutenu(II) połączonych z biologicznie aktywnymi cząsteczkami jako związków o potencjalnych właściwościach teranostycznych. Rozpatrywane właściwości teranostyczne to z luminescencja tych kompleksów, pozwalająca na wykorzystanie ich w diagnostyce, a z drugiej ich aktywność cytotoksyczna pozwalająca na zastosowanie ich w terapii antynowotworowej. Otrzymane zostały cztery nowe ligandy zawierające biologicznie czynne ugrupowanie: semikarbazon 5-(4-4′-metylo-[2,2′-bipirydyno]-4-ylbut-1-yn-1-ylo)pirydino-2-carbaldehydu (**L1**), 3-(5-4′-metylo-[2,2′-bipirydyno]-4-ylpentylo)imidazolidino-2,4-dion (**L2**), 5,5-dimetylo-3-(5-4′-metylo-[2,2′-bipirydyno]-4-ylpentylo)imidazolidino-2,4-dion (**L3**) oraz [1-(5-4′-metylo-[2,2′-bipirydyno]-4-ylpentylo)-2,5-dioxoimidazolidin-4-yl]mocznik (**L4**). Ligandy te zostały użyte do otrzymania dziewięciu nowych polipirydylowych kompleksów rutenu(II). Zsyntetyzowano sześć kompleksów z ligandem **L1** ($[Ru(bpy)_2(L1)]^{2+}$, $[Ru(Mebpy)_2(L1)]^{2+}$, $[Ru(tBubpy)_2(L1)]^{2+}$, $[Ru(Phbpy)_2(L1)]^{2+}$, $[Ru(dip)_2(L1)]^{2+}$, $[Ru(SO_3dip)_2(L1)]^{2-}$) oraz trzy kompleksy z ligandami **L2**, **L3** i **L4** ($[Ru(bpy)_2(L2)]^{2+}$, $[Ru(bpy)_2(L3)]^{2+}$, $[Ru(bpy)_2(L4)]^{2+}$) (bpy = 2,2′-bipirydyna, Mebpy = 4,4′-dimetylo-2,2-bipirydyna, tBubpy = 4,4′-tert-butylo-2,2′-bipirydyna, Phbpy = 4,4′-difenylo-2,2-bipirydyna, dip = 4,7-difenylo-1,10-fenantrolina i SO_3dip = 4,7-di-(4-sulfonatofenylo)-1,10-fenantrolina).

Wyznaczono właściwości spektroskopowe i fotofizyczne otrzymanych kompleksów. Obecność ligandów **L1-L4** w strukturze kompleksu obniżała wydajność kwantową luminescencji oraz skracała czas życia luminescencji w stosunku do niemodyfikowanego kompleksu $[Ru(bpy)_3]^{2+}$. Obliczenia teoretyczne wykazały, że ligandy **L1-L4** nie wpływają na geometrię wokół jonu centralnego kompleksu, jednakże znacznie zwiększają energię orbitalu HOMO. W rezultacie dochodzi do zmniejszenia przerwy energetycznej pomiędzy orbitalami HOMO a LUMO. Obliczone widma absorpcyjne wykazują dużą zgodność z danymi eksperymentalnymi.

Zbadane także zostało oddziaływanie pomiędzy otrzymanymi kompleksami rutenu a albuminą surowicy ludzkiej (human serum albumin, HSA). Wszystkie przebadane kompleksy silnie oddziaływały z albuminą. Otrzymane stałe wiązania wynoszą około 10^5 $M^{-1}s^{-1}$, co może sugerować tworzenie się adduktów kompleks Ru-albumina. Ponadto stwierdzono, że kompleksy te wiążą się najprawdopodobniej do hydrofobowej kieszeni białka, zlokalizowanej w miejscu wiążącym I (Sudlowa), w poddomenie II A cząsteczki albuminy.

Wstępne badania cytotoksyczności otrzymanych kompleksów rutenu wykazały, że posiadają one właściwości cytotoksyczne względem komórek nowotworowych. Wyniki te, wraz z dobrymi właściwości luminescencyjnymi otrzymanych kompleksów rutenu (czasy życia i wydajność kwantowa luminescencji) czynią je interesującymi kandydatami do potencjalnych zastosowań teranostycznych.

Résumé

L'objectif de cette these est de préparer et caractériser de nouveaux agents théranostiques potentiels a base de complexes de ruthénium portant des molécules biologiquement actives. Pour évaluer potentiel théranostique des nouveaux composés les propriétés de luminescence et la cytotoxicité ont été considérées. Quatre nouveaux ligands portant des substituants a activité biologique: 5-(4-4'-methyl-[2,2'-bipyridine]-4-ylbut-1-yn-1-yl)pyridine-2-carbaldehyde semicarbazone (**L1**), 3-(5-4'-methyl-[2,2'-bipyridine]-4-ylpentyl)imidazolidine-2,4-dione (**L2**), 5,5-dimethyl-3-(5-4'-methyl-[2,2'-bipyridine]-4-ylpentyl)imidazolidine-2,4-dione (**L3**) and [1-(5-4'-methyl-[2,2'-bipyridine]-4-ylpentyl)-2,5-dioxoimidazolidin-4-yl]urea (**L4**) ont été prepares, caractérisés et engagés dans la synthese des complexes de ruthénium correspondants. Six complexes ont été obtenus a partir du ligand **L1** ($[Ru(bpy)_2(L1)]^{2+}$, $[Ru(Mebpy)_2(L1)]^{2+}$, $[Ru(tBubpy)_2(L1)]^{2+}$, $[Ru(Phbpy)_2(L1)]^{2+}$, $[Ru(dip)_2(L1)]^{2+}$, $[Ru(SO_3dip)_2(L1)]^{2-}$) et trois a partir de L2, L3 and L4 ($[Ru(bpy)_2(L2)]^{2+}$, $[Ru(bpy)_2(L3)]^{2+}$, $[Ru(bpy)_2(L4)]^{2+}$) (bpy = 2,2'-bipyridine, Mebpy = 4,4'-dimethyl-2,2-bipyridine, tBubpy = 4,4'-tert-butyl-2,2'-bipyridine, Phbpy = 4,4'-diphenyl-2,2-bipyridine, dip = 4,7-diphenyl-1,10-phenantroline and SO_3dip = 4,7-di-(4-sulfonatophenyl)-1,10-phenantroline).

Les propriétés spectroscopiques et photophysiques des composés ont été étudiées. La présence des ligands **L1-L4** conduit a une décroissance du rendement quantique et de la durée de vie de l'état excité en comparaison des complexes non substitués $[Ru(bpy)_3]^{2+}$. Des calculs DFT montrent que les ligands **L1-L4** n'influencent pas la géométrie du complexe mais accroissent le niveau énergétique de la HOMO induisant des band gap HOMO-LUMO plus faibles.

Les interactions entre les complexes and l'human serum albumin (HSA) ont été étudiées determined. Tous les complexes préparaés montrent une tres forte affinité pour HSA - La constante d'association 10^5 $M^{-1}s^{-1}$ témoigne de la formation d'adduits Ru-HSA stables. Il a aussi été démontré que les complexes de ruthénium se lient préférentiellement a la poche hydrophobe des protéine, située dans le site 1 de Sudlow dans le sous domaine II A.

Des études préliminaires ont montré que les complexes de ruthénium préparés présentent une activité cytotoxique vis-*à*-vis de diverses lignées de cellules cancéreuses. Cette activité associée aux bonnes propriétés de luminescence (rendement quantique, durée de vie) fait des nouveaux complexes des candidats potentiels pour les applications théranostiques.

Contents

1. Introduction

1.1. History of medicinal inorganic chemistry

1.1.1. Metals in medicine

The natural evolution has incorporated many metal ions into essential biological systems. Metals play a wide variety of tasks. Zinc provides the structural framework for proteins such as zinc fingers which regulate the functions of genes in cells and also is an important component of insulin - an enzyme crucial for regulation of sugar metabolism. The iron-containing protein - hemoglobin - is responsible for carrying oxygen in blood. Additionally, metals such as iron, copper, manganese and zinc are incorporated into many catalytic proteins - the metaloenzymes which participate in many reactions essential for life[1].

The presence of metal ions in biological system directed people towards the use of them as a drugs. This concept is not new and the metals were used in medicine long before the discovery of their presence in humans body. Over 5000 years ago the ancient Egyptians used copper to sterilize water. Around 2000 B.C.E. the ancient Chinese and Arabs have known medical activities of natural gold however this knowledge had religious and philosophical origins. There was a believe that rare and precious metal must hold positive health properties. The origin of this believe can be found in the China's legend about Three Celestial Emperors - the founders of ancient China[2].

Five hundred years later, new metal - zinc was discovered in Europe and the Minoan civilization begin to use it as a drug. In the same time, the ancient Egyptians used various remedies based on iron and silver. They also used heavy metals salts to treat various skin diseases. In renaissance Europe mercury was used as a diuretic and it was continuously used till early 1950s[3]. However, the true medicinal inorganic chemistry slowly began to develop in early 1900s. Activity of $K[Au(CN)_2]$ towards tuberculosis and antibacterial activity of various gold salts was discovered in the number of different conditions.

In the beginning of the 20th century Paul Ehrlich synthesized and tested arsphenamine (also known as Salvarsan or Ehrlich 606)[4, 5] - an arsenic compound which is consider as first successful cure for syphilis. He also discovered favored accumulation of lead in central nervous system and introduce the "magic bullet"

concept, nowadays known as "drug targeting" which is the object of extensive research worldwide. In 1908, Paul Ehrlich was awarded the Nobel Prize for his research especially for the discovery of immunochemistry. He is considered as the founder of chemotherapy - "the use of drugs to injure an invading organism without injury of the host"[4].

Since the discovery of the antitumor activity of cisplatin (*cis*-[$Pt(NH_3)_2Cl_2$]) in 1965 by Barnett Rosenberg[6], medicinal inorganic chemistry exist as a separate discipline[7]. Cisplatin was the first chemical compound to become the subject of mechanistic studies. Its mechanism of action was widely investigated and its activity was optimized. Furthermore, medicinal inorganic chemistry studied the introduction of metal ions into a biological system either by fortuity or by intention. In case of fortuitous introduction, medicinal inorganic chemistry considers different ways to chelate ions out of biological system to avoid either a poisoning from an excess of a toxic metals or overload of essential metals. For example, 2,3-dimercapto-1-propanol, known as BAL is used as chelator in mercury and nickel poisoning, and disodium ethylenediaminetetraacetate is used for lead removal. The removing of essential metals may also leads to altering the homeostasis of them and induce biological respond (e.g. zinc binding matrix developed as metalloproteinase inhibitors for the treatment of inflammatory diseases and cancer[7]).

The intentional introduction of metal ions into a biological system can be either for therapeutic purpose (e.g. cisplatin) or diagnostic purpose. Barium sulfate ($BaSO_4$) is an imaging agent heavily used as X-ray contrast. Gadolinium complexes are used for magnetic resonance imaging (MRI) and ^{99m}Tc is γ-emitting radiopharmaceutical, with millions of applications per year[8]. As was noted by Peter Sadler in 1991[3], most of the elements from periodic table up to atomic number 83 (bismuth) have potential application in treatment or diagnostic.

1.1.2. Cisplatin - the first anticancer drug

Cisplatin - *cis*-diamminedichloridoplatinum(II) was discovered by Michele Peyrone in 1845[9] and for a long time was known as Peyrone's salt. In 1893, Alfred Werner deduced the structure of this molecule and together with its trans analogue used it as the first example of isomers in coordination chemistry[10, 11].

However till 1960s its activity against cancer remained unknown. In 1964, Barnett Rosenberg discovered that platinum electrodes used in one of his experiments inhibit cell division in *Escherichia coli*[6]. Later it was found that compound responsible for this was *cis*-[$Pt(NH_3)_2Cl_2$] complex, which was slowly formed by reaction of platinum electrodes with ammonium chloride electrolyte. In 1969, anticancer activity

of this compound was discovered and studied[12]. Two years later this drug entered clinical trials and in 1978, was approved for use in the U.S. by the Food & Drug Administration[13].

Unfortunately, Cisplatin exhibit antitumor activity against certain types of cancer and some tumors are resistant for its actions. In some cases, this resistance is intrinsic but also it can be developed. And finally, therapy with cisplatin produce severe side-effects, such as nephrotoxicity, neurotoxicity, nausea, bone marrow dysfunction etc. Some of those effects can be limited by reducing dose and by slower administration of drug. Understanding of drug distribution and cellular uptake of this drug helps to improve it.

Cisplatin mechanism of action

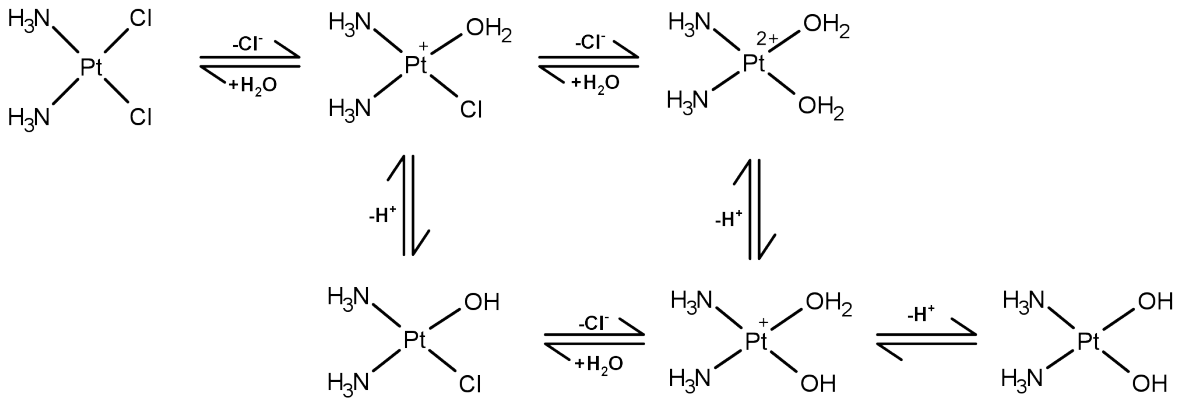

Figure 1.1: Mechanism of cisplatin aquatation in low chloride ions concentration[14]

After intravenous administration of Cisplatin as an aqueous solution, the molecule penetrate cell membrane via passive diffusion. Intracellular chloride ions concentration is almost 25 times lower then extracellular concentration[15] - ca. 100 mM in the plasma and 4 mM in cells. In high chloride concentration complex remains neutral. Its activation occurs after entering cell when chloride ligands dissociate and form much more reactive form of Cisplatin - aqua- and hydroxide- species (see fig. 1.1). This form of platinum complex can react with DNA and form a stable adduct. The most favored DNA coordination site is N7 atom of guanine and N7 atom of adenine. It can also binds the N1 of adenine and N3 of cytosine[16].

Cisplatin can bind with DNA monofunctionallu and bifunctionally. Monofunctional binding is unlikely to be responsible for cytotoxicity of Cisplatin because those adducts do not exhibit cytotoxicity. Similarly Transplatin (*trans*-diamminedichloridoplatinum(II)) which can form only monofunctional adducts and exhibits no cytotoxic activity[17]. Majority of Cisplatin form bifunctional

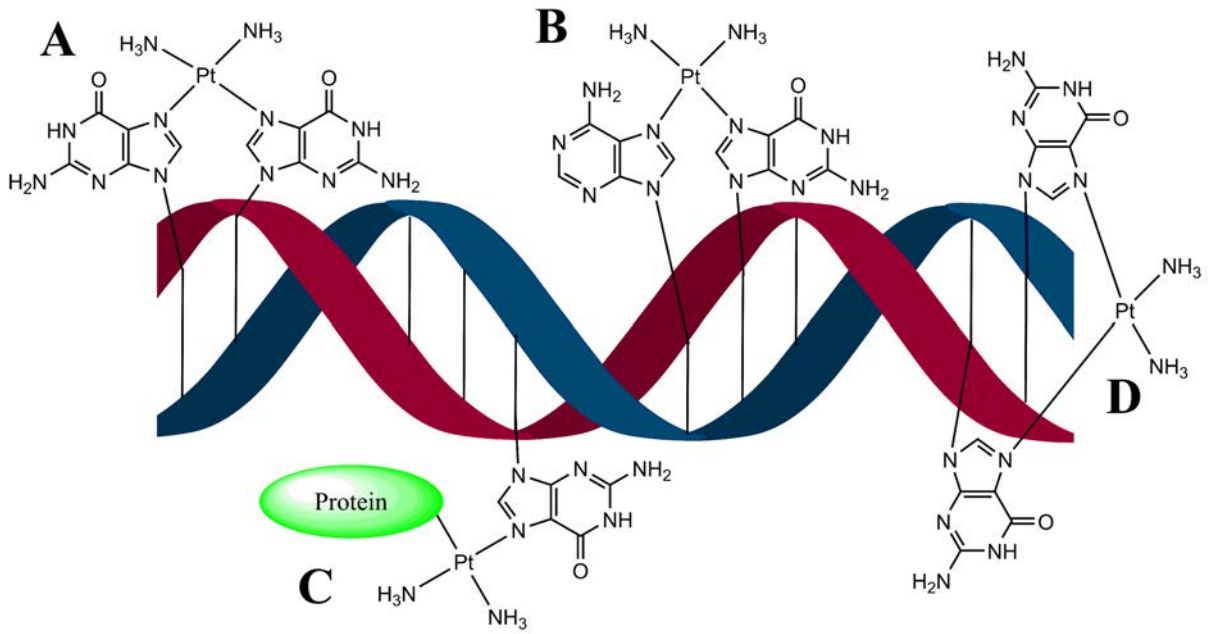

Figure 1.2: Schematic of double stranded DNA with most common Pt-DNA adducts. (A) Intrastrand 1,2-d(GpG) cross-link, (B) Intrastrand 1,2-d(ApG) cross-link, (C) DNA-protein cross-link, (D) Interstrand d(GG) cross-link.

intrastrand adducts with DNA. 1,2-intrastrand cross-link adduct with guanine (*cis*-[Pt(NH_3)$_2${d(GpG)}]) (fig. 1.2A) is most abundant adduct - around 60-65% of cisplatin binds that way. Another 23-28% of cisplatin form 1,2-intrastrand cross-link adduct with adenine and guanine (*cis*-[Pt(NH_3)$_2${d(ApG)}]) (fig. 1.2B) and less than 10% exist as as interstrand adducts (fig. 1.2D). Only traces (2-3%) of monofuctional adduct with guanine and cellular proteins (fig. 1.2C) were found [16].

It was discovered, that Cisplatin-DNA adducts block transcription of DNA by RNA polymerase II, inhibit DNA replication and forced apoptosis - programmed cell death[18]. Probably two most abundant Pt-DNA adducts - 1,2-d(GpG) and 1,2-(AdG) are responsible for majority of its cytotoxic activity. The formation of those adducts resulting in a loss of helix stability and a structural change of DNA[19]. Unwinding of the helix, provoking compression of major groove and opening up the minor groove[20]. As the result of this geometry changes, nonsequence-specific domain of DNA are recognized by several cellular proteins such as histones, DNA repair proteins and high mobility groups (HMG) of HMGB1 protein[21]. Adducts between Pt-DNA and those proteins are very stable and fail to fulfill their functions which lead to apoptosis.

1.1.3. Reducing side-effects - Cisplatin analogues

Low selectivity and many side effects of Cisplatin[22] leads to many studies about its analogues. After discovery that dissociation of chloride groups is important for its cytotoxic properties modification of ammine groups was studied in majority. As the results of those studies several generation of platinum-based drugs were developed.

Among all studied platinum based drugs, 33 have entered clinical trials after approval of Cisplatin as a drug in 1978. However, only Carboplatin® and Oxaliplatin® has received worldwide approval as a drug. Three others (Nedaplatin®, Lobaplatin® and Heptaplatin®) has received regionally limited approval and are used respectively in Japan, China and South Korea[23].

The vast majority of studied compounds keep unchanged, *cis*-configured square-planar platinum(II) complexes structure with general formula *cis*-$[PtA_2X_2]$, where X_2 means either two halogen ligands or one bidentate anionic leaving group and A_2 means either stable bidentate amino ligand or two monodentate amino ligands. Some of studied compounds possess however octahedral configuration with Pt(IV) in the center. Their general formula can be presented as *cis*-$[PtA_2X_2Y_2]$ where Y_2 are two monodentate leaving groups in configuration *trans* to each other.

Second and third generation of platinum-based drugs

Cisplatin is highly nephrotoxic unless it is slowly infused in prehydrated form. This procedure allowed to reduce severe renal toxicity of the drug, however vast majority of side effects (such as nausea, vomiting, ototoxicity, irreversible damage of the hair cells etc.) required administration of additional drugs. To reduce those effects, the second generation of platinum-based drugs was developed. The first complex, which was proved to have more tolerable toxicological profile was Carboplatin® - *cis*-diammine(1,1-cyclobutanedicarboxylato)platinum(II). It does not exhibit any nephrotoxicity and can be given without hydratation. Furthermore, its neurotoxicity and ototoxicity are much weaker and the gastric side effect is less severe and can be easily controlled. Carboplatin® is a good alternative for Cisplatin in aggressive, high-dose chemotherapy treatment[24, 14].

The third generation of platinum-based drugs focused mostly on overcoming intrinsic resistance of many tumors. There are four main mechanisms which were identified as responsible for cancer resitance[25]:

1. Reduction of drug uptake
2. Increased detoxification by glutathione or metallothionein
3. Increased repair of platinum-DNA adducts

4. Increased tolerance to platinum-DNA adducts

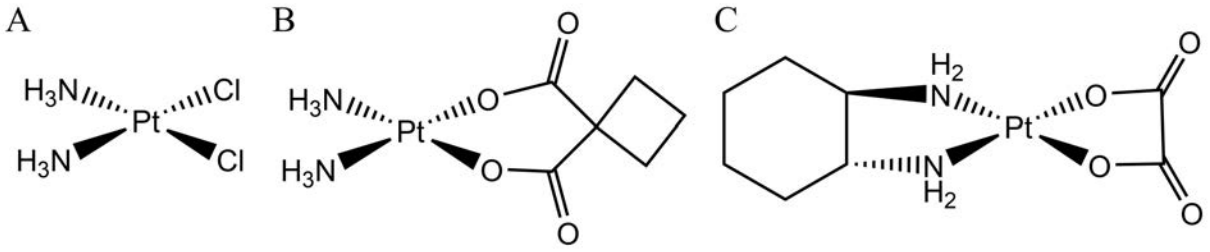

Figure 1.3: Examples of platinum(II)-based drugs. (A) Cisplatin, (B) Carboplatin, (C) Oxaliplatin.

To overcome those problems, modifications of amine groups were applied. *Trans*-R,R-1,2-diaminocyclohexane ligand was used to form a complex with platinum(II) shortly after discovery of Cisplatin activity. This complex - *cis*-dichloro(1,2-diaminocyclohexane)platinum(II) was recognized as a potent anticancer agents in some experimental tumor models, however its low water solubility prohibited intravenous administration. Exchanging of chloride anions onto oxalic acid resulting a new complex known as Oxaliplatin®. It is comparatively soluble in water and was first platinum-based drug which had proved to be active in metastatic colorectal cancer[26]. It has also exhibit good results in treatments where Cisplatin and Carboplatin® had failed[27, 28, 29].

Platinum(IV) drugs

The activity of square-planar platinum(II) complexes have been studied extensively. However, one more possibility had to be explored. By changing oxidation state of platinum metal from II to IV the geometry of the complex is changing from square-planar to octahedral. This may lead to change in Pt-base drug bioactivity and its mechanisms of action. Among all studied platinum(IV) complexes, three were investigated further and had entered clinical trials - Ormaplatin, Iproplatin and Satraplatin[23, 14]. Ormaplatin was evaluated in six different phase I clinical trials. After treating 118 patients with this drug, severe neurotoxicity was discovered and drug never has entered phase II[30]. Iproplatin and Satraplatin have successfully entered phase III of clinical trials. However it was determined that Iproplatin exhibit much lower activity then Carboplatin® and Cisplatin and it was not approved as a drug by any country.

Satraplatin is the first platinum-based drug which can be administrate orally. It has successfully completed phase III of clinical trials and it is currently evaluated in several clinical trials in composition with other drugs. Satraplatin is available in the United

States with the help of a special program of "early access" to severe cancer patients however it is not yet registered as a drug[30, 31, 32].

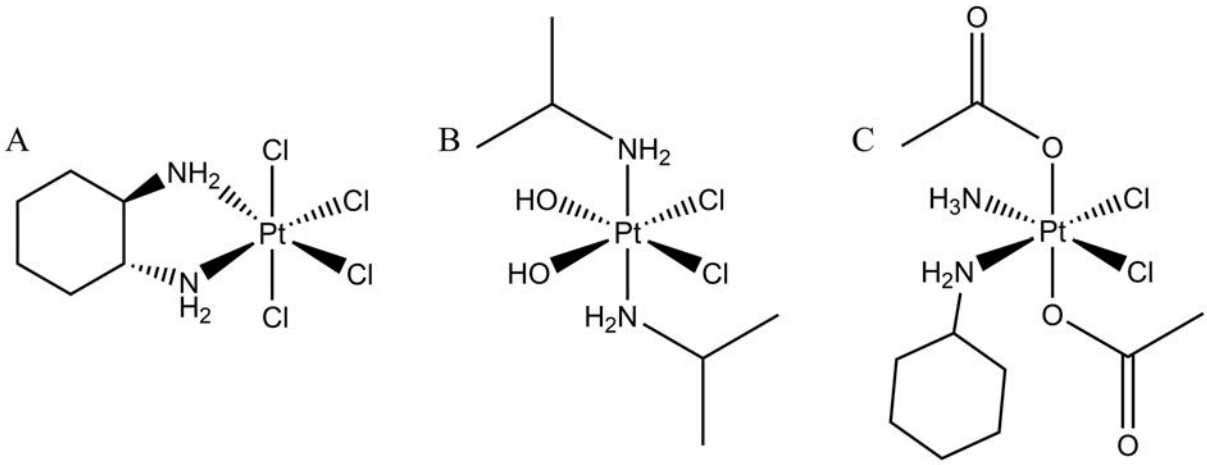

Figure 1.4: Three platinum(IV) complexes evaluated as potential anticancer drugs. (A) Ormaplatin, (B) Iproplatin, (C) Satraplatin.

1.2. Ruthenium complexes in cancer treatment

Success of Cisplatin and other platinum-based drugs in anticancer therapy inspired people to look into other rare noble metals. Since 1980, ruthenium is under intensive studies as a potential candidate to replace platinum in cancer treatment. Under physiological conditions ruthenium can exist in three oxidation states - Ru(II), Ru(III) and Ru(IV). Due to presence of biological reductants such as glutation and ascorbic acid and presence of oxidants ruthenium can easly change its oxidation state[33]. Most of complexes at these oxidation states form octahedral coordination complexes with nitrogen and sulfur donor ligands. Organometallic ruthenium(II) complexes however have tetrahedral geometry with at least one π-bond to an arene ligand - so-called piano-stool complexes.

1.2.1. Simple ammine and amine ruthenium complexes

First type of ruthenium complexes with anticancer properties were proposed in 1980 by Clarke and co-workers[34]. Ammine and amine ruthenium(III) complexes were clearly inspired by structure of Cisplatin and were suspected to act as a DNA binders. As was mentioned ruthenium(III) can be easily reduced by biological reducing agents[33]. In the hypoxia cells reverse oxidation is much slower due to lack of oxygen, therefore toxicity of *cis*-$[Ru(NH_3)_4Cl_2]$ anticancer agent is enhanced as a result of increased DNA binding[35]. Further development of these molecules however, was stopped due to their poor solubility in water.

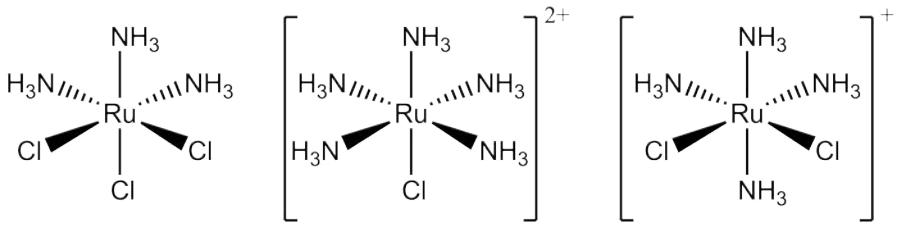

Figure 1.5: Examples of am(m)ine ruthenium(III) complexes.

1.2.2. Ruthenium dimethyl sulfoxide complexes

Low water solubility of the ammine and amine ruthenium(III) complexes is one of the main problem in their biological application[34]. The next major group of ruthenium complexes which has been studied are ruthenium(II) complexes with chloro and dmso ligand (where dmso is a S-bound dimethylsulfoxide). Those highly water-soluble complexes exhibit antimetastatic activity and relatively low cytotoxicity[36]. Dimethylsulfoxide ligands also increase inertness of ruthenium

complexes in water environment due to strong Ru-dmso bond. Coordinated dmso as well stabilized lower, less stable oxidation state of Ru(II) and helps to reduce Ru(III). Some of the complexes also posses two chloro ligands, which may easily dissociate in low chloride concentration (such as intracellular environment) and form more active aqua complexes - similarly to Cisplatin[37, 38].

Analogously to platinum complexes *cis* and *trans* isomers of Ru-dmso complexes exhibit different therapeutic activity. It was found that *trans* isomers are much more cytotoxic then their *cis* analogues[39]. It has been proven that both isomers form thermodinamically stable bidentate adducts with oligonucleotides but the *trans* isomer was much more reactive[40]. It may pointed the differences in anticancer mechanism of platinum(II) and ruthenium(II) complexes. Both *cis* and *trans* isomers cause a disruption in DNA structure by forming crosslink bond, however *trans* isomer form five-fold higher content of ruthenium in DNA which may indicate that it binds to DNA much stronger[37]. Furthermore, some of dichloro dmso complexes of ruthenium exhibit no cytotoxic effect towards primary tumors, however possessed antimetastatic activity (particularly in non-small cell lung cancer)[41].

1.2.3. NAMI-A, KP1019 and their analogues - ruthenium antimetastatic agents

In 1986, Bernhard Keppler described a new ruthenium(III) complex (imidazolium *trans*-[tetrachloride-bis(1*H*-imidazole)ruthenate(III)], KP418) which is consider as an inspiration of so-called "Keppler type" ruthenium complexes. This complex was proved therapeutic activity against P388 leukaemia, B16 melanoma and SA-1 (murine fibrosarcoma cells) cells lines[42, 43]. Moreover *in vivo* studies have shown a significant reduction of tumor burden in a colorectal cancer rats model[42]. Among all ruthenium(III) complexes synthesized on base of KP418, three are considered to be most important.

Imidazolium *trans*-[tetrachloride(1*H*-imidazole)(S-dimethylsulfoxide)ruthenate(III)] (NAMI-A) was firstly synthesized and studied in 1992 by Sava and co-workers[44]. In opposite to KP418, NAMI-A has much higher Ru(III/II) reduction potential due to π-acceptor effect of the S-bound dmso which also exerts a kinetic trans effect. NAMI-A was proved to affect the process of metastasing rather than acting against primary tumors. Its activity is probably based on enhanced cell adhesion and inhibition of neoangiogenesis in tumors[45, 46]. It was also proven that its mechanism of action does not involve DNA binding and its activity is rather independent of its concentration in cancer cells[37, 47, 48].

The other two significant Keppler complexes - KP1019 and NKP-1339 (respectively indazolium and sodium *trans*-[tetrachloridebis(1*H*-indazole) ruthenate(III)]) were

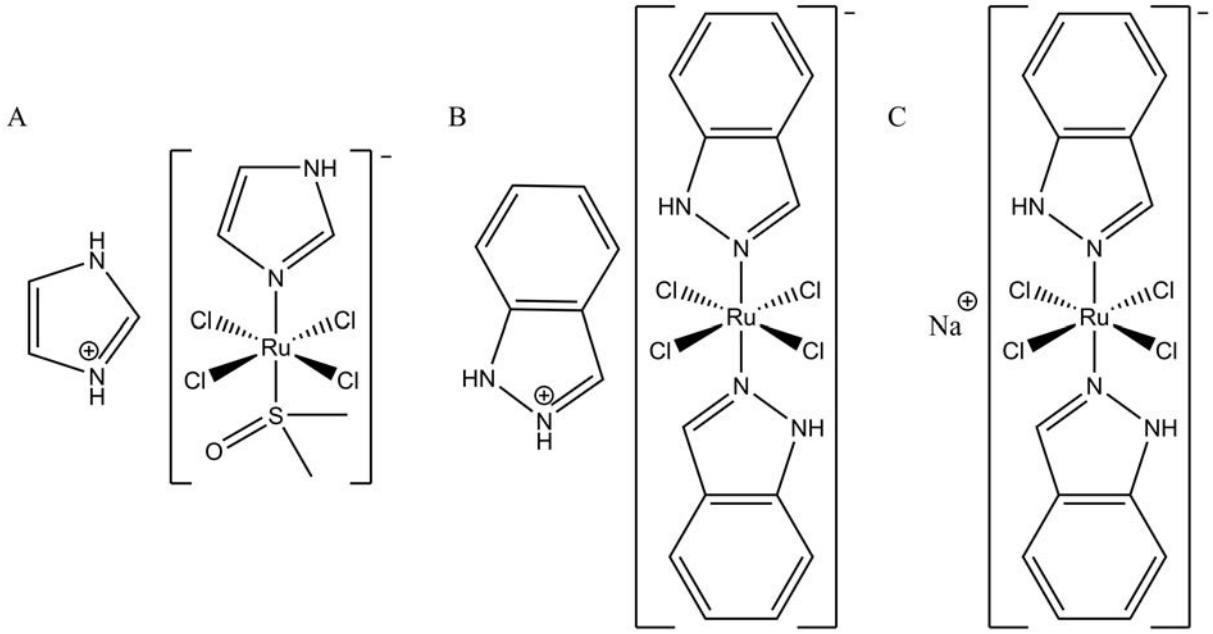

Figure 1.6: Ruthenium-based drugs in clinical trials. (A) NAMI-A, (B) KP1019, (C) NKP-1339.

described in 1989[49]. KP1019 was found to be superior in its activity against a colorectal cancer rats model then KP418. Treatment with KP1019 yielded efficiency with around 95% reduction of tumor volume with mortality at 0%. It was also found to be superior to 5-fluorouracil - a standard against colorectal cancer[43, 49]. Its activity comes from interactions between complex and DNA and inhibition of DNA synthesis[50].

One of the disadvantage of KP1019 is its solubility in water which may hinder the transfer in bloodstream. It also limit the administrative dose in clinical trials at maximum 600 mg/patient[51]. Its sodium salt (NKP-1339) on the other hand is much more water soluble. NKP-1339 exhibit similar activity as KP1019 in both *in vitro* and *in vivo* studies. It was determined that both compounds interact with serum proteins particularly albumin and transferrin similary to NAMI-A[52, 53]. It has been suggested that both proteins act as transport and delivery system for those complexes and play significant role in their cancer targeting mechanism.

In presence of biological reductants such as glutathione and ascorbic acid ruthenium(III) is easily reduced to Ru(II). Ruthenium(II) complexes are much more labile and exchange their ligands much faster than Ru(III) complexes. The hydratation of more labile ruthenium(II) complexes is proposed as the mechanism of their activation (similar as in platinum(II) drugs). This concept is so-called "activation-by-reduction" and is based on the concept that ruthenium(III) complexes may serve as prodrugs which are activated in oxygen-poor environment (such as solid tumors) and remain inactive

in normal tissue[37, 54]. Moreover ruthenium(II) complexes exhibit higher reactivity towards nucleotides then Ru(III) complexes[55].

The activation process highly depends on the redox potential of Ru(III)/Ru(II) couple. This potential strongly depends on the ligands coordinated to ruthenium center. All three studied ruthenium(III) complexes (NAMI-A, KP1019, NKP-1339) can be reduced under physiological conditions to their ruthenium(II) forms[56, 57]. NAMI-A due to S-dmso ligand is much easier reduced then KP1019 or NKP-1339. This may explain why it exhibits much stronger side effect in clinical trials[58].

Clinical trials evaluation

NAMI-A, KP1019 and NKP-1339 belongs to small group of ruthenium complexes which have been already evaluated in clinical trials[58, 59, 60].

NAMI-A

Phase I of clinical trials for NAMI-A was conducted on 24 patients. During treatment several side effects including nausea, vomiting, diarrhea, fever, painful blisters on hands and feet were observed[58, 61]. For final results 20 patients were evaluated and 19 of the twenty shown disease progression while one patient shown no progression. Due to these results, NAMI-A was not evaluated as stand-alone drug in phase II.

Due to previous *in vivo* results which has shown that NAMI-A slows down progression of metastasis and not growth of the initial tumor, phase I and II were conducted in combination with gemcitabine. This nucleoside analog has previously shown successful results in cancer treatment [62]. During phase I, minimal dosage was determined to be 300 mg/m^2 and maximum dosage was determined to be 600 mg/m^2 over 21 days. In phase II impact of NAMI-A in combination with gemcitabine was evaluated. 27 patients were chosen for the final results. In 15 patients anticancer activity was determined, 10 have shown stable disease progression 1 patient exhibited a partial remission. However the criteria for expansion based on the obtained efficacy results were not met in the second stage of the study. The treatment was insufficiently effective and the efficacy was lower than could be expected of a treatment with gemcitabine alone. Due to these results protocol was not followed and clinical trials were terminated[61].

KP1019 and NKP-1339

In phase I of clinical trials, eight patients with advanced solid tumors without further therapeutic option were treated with KP1019[60]. The drug was administrated intravenously in doses ranging 25 - 600 mg/m^2 to determine therapeutic dose for further studies. In 83% of patients evaluated for the study (5 of 6) disease stabilized for 8-10 weeks. However there was no correlation between this effect and applied dose. Also, KP1019 was extremely well tolerated and only few weak side-effects were noted. Due to solubility problems however, maximum tolerated dose was not achieved[43, 51, 60]. For phase II of clinical trials, dose in range 400-600 mg with longer application time (10 weeks) was proposed based on previous animals *in vivo* studies. However, phase II was not yet evaluated in literature.

In case of NKP-1339, dose limitation due to low solubility was avoided. The results of phase I were presented in 2012 on American Society of Clinical Oncology annual meeting[63]. 34 patients were treated with this drug in 9 different doses. Similar to KP1019 only minor side effects have been observed. Biological response for NKP-1339 was higher than for KP1019. Stable disease was observed in seven patients for a long period of time (up to 88 weeks). And in case of one patient partial remission was observed. For now, phase II single agent NKP-1339 and phase I NKP-1339 combination trials are planned.

1.2.4. Ruthenium-arene complexes

The ability to change oxidation state and exchange ligands of previously described ruthenium complexes may be their advantage (activation by reduction theory) but also unpredictability of this complicated ligand exchange chemistry is a huge disadvantage. In terms to increase the stability of the oxidation state, organometallic ruthenium complexes were developed[64]. As was mentioned before, those complexes in contrast to other Ru complexes posses unique tetrahedral geometry - so-called piano-stool. Their general structure can be described as [Ru(η^6-arene)(A)(B)(X)]$^+$, where X is a halogen atom (mostly chloride) and A,B are either two monodentate ligands or one bidentate ligand. This configuration stabilize ruthenium +2 oxidation state and prevent undergoong oxidation to Ru(III). In most cases, those complexes exchange only one ligand (labile halogen ligand) and exhibit good water solubility due to their ionic character [37, 64, 65].

The other important factor for cytotoxic activity of those molecules is their cellular uptake. Organometallic ruthenium complexes have increased lipophilicity due to arene molecule which may enhance biomolecular recognition process and assist cellular uptake. In fact, there is a direct correlation between *in vitro* cytotoxic activity of the

molecules and their lipophilicity[66]. Presence of arene molecule may also induce other mechanisms of actions such as intercalation to biomacromolecules (e.g. DNA)[67].

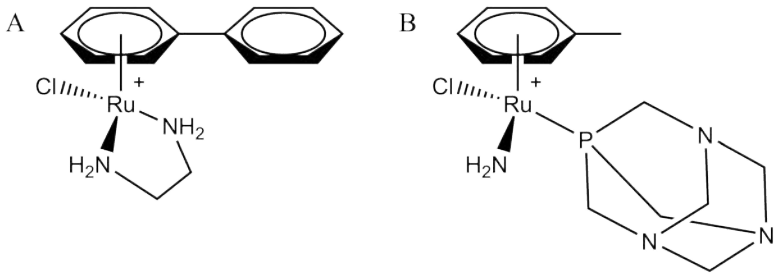

Figure 1.7: Examples of ruthenium(II)-arene complexes. (A) RM175, (B) RAPTA-T.

It was discovered, that Ru(II)-arene complexes with bidentate ethylenediamine ligand (Ru(η^6-arene)Cl(en)]$^+$) exhibit anticancer activity in both *in vitro* and *in vivo* studies, including activity towards Ciplatin-resistant cancer cells[65]. Ethylenediamine ligand was chosen due to the analogy of platinum complex with ammonia ligands. It was thought that hydrogen bonds between this ligand and DNA may be formed in addition to covalent interactions. Studies have shown that this complex binds selectively to N7 atom of guanine base in DNA. The interaction with different binding sites of DNA also confirmed influence of ethylendiamine group on the selectivity of those interactions. Interestingly, influence of arene group was also found. The best activity was found for complex containing most hydrophobic η^6-arene group. Probably the aren-purine base stacking plays a role in stabilizing the transition state in complex-DNA reaction. In fact RM175 ([(biphenyl)RuCl(en)](PF_6)) exhibit significant anticancer activity in multidrug resistant cells and is a potential candidate for clinical trials.

The other Ru(II)-arene complex which is on the edge of clinical trials is RAPTA-T. This obtained by Dyson and co-workers complex belong to the larger group of complexes called RAPTA. They contain the ruthenium(II) center, two labile chloride ligands and hydrophilic phosphine ligand PTA (1,3,5-triaza-7-phosphaadamante). Presence of PTA moiety cause selective activation of the complexes in the hypoxic tumor cells. In the low pH, PTA group easily undergo protonation and its protonated form is consider as an active agent. Due to this effect, RAPTA complexes exhibit pH-dependent DNA binding in lower pH (such as hypoxic cells pH). It was proven that RAPTA complexes also exhibit anticancer activity especially in multidrugs resistant tumors and selectively reduces the growth of lung metastases[50, 68, 69, 70].

1.2.5. Ruthenium polypyridyl complexes

Last group of molecules which will be discussed here is ruthenium(II) polypyridyl complexes. They have been investigated in greater details than any other class of luminescent metal complexes over last 50 years. Thousands of compounds have been prepared and investigated for the various applications (e.g. biosensors, solar cells sensitizers, specific electrodes, anticancer agents). In term of cancer treatment, Ru(II)-polypyridyl complexes interactions with DNA are most interesting. In case of this group of complexes, ligand exchange is almost impossible and so, covalent bonds with DNA cannot be form. In general, two other possible mechanisms may be involved: intercalation between base pairs of nucleotides or/and DNA groove binding through a combination of electrostatic, hydrophobic and hydrogen-binding interactions.

One of the first complex which has shown strong DNA binding was $[Ru(bpy)_2(HATP)]^{2+}$ complex, where bpy are 2,2′-bipyridines and HATP is 1,4,5,8,9,12-hexaazatriphenylene[71]. After binding to DNA, complex exhibited massive absorption change and significant enchantment of emission which were presumably a consequence of environment change due to intercalation of HATP ligand between base pairs of DNA. However, the most significant increase of luminescence in presence of DNA was observed after increasing the size of heteroaromatic ligand. $[Ru(bpy)_2(dppz)]^{2+}$ where dppz is dipyridophenazine, is a non-luminescent complex in water but when intercalated into DNA exhibit strong emission. This mechanism was called light-switch effect and the complex was proposed as specific DNA probe[72, 73].

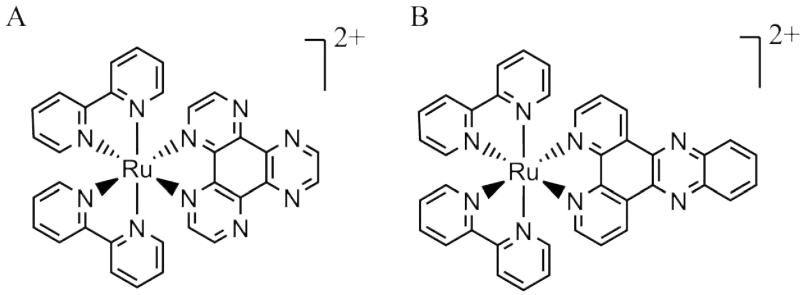

Figure 1.8: Examples of ruthenium(II) polypyridyl complexes which can intercalate with DNA. (A) $[Ru(bpy)_2(HATP)]^{2+}$, (B) $[Ru(bpy)_2(dppz)]^{2+}$.

Photodynamic therapy and photoactivated therapy

The photosensitivity of ruthenium(II) polypyridyl complexes prompted them for testing as sensitizers in PDT - photodynamic therapy of cancer[74]. Recently several Ru(II) complexes, previously used in DSSC (dye-sensitized

solar cells) or in biological staining were evaluated as potential agents in photodynamic cancer therapy. Homoleptic ruthenium(II) complexes with dip ligands (4,7-diphenyl-1,10-phenantroline) and with SO_3dip ligands (4,7-diphenylsulfonyl-1,10-phenantroline) were tested against several different cells lines such as human non-small lung cancer cells (A549) or human promyelocytic leukemia cells (HL60). Both complexes despite similar structures exhibit extremely different physical properties mainly due to their different charges (respectively +2 and -4)[75]. $[Ru(dip)_3]^{2+}$ showed a very good cytotoxicity both in darkness and after light-irradiation. Surprisingly, $[Ru(SO_3dip)_3]^{4-}$ seems to be non-toxic in darkness but after irradiation with light it became toxic in low micromolar concentration.

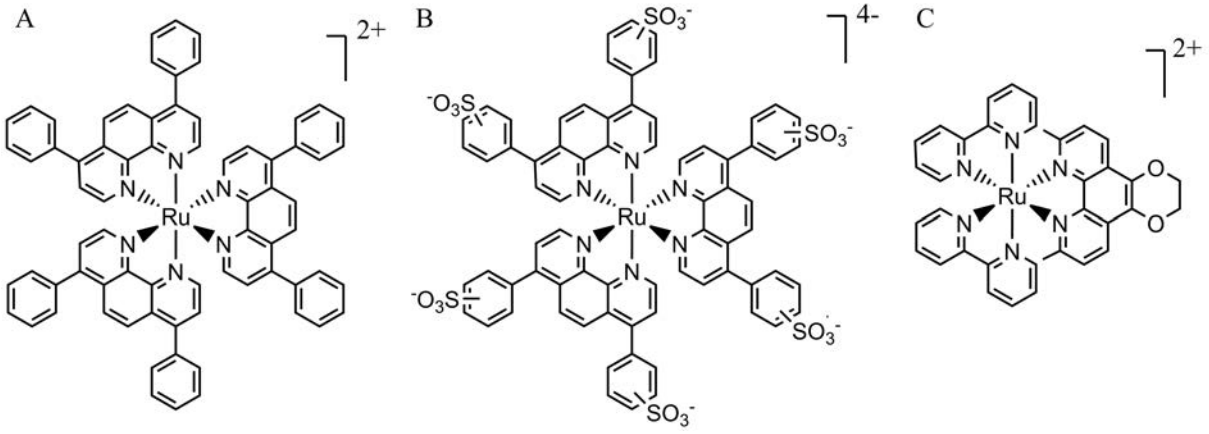

Figure 1.9: Examples of ruthenium(II) polypyridyl complexes evaluated for photodynamic therapy. (A) $[Ru(dip)_3]^{2+}$, (B) $[Ru(SO_3dip)_3]^{4-}$, (C) $[Ru(bpy)_2(dmdop)]^{2+}$.

The main problem with photodynamic therapy is its dependence on the presence of oxygen in the cells. Many ruthenium-based PDT agents relied on generation of reactive oxygen species. However, most tumors are in the state of hypoxia, which means that oxygen concentration is limited and efficiency of the PDT is decreasing. One strategy to overcame this problem is photoactivation of ruthenium complexes. After photo-irradiation, octahedral geometry of ruthenium complex can be distorted which leads to dissociation of one ligand and formation of aqua complex. This complex similary to Cisplatin and other described previously Ru complexes can interact with DNA by forming covalent bonds with nucleotides in DNA[76]. Finally, some ruthenium complexes (such as $[Ru(bpy)_2(dmdop)]^{2+}$ where dop is 2,3-dihydro-1,4-diohino[2,3-f]-2,9-dimethyl-1,10-phenanthroline) posses dual mode of action. They can bind to DNA causing DNA distortion and also form single strand breaks due to formation of singlet oxygen[77].

1.2.6. Ruthenium complexes bearing biologically active molecules - theranostic application

As was mentioned in previous chapter, photophysical properties of ruthenium(II) polypyridyl complexes make them good candidates for luminescence probes. Recent studies have shown that the luminescence of those complexes is increased under the hypoxic conditions. However, the hydrophilic character of the complexes prevents them from crossing biological membranes and limits their applications. A series of novel ruthenium(II) complexes with better hydrophobic properties were synthesized few years ago. The complexes were composed of two 2,2'-bipyridine molecules and one 1,10-phenantroline bearing a long alkane chain or pyren unit. It was resulting in increased lipophilicity of the complex and better cells accumulation. Moreover, the luminescence properties of the complex were not affected by presence of the moieties attached to the 1,10-phenantroline ligand[78].

The ruthenium(II) complex bearing the estradiol was designed as a specific probe for estrogen receptor α. This receptor respond is the most accurate indicator of cancer in particular, estrogen-dependent cancer such as breast, colon, ovarian and prostate[79]. The other example of specific probes are ruthenium polypyridyl complexes bearing cumarin moiety. Those molecules were designed as esterase-specific sensors to measure the activity of the enzyme[80]. In order to target the nuclear enzymes, the ruthenium complexes were modified with the short peptides chains. The specific sequence of peptide can be recognize by specific enzyme. In this way, the complex can be modulate as a probe for only one enzyme.[71, 81].

However, the modulation of pharmacokinetic profile is not the only reason for introduction of additional groups into ruthenium complex structure. Recently, theranostic application of ruthenium complexes are extensively explored by many research groups. This novel approach is based on combining of therapeutic and diagnostic properties into one molecule. This method not only allows to monitor the therapeutic effect of the treatment in real time, but also helps to visualize the biodistribution and accumulation of the drug.

In the most cases, conjugates of the ruthenium are received by binding the biologically active molecules with the complexes via linker. In general, the linker is a short, unbranched chain which can contain heteroatoms in its structure. The linker structures could have an important influence on properties of the ruthenium complexes. It was confirmed that structure of the linker have an influence on the cellular uptake and subcellular localization of the complex[82]. The complexes with the most hydrophilic linkers have the lowest cellular uptake and are mostly present in cytoplasm, while the complexes with the most hydrophobic linkers are localized mostly in mitochondria.

The ruthenium complex bearing 2-nitroimidazole was introduced recently as a new conjugate for treatment and visualization of cancer[83]. This molecule binds polypyridyl ruthenium(II) complex with the bioreductive prodrug, developed towards application in therapy of hypoxic cells, characteristic for tumors. The results have shown that this complex posses not only cytotoxic activity but also antiproliferative activity[84]. Ruthenium complexes were also adapted as luminescence probes[85] and photosensitizers in photodynamic therapy. A series of ruthenium complexes bearing porphyrins were designed as potential two-photon tumor-imaging and photodynamic agents[82, 86, 87]. The complexes had higher solubility and absorption band in the range between 600-800 nm - so called "therapeutic window" more appropriate for PDT - than porphyrins.

The theranostic concept was originally applied to much larger systems such as nanoparticles. Recent studies have shown that gadolinium based nanoparticles modified with ruthenium(II) phenantroline complexes can be used as imaging agents in MRI and simultaneously as photodynamic therapy agents[88]. Also binding ruthenium(II) bipyridine homoleptic complex with silver nanoparticles leads to drastically increased photoinduced oxidation activity[89].

1.3. Biological activity of semicarbazones and thiosemicarbazones

Semicarbazones and thiosemicarbazones are formed when semicarbazide - an ammonia related nucleofile - is added to carbonyl group (aldehyde or keton) and imine bond is formed. Historically, semicarbazones were used in qualitative analysis of aldehydes and ketons[90]. However, their wide spectrum of biological activity is known for more than 50 years. Many semicarbazones and thiosemicarbazones were evaluated as antibacterial, antiviral, antifungal, antifilarial and anticancer agents[91]. Properties and activity of those molecules strongly depends on substituent groups attached to both nitrogen atoms (N1 and N4) of semicarbazon or thiosemicarbazone. Also coordination to metal center plays important role in their activity.

The activity of some semicarbazones and thiosemicarbazones against Plasmodium parasites makes them a good candidates as an antimalarial drug mostly due to their inhibition of cysteine proteases[92]. They were also tested as anticonvulsant drugs due to their lesser neurotoxicity then other drugs[93, 94].

1.3.1. Anticancer activity

Evaluation of semicarbazones derivatives anticancer activity has begun in early 1970s[95]. Since that time many compounds (semicarbazones, thiosemicarbazones and their metal complexes) were tested at this field. Among all studied molecules, heterocyclic derivatives and their metal complexes seems to posses best activity towards primary tumors[91, 93, 96, 97].

Despite good *in vitro* and *in vivo* results towards cancer, only one molecule was evaluated in clinical trials so far. 3-aminopyridine-2-carboxaldehyde thiosemicarbazone also known as Triapine® is a potential ribonucleotide reductase inhibitor which may also induce endoplasmatic reticulum stress in cancer cells[54]. Mechanism of its action is not known yet however it is postulated that Triapine® binds with iron center of ribonucleotide reductase (RNR) and quench thyrosyl radical which is crucial for RNR activity.

1.3.2. Ribonucleotide reductase - potential target in cancer treatment

Ribonucleotide reductase is an enzyme which is responsible for reduction of ribonucleotides into corresponding deoxyribonucleotides. Ribonucleotides reduction is a limiting step in DNA synthesis and hence inhibition of this step leads to inhibit cells proliferation. RNR exist in almost all living organisms - from bacteria to eukaryotes. It was even found in some viruses like bacteriophage or in archaea. It means that catalytic cycle of this enzyme is one of the oldest in the life cycle.

There are three main classes of ribonucleotide reductase which were discovered[98]. They differ in structure, the metal site and place of radical. Moreover class II and III can operate in anaerobic conditions while class I require oxygen. Main differences were collected in table 1.2. Class I is most widely distributed in all eukaryotes. Presence of class II and III in eukaryotes is marginal (see table 1.1). Class I is further divided into two subclasses: Ia and Ib. Subclass Ib is mostly present in bacteria and Ia subclass is an enzyme present in eukaryotes' cells[99].

Table 1.1: Distribution of RNR depending on the class

	Class I	**Class II**	**Class III**
In archaea	Limited distribution	Yes	Yes
In bacteria	Yes	Yes	Yes
In eukaryotes	Yes	Limited distribution	Limited distribution
In dsDNA viruses	Yes	Bacteriophage	Bacteriophage

Class Ia ribonucleotide reductase is tetrameric holoenzyme ($\alpha_2\beta_2$) with a large α_2-homodimer defined as R1 or NrdA and smaller β_2-homodimer defined as R2 or NrdB. However, the crystal structure of R1-R2 holoenzyme is not available yet. R1 is the part of enzyme which harbors the substrate binding site (active site), allosteric site and also redox active disulfides between two cysteines (Cys462 and Cys225) which participate in reduction of substrates (see Fig. 1.10). R2 part contains oxygen-linked diferric center and tyrosyl radical (Tyr122). This radical is an essencial for enzymatic activity of RNR. The stability, formation and transfer of this radical highly depends on binuclear iron(III) center.

Table 1.2: Differences of ribonucleotide reductse classes

	Class Ia	**Class Ib**	**Class II**	**Class III**
Structure	$\alpha_2\beta_2$	$\alpha_2\beta_2$	α or α_2	α_2 + β_2
Operation	Aerobic	Aerobic	Oxygen independent	Anaerobic
Radical	Tyr122 in β	Tyr122 in β	Ado-cobalamine	Gly580 in α
Metal center	Fe-O-Fe	Fe-O-Fe or Mn-O-Mn	Co	Fe-S
Substrate	NDP	NDP	NDP/NTP	NTP

Mechanism of RNR reduction

The main catalytic part of class I RNR is Tyrosyl radical (Tyr122). This radical is stabilized by diferric metal center (Fe_2O_2) and is localized in R2 subunit of the enzyme.

However, reduction takes place in R1 subunit, so it is necessary to transfer this radical to more suitable place. The final amino acid which take place in direct mechanism is Cysteine439. The distance between Tyr122 and Cys439 is approximately 35 Å [100, 101]. The radical is probably transferred through Tyr122 - Tyr356 - Tyr731 - Tyr730 and finally Cys439 in the active site of enzyme[102]. Presence of such pathway introduce the new possible ways for the inhibition of this enzyme.

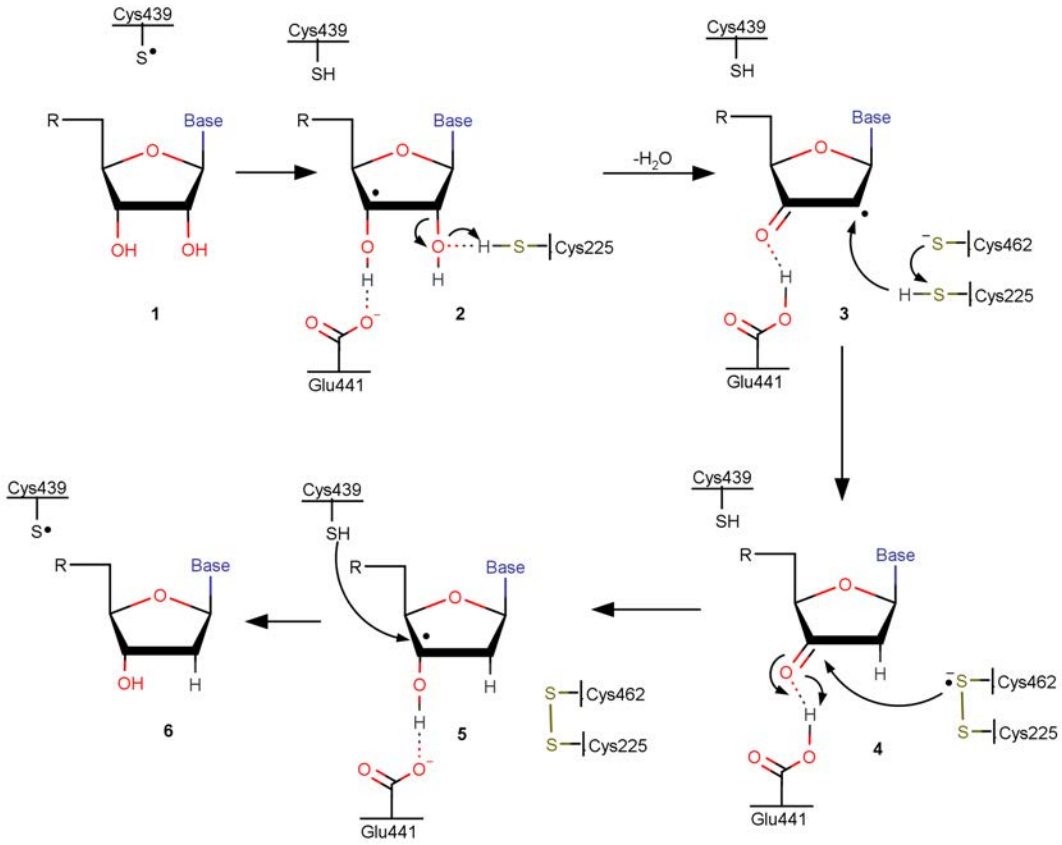

Figure 1.10: Mechanism of ribonucleotide reduction by class Ia RNR.

RNR inhibition and metal complexes

Among all studied molecules which inhibits ribonucleotide reductase, metal complexes take a special place. As was mentioned before, the most important part of the enzyme is thyrosyl radical so, quenching of this species inhibit an enzyme. Metal complexes - especially iron(II) and (III) complexes can produce reactive oxygen species (ROS) under physiological conditions. It is postulated that ROS can react with thyrosyl radical and quenching it.

Several different complexes, mostly bearing α-heterocyclic thiosemicarbazones as ligands (e.g. Trapine®) were tested as inhibitors of RNR. Most of the complexes were much more efficient in thyrosyl radical quenching than hydroxyurea which is consider as a standard in those kind of studies. Iron(III) complex with Triapine® had exhibited best activity towards thyrosyl radical[103]. It was also confirmed that this kind of complex can be formed spontaneously under physiological conditions by chelating of iron from environment or from RNR metallic center[104].

1.4. Hydantoins - anticonvulsant drugs in cancer treatment

1.4.1. Seizures and cancer

Anticonvulsant activity of hydantoins is known since 1930s[105]. The most known hydantoin derivative which is used as anticonvulsant drug worldwide is phenytoin (5,5-diphenylhydantoin)[106] and despite severe side-effects remain one of the lead drugs at the market. The major advantage of hydantoin-based drugs is possibility to administrate them orally. However, this advantage had became disadvantage in case of seizures induced by tumors.

One of possible sequelae of cancer are epileptic seizures. The cause of it may have a variety of sources, including cytotoxic drugs administration or toxic metabolic encephalopathy of brain parenchymal[107]. To extentuate those symptoms, drugs with rapid onset are administrated as a loading dose during chemotherapy. Orally administrated drugs are not good for this purpose due to reduction of their activity and uptake caused by the toxic effect of cancer drugs on the gastrointestinal muscosa. Most of antiepileptic drugs also interfere with serum level of chemotherapeutics and may impair the efficiency of cancer treatment[108].

1.4.2. Hydantoins in cancer treatment

Besides antiepileptic properties of hydantoins, many of them were studied as potential anticancer agents[109, 110]. In fact, biological activity of hydantoins strongly depends on substituents attached to the hydantoin ring[109]. In general, hydantoins molecules can be divided into two parts[111]: N3-C4(=O)-C5-R which is consider as anticonvulsant pharmacophore and C2(=O)-N3(H) part which is mostly responsible for cytotoxic and mutagenic properties of the molecule. It is postulated, that modification of second part do not affect anticonvulsant properties of the molecules but may result in changing toxicity and mutagenic properties of it.

Many new hydantoins derivatives had confirmed anticancer activity over last few years[110, 112, 113]. In major group of molecules only substituents at position 5 were changed, however also modification of N1 and N3 subtituents took place and even exchange of oxygen to sulfur[114] or selenium[113]. Results of this evaluation shown that some of the hydantoins posses high cytotoxicity towards cancer cells. They also are good antioxidants and antimetastatic agents.

2. Aim and scope of the thesis

The photophysical properties of ruthenium(II) polypyridyl complexes open wide possibilities of using them in biological applications for example as bioimaging agents. In recent years, those types of complexes are extensively studied as theranostic agents, with both therapeutic and diagnostic activities.

The main goal of the project is synthesis and preliminary characterization of novel ruthenium(II) polypyridyl complexes bearing biologically active molecules as potential theranostic agents. Two groups of biologically active moieties are chosen based on their previously reported biological activity. Pyridine-2-carboxyaldehyde semicarbazone is chosen as a model of α-heterocyclic semicarbazones molecules with known anticancer activity. 3-aminopyridine-2-carboxaldehyde thiosemicarbazone (Triapine®) is the most known molecule of this type. It was confirmed in clinical trials that Triapine® is a ribonucleotide reductase inhibitor and an anticancer agent. The second group of chosen molecules is represented by three molecules - hydantoin, 5,5-dimethylhydantoin and allantoin. The hydantoins are well-known anti-seizure drugs which are recently extensively studied in combined cancer therapy.

The first part of the study is focusing on synthesis of the appropriate ligands for ruthenium complexes. Those ligands are conjugates of three molecules: 2,2-bipyridine, linker molecule and biologically active moiety - pyridine-2-carboxyaldehyde semicarbazone, hydantoin, 5,5-dimethylhydantoin or allantoin (ligands **L1** - **L4**). As a linker alkyn chain was used in ligand **L1** and alkane chain in ligands **L2-L4**. Several trials with various synthesis conditions and linker structures are undertaken in order to find optimal conditions of synthesis. The ligands are used to synthesize desired ruthenium(II) polypyridyl complexes in reaction with *cis*-bis(polypyridine)dichlororuthenium(II) core complexes. The schematic structure of designed ruthenium(II) complexes is presented in the figure 2.1.

The second part of the studies is focused on spectroscopic and photophysical properties of the ruthenium(II) polypyridyl complexes with ligands **L1** - **L4**. The influence of those ligands on spectroscopic and photophysical properties of the Ru(II) polypyridyl complexes are discussed based on the experimental results (absorption spectra, luminescence quantum yield, luminescence lifetime) and the theoretical

calculations (geometry optimization, natural bond orbitals (NBO) energy and shapes, simulated electronic absorption spectra).

The preliminary evaluation of the studied ruthenium complexes biological activity is performed. The interactions between those ruthenium complexes and human serum albumin are shown and the influence of the various polypyridyl ligands in ruthenium complexes on those interactions is discussed.

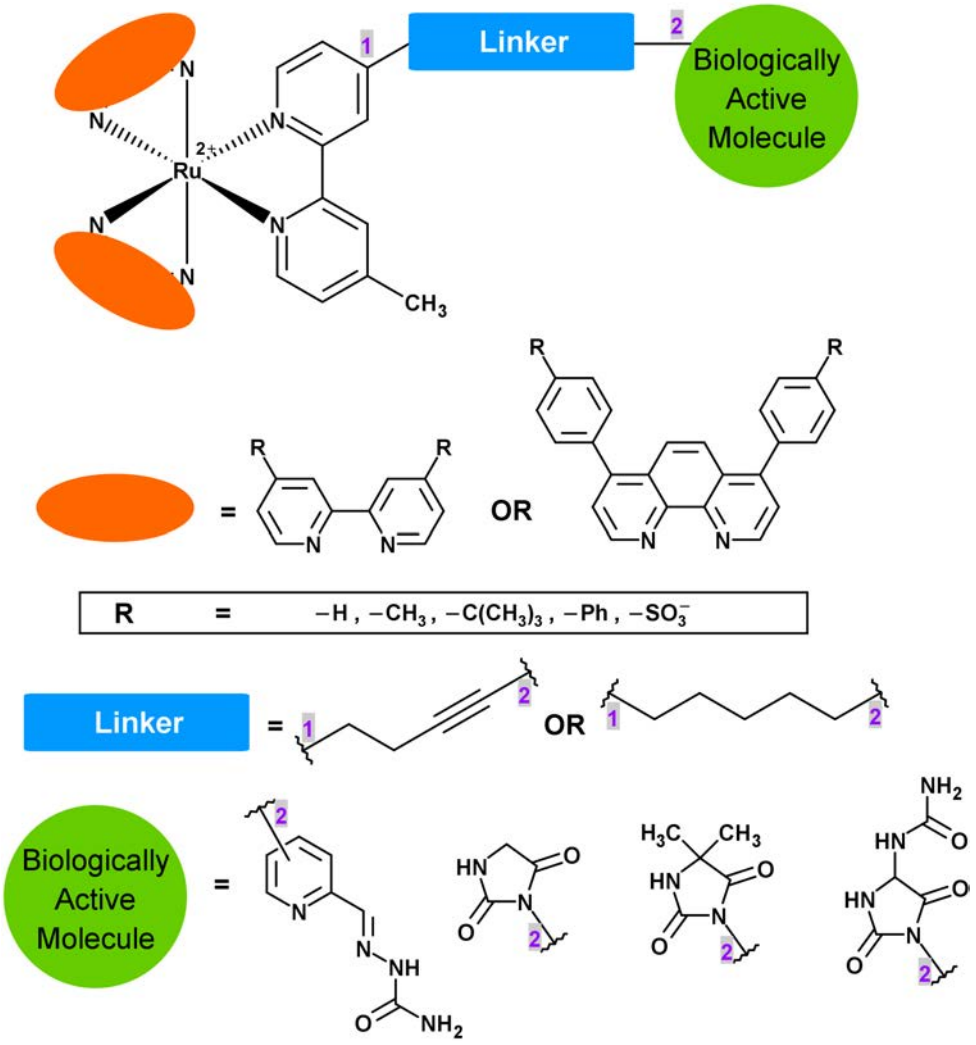

Figure 2.1: The structure of designed ruthenium(II) complexes

3. Methods

3.1. Electronic apsorption spectroscopy

UV-Vis absorption spectra of the ruthenium complexes were recorded at 25°C in water using Perkin Elmer Lambda 35 spectrophotometer. Molar absorbtion coefficients were determined using Lambert-Beer equation (3.1 and 3.2). Samples of the ruthenium complexes with a known mass were dissolved in dmso to get concentration of 32 mM. After that small amount (1-10 μL) of this solution was added to 1.6 mL of water in the cell with 1 cm optical pathway and spectra were recorded. For each complex ten points were measured and molar absorption coefficients (ϵ) were determined from the plot. For each ruthenium complex procedure was performed three times.

$$A = c \cdot \epsilon \cdot l \tag{3.1}$$

$$\epsilon = \frac{A}{c \cdot l} \tag{3.2}$$

3.2. Luminescence studies

Luminescence measurements were registered on Perkin Elmer LS55 spectrofluorimeter in the range 480 - 900 nm upon excitation at the maximum of metal-to-ligand charge transfer band for each ruthenium complex. The average of three scans was subjected to smoothing.

Quantum yield of luminescence was determined using $[Ru(bpy)_3]Cl_2$ as an internal standard[115]. Spectra were recorded with concentration lower than 0.05 absorbance unit at excitation band to avoid inner filter effect. Quantum yield was calculated according to the following equation:

$$QY = QY_r \cdot \frac{I}{I_r} \cdot \frac{A_r}{A} \cdot \frac{n^2}{n_r^2} \tag{3.3}$$

where I is the integrated intensity of luminescence, A is the optical density, and n is the refractive index, r refers to the values for reference. Three independent measurements were performed and mean value was calculated.

Luminescence lifetime experiments were performed at room temperature using Fluorolog-3 Horiba Jobin Yvon with single photon counting technique. The excitation wavelength was fixed at 464 nm (NanoLED diode) and average luminescence lifetime was measured at emission maximum. The instrument response functions were measured using a light scattering solution of Ludox (colloidal silica, Sigma-Aldrich). The DAS6 software (HORIBA Scientific) was used for deconvolution of the obtained decays and for calculation of the lifetime values. Two or three exponential fits were chosen based on χ^2 parameter (the goodness of fit evaluation).

3.3. Computational studies

3.3.1. Geometry optimalization and molecular orbitals energy calculations

The hybrid density functional B3LYP (Becke-Lee-Young-Parr composite of Exchange-correlation functional) was used for geometry and orbital energy calculation of studied ruthenium(II) complexes. For all complexes LANL2DZ basis-set [116, 117] was used for ruthenium atom and 6-31G(d,p) basis set for other atoms. The initial structure of ruthenium complex was based on crystallographic data of tris(2,2'-bipyridyl)dichlororuthenium(II)hexahydrate complex[118]. All calculations were performed with Gaussian 09 program[119] using PLGrid infrastructure. Orbitals were visualized using Gabedit software[120]. Structure figures and geometry parameters were obtained with Avogadro 1.1.1 software[121].

3.3.2. Electronic absorption spectra simulation

Electronic absorption spectra were simulated with time-dependent density functional theory (TD-DFT). Number of excited states to be determined was set to 40.The hybrid density functional B3LYP (Becke-Lee-Young-Parr composite of Exchange-correlation functional) was used with 3-21G basis-set for ruthenium atom and 6-31G(d,p) basis set for other atoms. The spectra were visualised with Gabedit software[120].

3.4. Synthesis

All solvents were used with analytical grade purity. THF was dried over sodium wire and its dryness was determned with Carl-Fisher method. DMF was stirred over calcium hydride for 12h, filtrated and distilled from over potassium carbonate[122].

Diisopropylamine was distilled over NaH and stored under argon[122]. nBuLi solution concentration was determined by titration with diphenylacetic acid in dry THF[123].

All reagents were purchased from Sigma-Aldrich or Alfa Aesar and were used without further purification.

Microwave syntheses were performed on a CEM Discover oven with infrared probe temperature control.

Molecules characterization

^{1}H and ^{13}C NMR spectra were recorded on Brucker 200MHz, 400MHz or 600MHz spectrometer.

High Resolution Mass Spectra (HRMS) were recorded on Brucker micrOTOF spectrometer in various solvents.

3.5. Spectrofluorimetric titration of human serum albumin with ruthenium complex

The solution of protein was prepared by dissolving of human serum albumin (HSA) in water and its concentration was determined spectrophotometrically from the molar absorbance coefficient of $4.40 \cdot 10^4$ $M^{-1}cm^{-1}$ at 280 nm [124]. The emission spectra were recorded upon excitation at 295 nm resulting in selective excitation of Tryphtophan 214 residue. Three scans were subjected to smooth spectra and fluorescence intensity was corrected due to inner filter effect according to equation 3.4.

$$F_c = F_0 \cdot 10^{\left(\frac{A_{ex}+A_{em}}{2}\right)} \quad (3.4)$$

where F_0 is recorded fluorescence intensity, F_c is corrected fluorescence intensity, A_{ex} is absorbance of solution at excitation wavelength (295 nm) and A_{em} is absorbance of solution at emission wavelength (355 nm).

Protein binding experiments were performed by measuring fluorescence intensity of HSA solution (concentration 1 μM) in the absence and the presence of various ruthenium complex concentration (up to 5 μM) in TRIS-HCl buffer pH 7.4, concentration 0.1 M at 37°C and concentration of NaCl 0.1 M. Ru-protein solution was incubated for 10 minutes befor measurement.

4. Results and discussion

4.1. General strategy of ruthenium(II) polypyridyl complexes synthesis

The main goal of this work was synthesis and characterization of novel polypyridyl ruthenium(II) complexes bearing biologically active molecules - pyridine-2-carboxyaldehyde semicarbazone or hydantoin derivatives. The general retrosynthetic analisys of the ruthenium complex synthesis is presented in figure 4.1. The designed complexes were divided into two parts: 2,2′-bipyridine ligands modified with biologically active moieties, and ruthenium core complexes - *cis*-bis(polypyridine)dichlororuthenium(II).

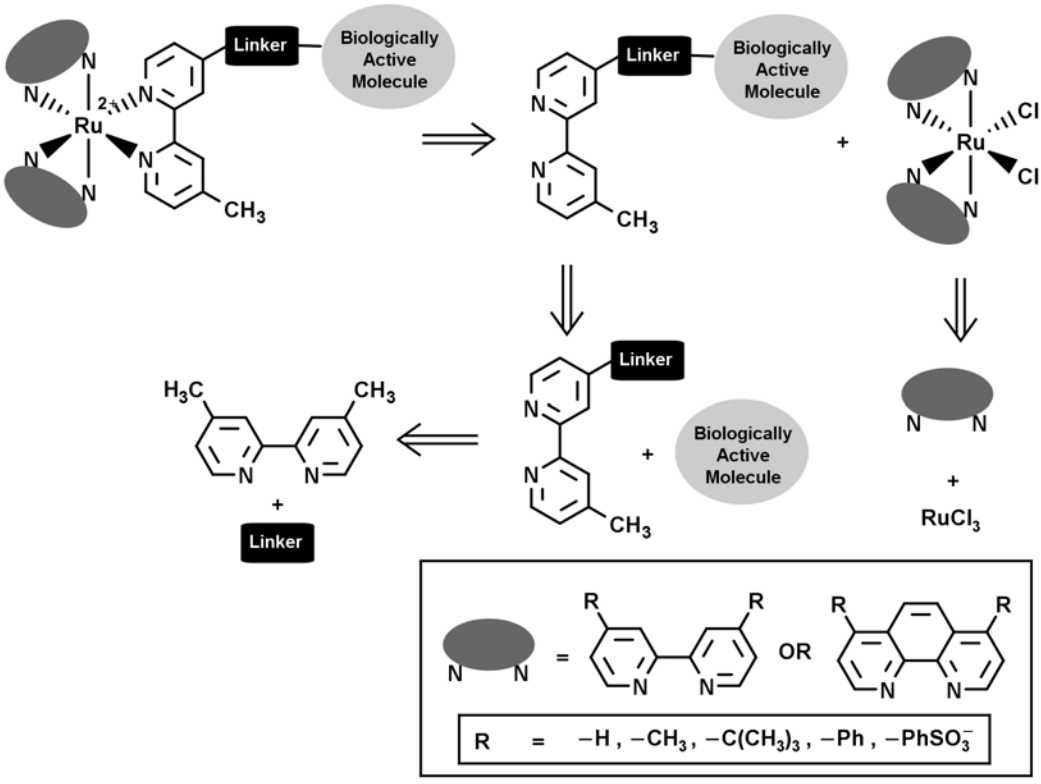

Figure 4.1: Retrosynthetic analisys of designed ruthenium complex

Firstly, the 4,4′-dimethyl-2,2′-bipyridine was modified with the linker molecule. As a linker, various molecules such as hydrocarbons (alkane, alkene, alkyne) or ethers were considered. However, the final conjugates between 2,2-bipyridine and biologically active molecules were obtained only for alkyne linker (ligand **L1**) and alkane (ligands **L2**, **L3** and **L4**). The results for all studied linkers are presented in this work in order to show the synthetic pathways leading to the final compounds.

The obtained 2,2′-bipyridine molecules with the linker were then bonded with the chosen biologically active moieties in order to form desire ligands. In following chapters, the detailed synthesis of all designed ligands are presented first and next, synthesis of the ruthenium complexes are presented in chapter 4.4.

4.2. Synthesis of 2,2′-bipyridine ligands modified with pyridine-2-carboxyaldehyde semicarbazone and the linker - various approaches

The first ligand which was designed was a 2,2′-bipyridine bound to pyridine-2-carboxyaldehyde semicarbazone. Semicarbazones and thiosemicarbazones are good chelators for many metals[125]. They also possess wide spectrum of biological activity. For example 3-aminopyridine-2-carboxaldehyde thiosemicarbazone also known as Triapine® is a potent ribonucleotide reductase inhibitor and also it may induce endoplasmatic reticulum stress in cancer cells [54]. This molecule was in a few clinical trials and currently it is investigated as a drug in combined cancer therapy[126, 127].

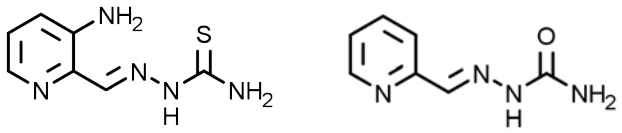

(a) Triapine®

(b) pyridine-2-carboxyaldehyde semicarbazone

Figure 4.2: (a) 3-aminopyridine-2-carboxaldehyde thiosemicarbazone (Triapine®) and (b) pyridine-2-carboxyaldehyde semicarbazone structures

It was decided to use semicarbazone in place of thiosemicarbazone and also simple pyridine ring instead of aminopyridine. Several trials to obtain the final ligand were attended. The main difference between all synthetic approaches was the length and the structure of the linker between 2,2′-bipyridine and pyridine-2-carboxyaldehyde semicarbazone. In this section all approaches - unsuccessful and final successful

synthesis are presented. All unsuccesfull synthesis allowed to better understand the reactivity of the studied molecules and help to propose the final procedure for ligand **L1** synthesis.

Ligand with alkane linker

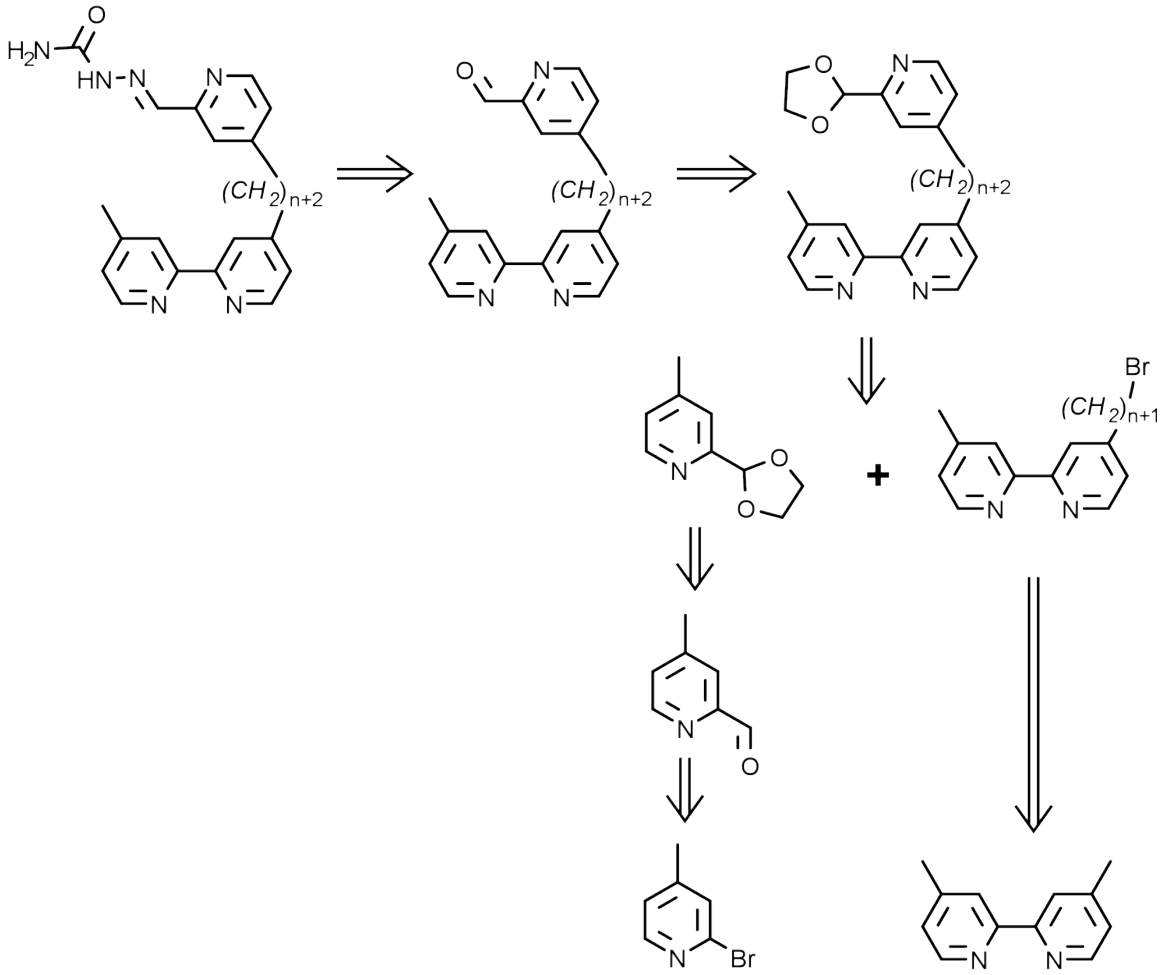

Figure 4.3: Retrosynthetic analysis of ligand with alkane linker

Initial approach was to bind 2,2′-bipyridine and pyridine-2-carboxyaldehyde semicarbazone with simple alkane chain. A retrosynthetic analysis was performed (see fig.4.3) and the synthesis was divided into two parts.

First pyridine-2-carboxyaldehyde had to be synthesized and protected. For this three different methods were tested. Reaction of 4-methylpyridine with n-butyllithium in presence of Li-DMAE[128, 129] gave small yield below 30% (fig. 4.4c), so it was decided to change initial molecule to 2-bromo-4-methylpyridine. First attempt with this molecule and n-butyllithium solution[130] gave even lower yield (20%). In contrast reaction with Grignard reagent (isopropylmagnesium chloride solution)[131] gave an excellent yield around 90% (see fig. 4.4[a-b]). The aldehyde group

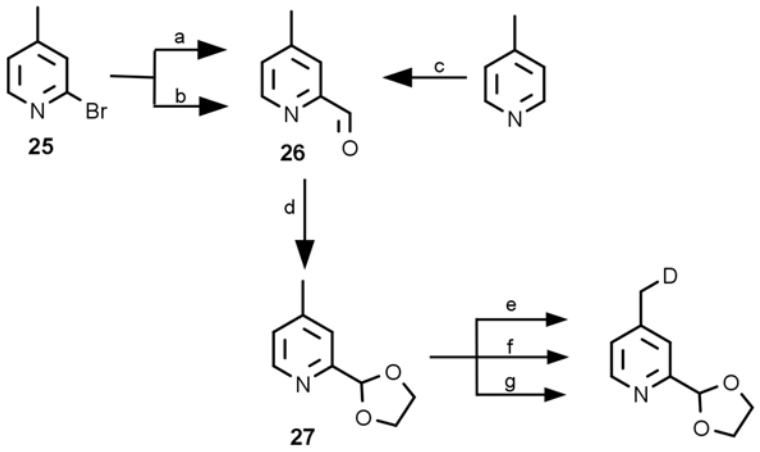

Figure 4.4: Synthesis of 2-(1,3-dioxolan-2-yl)-4-methylpyridine a neccessery substrate for ligand synthesis and attempts to deprotonate p-methyl group. Conditions: (a) 1) nBuLi, -78°C, THF 2) DMF; (20%) (b) 1) iPrMgCl, rt, THF, 2) DMF; (94%) (c) 1) nBuLi/Li-DMAE, -5°C, n-hexane 2) DMF; (28%) (d) ethylene glycol, pTSA, Toluene, reflux, 24h; (100%) (e) 1) DiPA/nBuLi, 0°C, THF 2) CH_3OD (product not formed) (f) 1) nBuLi, -78°C, THF 2) CH_3OD (product not formed) (g) 1) LiTMP, THF 2) CH_3OD (product not formed).

was then protected by condensation reaction with ethylene glycol in presence of p-toluenesulfonic acid[132]. 2-[1,3]-dioxolan-2-yl-4-methylpyridine was obtained with quantitive yield (see fig. 4.4d).

The second part of the synthesis was to obtain 2,2′-bipyridine bearing a bromoalkane chain. At the begining one methyl group of 4,4′-dimethyl-2,2′-bipyridine was lithated with freshly generated LDA[133, 134]. The resulting brown intermediate was next reacted with 1,n-dibromoalkane (for example 1,4-dibromobutane) (fig. 4.5). The yield of this reaction depends on the linker length and is set in the 60-85% range.

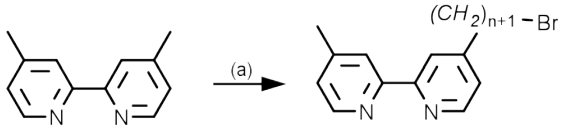

Figure 4.5: Synthesis of 4,-methyl-4′-(n-bromoalkano)-2,2′-bipyridine, the second part of the ligand Conditions: (a) 1) LDA, 0°C, THF 2) Br-$(CH_2)_n$-Br 66% (n = 4), 82% (n = 6)

Problems arose during the reaction that should bind both molecules together. A series of experiments showed that the methyl group in 2-(1,3-dioxolan-2-yl)-4-methylpyridine is very stable and despite using various bases (see fig. 4.4[e-g] for more details) deprotonation was impossible to achieve. Either only

the starting material was recovered or untraceable mixture of products was obtained. CH_3OD was used as highly negative electrophile found organolithiated compound deuterated. The reaction was monitored by ^1H NMR.

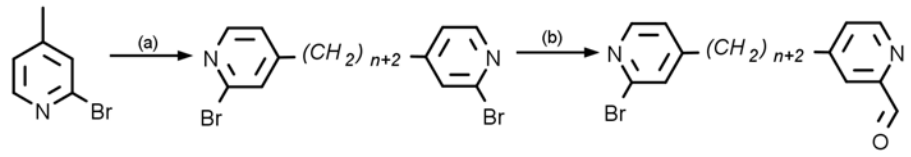

Figure 4.6: Synthesis of 4-[(2-bromopyridin-4-yl)methyl]pyridine-2-carbaldehyde - substrate for ligand1 synthesis. Conditions: (a) 1) LDA, 0°C, THF 2) Br-$(CH_2)_n$-Br , (b) various conditions.

Because of this problem the other approach presented in figure 4.6 was applied. 2-bromo-4-methylpyridine was reacted with LDA to prepare 2-bromo-4-(lithiomethyl)pyridine. This intermediate was reacted with 1,n-dibromoalkane. The product of this reaction was a dimer (figure 4.6(a)). Based on previous experiments both nBuLi and Grignard reagents (isopropylmagnesium chloride solution) were tested in several ratios. However, the selectivity of exchange was not achieved. Either both bromine was exchanged in the same time or neither of them.

Ligand with ether linker

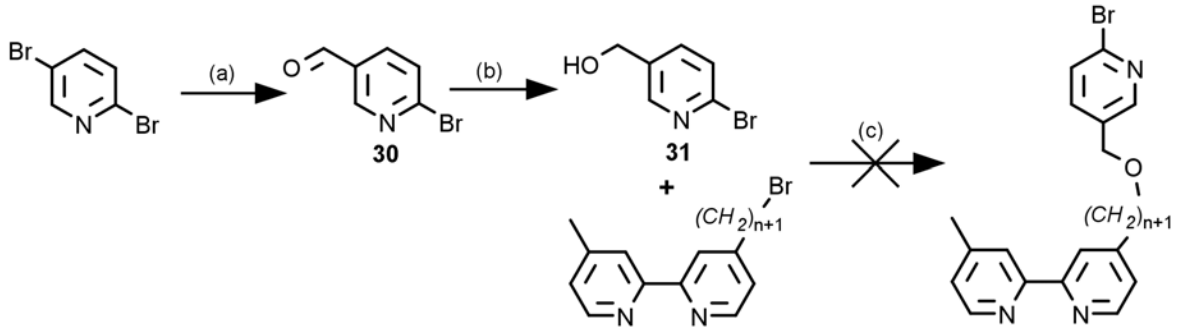

Figure 4.7: Synthesis of ligand with ether linker. Conditions: (a) 1) nBuLi, -78°C, THF 2) DMF, -78°C→ 0°C, (b) $NaBH_4$, MeOH, (c) NaH, 0°C, 4,-methyl-4'-(n-bromoalkano)-2,2'-bipyridine.

The second route applied was the introduction of the heteroatom into the linker's structure. Oxygen was chosen as binding atom because of its high reactivity and relatively high biostability of the ether bonding[135]. First, one of the bromine (position 5) in 2,5-dibromopyridine was selectively exchanged with nBuLi in dry

THF[136]. The obtained intermediate was reacted with dry N,N-dimethylformamide to form 2-bromopyridine-5-carboxyaldehyde. Next, aldehyde group was reduced by sodium borohydride in methanol to form 2-bromo-5-hydroxymethylpyridine[137]. After that, sodium hydride was used to deprotonate the hydroxyl group and form sodium alkoxide which was reacted directly (without purification) with 4-methyl-4′-n-bromoalkane-2,2′-bipyridine. Unfortunately the yield of this reaction was extremely small (less than 10%), probably due to the reaction of the alkoxide with bromine at position 2 or poor reactivity of the bromoalkane.

Ligand with alkene linker

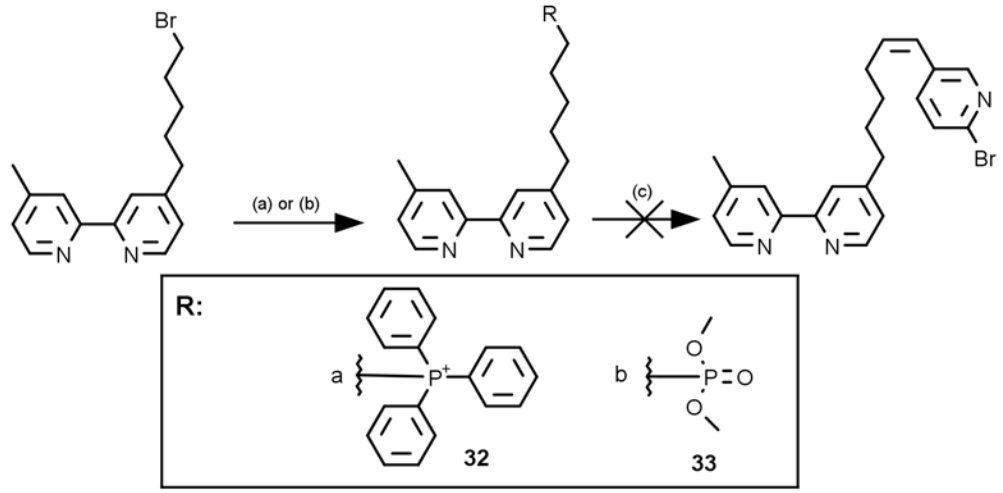

Figure 4.8: Synthesis of ligand with alkene linker. Conditions: (a) PPh_3, toluene, Ar, reflux, (b) $P(OEt)_3$, Ar, reflux (c) tBuOK, 2-bromo-5-formylpyridine, THF, Ar.

Next possibility to obtain the desired ligand was introduction of the alkene chain as linker. To reach this goal 4-methyl-4′-(n-bromoalkane)-2,2′-bipyridine had to be modified. The terminal bromine atom was turned into phosphine derivative and the new compound was reacted with 2-bromopyridine-5-carboxyaldehyde. The Wittig reaction leads to creation of the double bond exclusively in the Z configuration. Further parts of synthesis were the exchange bromine into formyl group in position 2 of pyridine and modified it into semicarbazone group.

Two different phosphine compounds were used to form precursors for the Wittig reaction. First of them was triphenylphosphine and second was triethylphosphite. Both compounds formed the desired products - respectievly ({4′-methyl-[2,2′-bipyridine]-4-yl}pentyl)triphenylphosphonium bromide was formed from triphenylphosphine and diethyl ({4′-methyl-[2,2′-bipyridine]-4-yl}pentyl)phosphonate was formed from

triethylphosphite. However both of those compounds were found unreactive in the Wittig reaction. This was the main reason why this synthetic pathway was also abandoned.

Synthesis of ligand L1 -
5-(4-{4′-methyl-[2,2′-bipyridine]-4-yl}but-1-yn-1-yl)pyridine-2-carbaldehyde semicarbazone

Retrosynthetic analysis

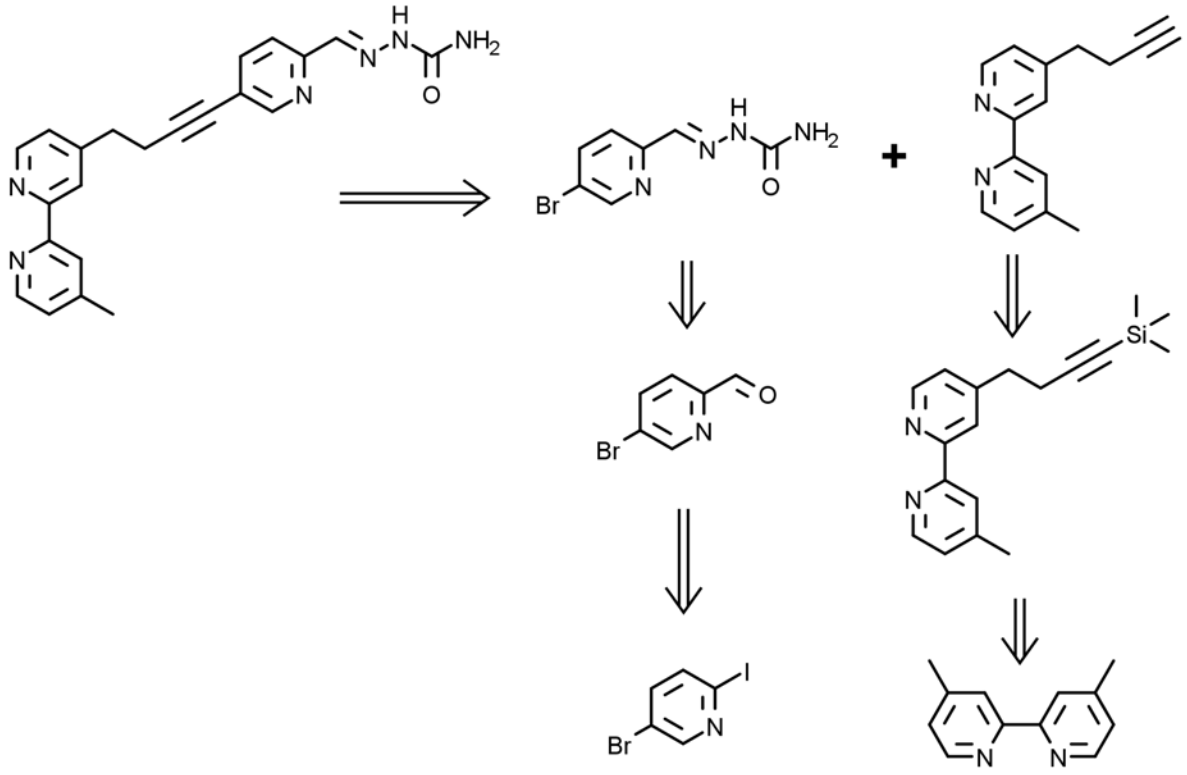

Figure 4.9: Retrosynthetic analizys of Ligand 1 synthesis.

The first part of this approach was to synthesize 5-bromopyridine-2-carboxyaldehyde semicarbazone. This product was obtained by the selective formylation[138]. 5-bromo-2-iodopyridine was reacted with isopropyl magnesium chloride solution to form the Grignard reagent. After that, freshly distilled, dry N,N-dimethylformamide was added and the desired aldehyde was obtained in a a good yield (80%). To prepare the desired semicarbazone, the obtained aldehyde was reacted with semicarbazide hydrochloride under anhydrous conditions. The product was obtained as a precipitate in 99% yield. Details of this experiments are presented in the figure 4.10.

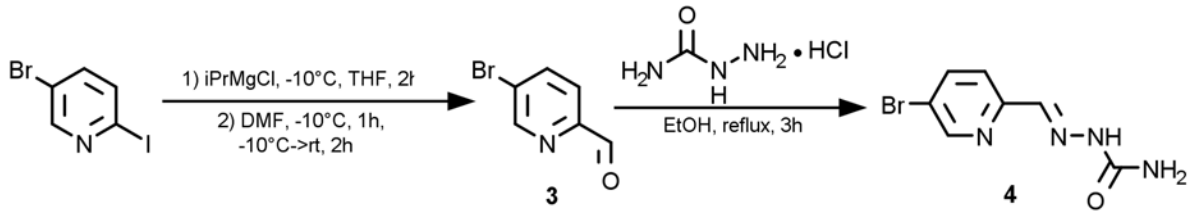

Figure 4.10: Synthesis of 5-bromopyridine-2-carbaldehyde semicarbazone

The second part of ligand **L1** synthesis was to obtain 2,2′-bipyridine bearing a terminal alkyne. 4,4′-dimethyl-2,2-bipyridine was used as the starting compound. One of the methyl groups was selectively lithiated by freshly prepared LDA[133, 134]. The obtained intermediate was reacted with trimethylsilyl propagyl bromide. After that, trimethylsilyl group was removed under basic conditions and the desired product was obtained. Details are presented in the figure 4.11.

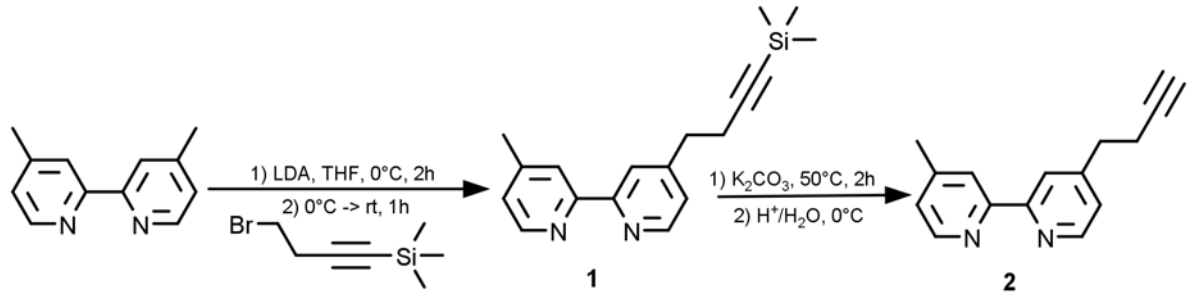

Figure 4.11: Synthesis of 4-(prop-2-yn-1-yl)-4′-methyl-2,2′-bipyridine

Finding Sonogashira coupling conditions

Last part of the ligand **L1** synthesis was to bind together both parts of it - 4-(prop-2-yn-1-yl)-4′-methyl-2,2′-bipyridine and 5-bromopyridine-2-carbaldehyde semicarbazone by a Sonogashira coupling. The main issue during this reaction which may have occurred was the coordination of the catalysts (copper(I) iodine or tetrakis(triphenylphosphine)palladium(0)) to bipyridine and significant reduction of yield. To eliminate this problem and find proper conditions for coupling, 4-(prop-2-yn-1-yl)-4′-methyl-2,2′-bipyridine was reacted with 3-bromopyridine under various conditions (table 4.1, fig 4.12). Two entries gave the desired product with diisopropylamine used as a base. It was decided to use a mixture of acetonitrile and this amine in volume ratio 1/1.

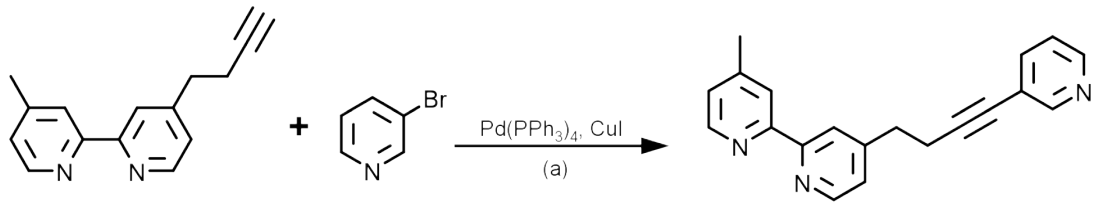

Figure 4.12: Model reaction used for finding right conditions of Sonogashira's coupling. (a) various solvents listed in table 4.1

Table 4.1: Tested conditions of Sonogashira coupling

Entry	Base	Solvent	Ratio (v/v)	Result	Yield
1	triethylamine	toluene	1/2	no reaction	X
2	triethylamine		X	no rection	X
3	diisopropylamine		X	product formed	28%
4	diisopropylamine	DMF	1/1	side products	X
5	diisopropylamine	ACN	1/1	product formed	52%

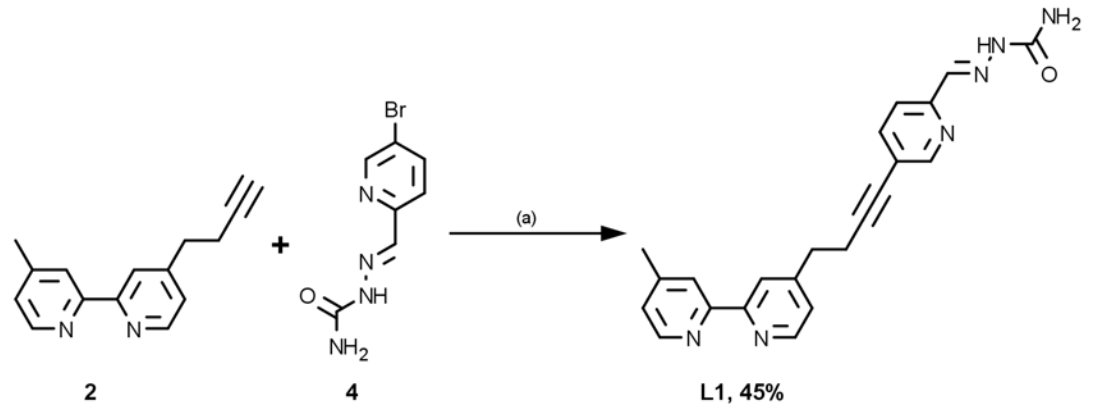

Figure 4.13: Synthesis of ligand 1 with Sonogashira coupling. (a) 0.3 eq CuI, 0.1 eq $Pd(PPh_3)_4$, ACN/DiPA 1/1

Final coupling

For the final coupling, conditions that gave the best results in previous experiments were used. The only modification of this procedure was the small amount of anhydrous methanol that was used to solubilize 5-bromopyridine-2-carbaldehyde semicarbazone. After the reaction, all solid particles were removed by filtration through Celite®, the filtrate was concentrated and washed with concentrated ammonia to remove copper.

Because of the size and polarity of the compound purification by flash chromatography was an impractical method. Nevertheless, product was crystallized in pure form (45% yield) as white-cream plates from mixture of chloroform and cyclohexane.

4.3. Synthesis of 3-(5-{4′-methyl-[2,2′-bipyridine]-4-yl}pentyl) -imidazolidine-2,4-dione (L2), 5,5-dimethyl-3-(5-{4′-methyl-[2,2′-bipyridine]-4-yl}pentyl) -imidazolidine-2,4-dione (L3) and [1-(5-{4′-methyl-[2,2′-bipyridine]-4-yl}pentyl) -2,5-dioxoimidazolidin-4-yl]urea (L4) - General procedure

Ligands **L2** (3-(5-{4′-methyl-[2,2′-bipyridine]-4-yl}pentyl)imidazolidine-2,4-dione), **L3** (5,5-dimethyl-3-(5-{4′-methyl-[2,2′-bipyridine]-4-yl}pentyl)imidazolidine-2,4-dione) and **L4** ([1-(5-{4′-methyl-[2,2′-bipyridine]-4-yl}pentyl)-2,5-dioxoimidazolidin-4-yl]urea) were synthesized using a similar procedure. Commercially available imidazolidine-2,4-dione (also known as hydantoin) derivatives were reacted with potassium hydroxide (see fig. 4.14a) to selectively deprotonate the nitrogen in position 3 [139, 140]. The reaction had to be carried out in anhydrous conditions due to the instability of obtained salts in water. Anhydrous methanol was used as solvent and the product was dried in oven to remove leftover water traces. The obtained salt was used without further purification. Three different imidazolidine-2,4-dione derivatives were used to obtain these ligands.

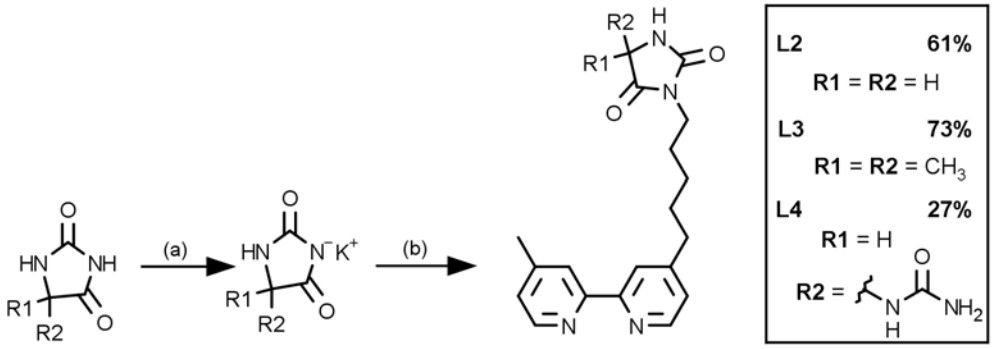

Figure 4.14: Synthesis of ligands with hydantoins derivative. Conditions: (a) KOH, 50°C, 1h, MeOH, (b) 4,-methyl-4′-(5-bromopentyl)-2,2′-bipyridine, 100°C, 3h, DMF

The next step was to bind imidazolidine-2,4-dione derivatives with the 2,2′-bipyridine ligand. To do this, 4-(5-bromopentyl)-4′-methyl-2,2′-bipyridine which was synthesized (see fig. 4.5 on page 43) during ligand **L1** synthesis was reacted with the appropriate hydantoin salt in dry N,N-dimethylformamide at a temperature above 100°C. The hydantoin salt was used in small excess and after the reaction, all impurities were removed by washing ligands **L2**, **L3** and **L4** with water. The three new ligands **L2**, **L3** and **L4** were obtained respectievly in 61%, 73% and 27% yield depending on used

hydantoin. The lowest yield was obtained for allantoin (Ligand **L4**) probably because of it higher water solubility.

4.4. Ruthenium complexes synthesis

4.4.1. Synthesis of cis-bis(polypyridine)dichlororuthenium(II)

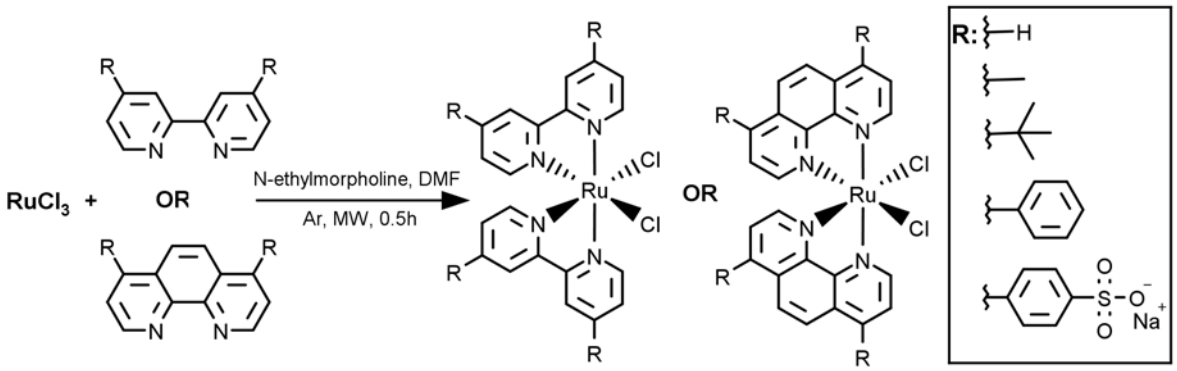

Figure 4.15: Synthesis of used cis-bis(polypyridine)dichlororuthenium(II) complexes.

After the succesful synthesis of ligands the last step to obtain the target molecules was the coordination of those ligands to ruthenium(II) core complexes. As core complexes it was decided to use cis-bis(polypyridine)dichlororuthenium(II) complexes, where polypyridine means derivatives of 2,2'-bipyridine or derivatives of 1,10-phenantroline. This kind of complexes are well known and are widely described in the literature[141, 142, 143]. Two methodes were investigated: the thermal method and the microwave irradiation. The thermal method[144] was not very efficient and the yield was quite low (below 20%). Extending the reaction time (16 h instead of 2 h) improved the yield up to 40%. Much faster was microwave irradiation[145]. The yield of the reaction was almost the same after only half an hour. Using this method six complexes with different ligands were synthesized (see fig.4.15).

4.4.2. Synthesis of ruthenium(II) complexes with ligand L1

The final step of synthesis was the coordination of ligand **L1** to the ruthenium(II) complex. The appropriate cis-bis(polypyridine)dichlororuthenium(II) complex was dissolved in absolute ethanol under argon conditions and ligand **1** in slight excess was added. The mixture was refluxed in darkness and reaction was followed by TLC (neutral Al_2O_3, 5% methanol in dichloromethane) till all starting ruthenium(II) complex was consumed. After that time, the ethanol was removed under reduced pressure and the red residue was purified by crystallization or flash chromatography.

As the result of synthesis, six different ruthenium(II) complexes bearing ligand **L1** were obtained. The complexes were characterized by ^{1}H NMR and HRMS-ESI. General synthesis and complexes structures are presented in figure 4.16.

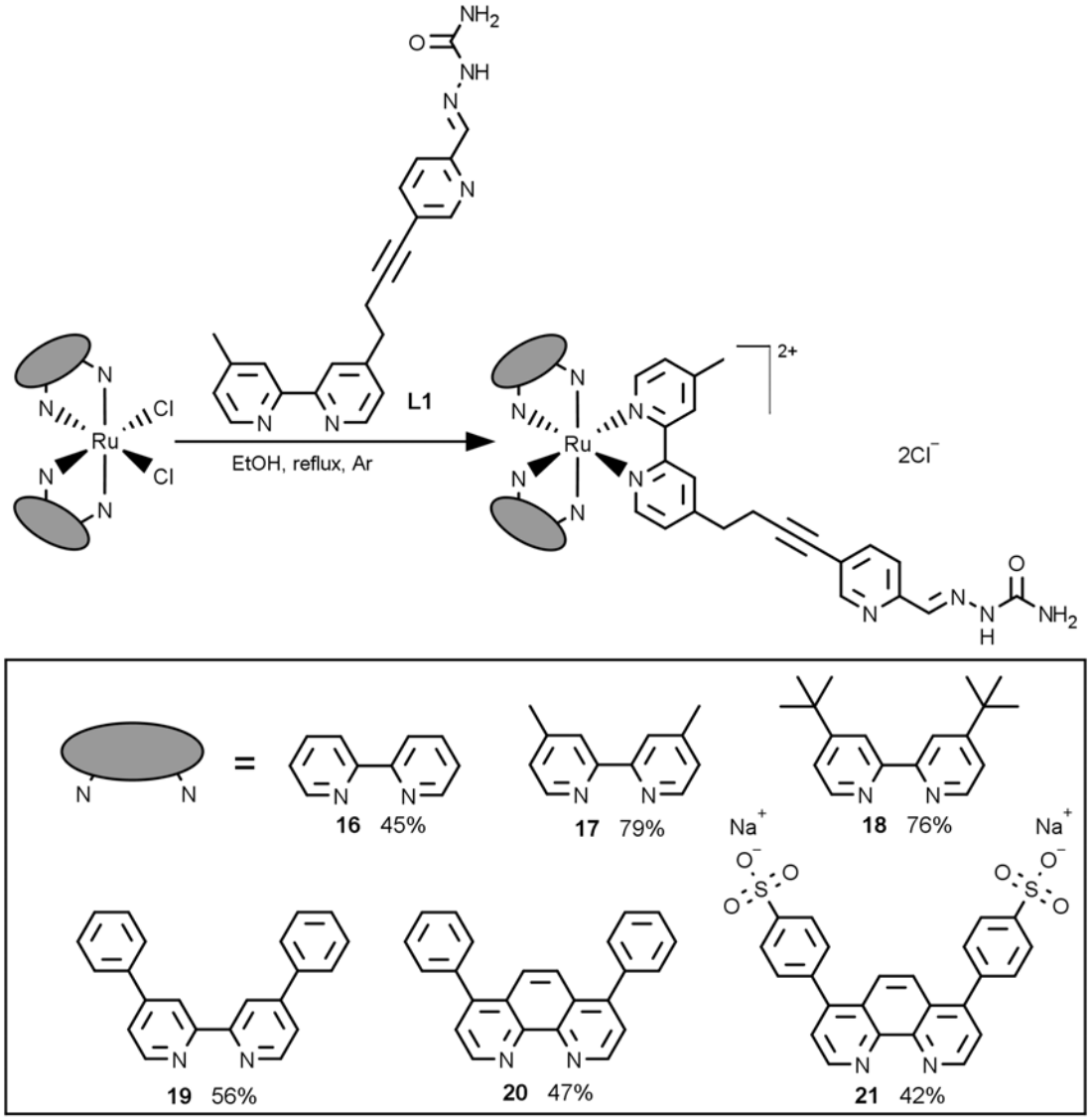

Figure 4.16: Synthesis of ruthenium(II) complexes with ligand **1**

4.4.3. Synthesis of ruthenium(II) complexes with ligands L2, L3 and L4

Similar procedure with few changes was applied to synthesize ruthenium(II) complexes with ligands **L2**, **L3** and **L4**. For those ligands only one complex was used as the starting material - cis-bis(2,2′-bipyridine)dichlororuthenium(II). The complex was dissolved in absolute ethanol and proper ligand was added. Mixture was refluxed under argon for 18 h (followed by TLC) and solvent was removed under reduced pressure. The residue was dissolved in small amount of acetonitrile and saturated solution of potassium hexafluorophosphate was added in large excess. The orange solid was filtrated, washed with cold water and dried. The pure product was obtained

after flash chromatography (neutral Al_2O_3, dichloromethane/methanol 9/1). Synthesis of those complexes is presented in the figure 4.17.

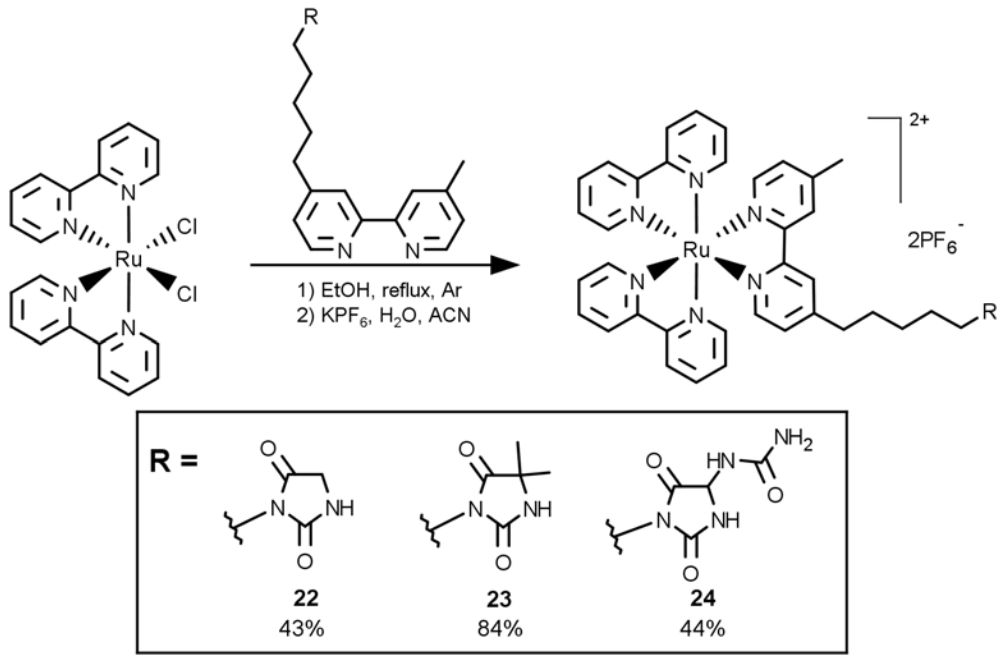

Figure 4.17: Synthesis of ruthenium(II) complexes with ligands **L2**, **L3** and **L4**

4.5. Photophysical properties of ruthenium complexes

4.5.1. Absorption properties

Ruthenium(II) polypyridyl complexes have been studied extensively over last few decades for their rich optical and optoelectronic properties. The absorption spectra of those complexes usually exhibit strong absorption band in visible region of spectra (400 - 600 nm) caused by metal-to-ligand charge transfer (MLCT) transition.

All studied ruthenium(II) complexes exhibit broad and intense MLCT absorption band in the visible region of spectrum (400-500 nm). This band may be assigned to electronic transitions from ruthenium(II) based t_2g orbital to the ligand based π^* orbitals[146, 147]. In the MLCT band region two bands can be distinguished due to the heteroleptic character of the studied complexes. Additionally, the studied ruthenium complexes exhibit intense absorption band in the UV region of the spectrum (around 250-300 nm). These bands were assigned to the intraligand $\pi \rightarrow \pi^*$ transition of ligands. Electronic absorption spectra of the studied complexes are presented in figure 4.18. The main absorption bands with molar absorption coefficients are collected in table 4.2.

Table 4.2: Molar absorption coefficients of the studided ruthenium(II) complexes in water

Ruthenium complex	$\lambda_{\pi\rightarrow\pi*}$ (ϵ)	λ_{MLCT} (ϵ)	λ_{MLCT} (ϵ)
	(nm ($M^{-1}cm^{-1}$))		
$[Ru(bpy)_3]^{2+}$			452 (14 000)[a]
$[Ru(bpy)_2(L1)]^{2+}$	286 (108 600 ± 400)	427 (15 400 ± 100)	455 (18 100 ± 100)
$[Ru(Mebpy)_2(L1)]^{2+}$	286 (107 900 ± 300)	431 (17 600 ± 100)	459 (19 600 ± 200)
$[Ru(tBubpy)_2(L1)]^{2+}$	286 (91 200 ± 500)	431 (13 000 ± 400)	458 (14 600 ± 300)
$[Ru(Phbpy)_2(L1)]^{2+}$	259 (137 500 ± 500) 290 (158 400 ± 600) 308 (152 500 ± 500)	443 (29 800 ± 300)	474 (33 800 ± 200)
$[Ru(dip)_2(L1)]^{2+}$	279 (204 800 ± 800)	435 (42 100 ± 300)	457 (43 000 ± 300)
$[Ru(SO_3dip)_2(L1)]^{2-}$	279 (159 000 ± 900)	440 (30 500 ± 400)	464 (29 600 ± 200)
$[Ru(bpy)_2(L2)]^{2+}$	287 (85 200 ± 200)	427 (12 600 ± 100)	456 (14 600 ± 100)
$[Ru(bpy)_2(L3)]^{2+}$	287 (83 500 ± 300)	427 (13 000 ± 200)	456 (14 400 ± 100)
$[Ru(bpy)_2(L4)]^{2+}$	287 (86 100 ± 200)	427 (12 400 ± 100)	456 (14 400 ± 100)

[a] Data from[115]

Energy of metal-to-ligand charged transfer band can be easily tuned by modification of ligands around ruthenium core (see fig. 4.18). The MLCT band with the lowest energy is observed for $[Ru(Phbpy)_2(L1)]^{2+}$ complex. The band is red shifted (19 nm) compared to MLCT band of the $[Ru(bpy)_2(L1)]^{2+}$ complex. The lower energy absorption of this complex is the result of the presence of the electron donating phenyl groups

which lowers the energy of the π^* orbital in 2,2-bipyridine[147, 148]. For this ruthenium complex additional $\pi \rightarrow \pi*$ intraligand transitions are observed at high-energy (UV) region of the spectrum.

Ligands **L1**, **L2**, **L3**, and **L4** have no influence on MLCT bands absorption energy. The change of lignads results only in a slight alteration of molar absorption coefficient (see table 4.2). For the $[Ru(bpy)_2(L1)]^{2+}$ complex the molar absorption coefficient for MLCT band at 455 nm equals 18 100 $M^{-1}cm^{-1}$ and for complexes with ligands **L2**, **L3**, and **L4** it has a value around 14 500 $M^{-1}cm^{-1}$ at 456 nm.

4.5.2. Emission properties

It is known, that ruthenium(II) polypyridyl complexes bearing 2,2'-bipyridine or 1,10-phenantroline derivatives as ligands exhibit strong luminescence after excitation in MLCT region. Their emission band is usually in the range between 600 and 700 nm and strongly depends on ligands around ruthenium center[149, 150, 151, 152]. All studied ruthenium complexes also exhibit luminescence after excitation at a maximum of MLCT band and the emission bands are observed in the range between 610 - 640 nm (see fig. 4.19). The quantum yield (QY) of luminescence was determined using $[Ru(bpy)_3]^{2+}$ aqueous solution as standard under air-equilibrated and anaerobic conditions[115].

The obtained values of luminescence's quantum yield for all studied ruthenium complexes are collected in table 4.3. The values for complexes with ligand **L1** and 2,2'-bipyridine derivatives are lower than for $[Ru(bpy)_3]^{2+}$ complex. Under air-equilibrated conditions QY is below 1% (2.4% for $[Ru(bpy)_3]^{2+}$) while under anaerobic conditions is in the range between 1 and 2% (4.2% for $[Ru(bpy)_3]^{2+}$). For the complexes with ligands **L2**, **L3** and **L4** results are similar. Quantum yield of luminescence is ca. 1% under air-equilibrated conditions and ca. 2% under anaerobic conditions.

The lower values of QY for complexes with ligands **L1**, **L2**, **L3** and **L4** in comparison with the standard ($[Ru(bpy)_3]^{2+}$) can be caused by forming the hydrogen bonds between the ligands **L1**, **L2**, **L3** and **L4** and the solvent. Similar changes were reported for ruthenium complexes with other ligands which are able to form hydrogen bonds with the solvent[149, 152].

For the complexes with more rigid ligands - 1,10-phenantroline derivatives - $[Ru(dip)_2(L1)]^{2+}$ and $[Ru(SO_3dip)_2(L1)]^{2-}$, the obtained values of QY are higher than for complexes with 2,2'-bipyridine ligands. This was expected based on previously reported results[153, 154, 79]. Exchange of bpy ligands into dip ligands increase luminescence quantum yield of the ruthenium complex. The highest value of luminescence quantum yield was obtained for $[Ru(SO_3dip)_2(L1)]^{2-}$ complex - under

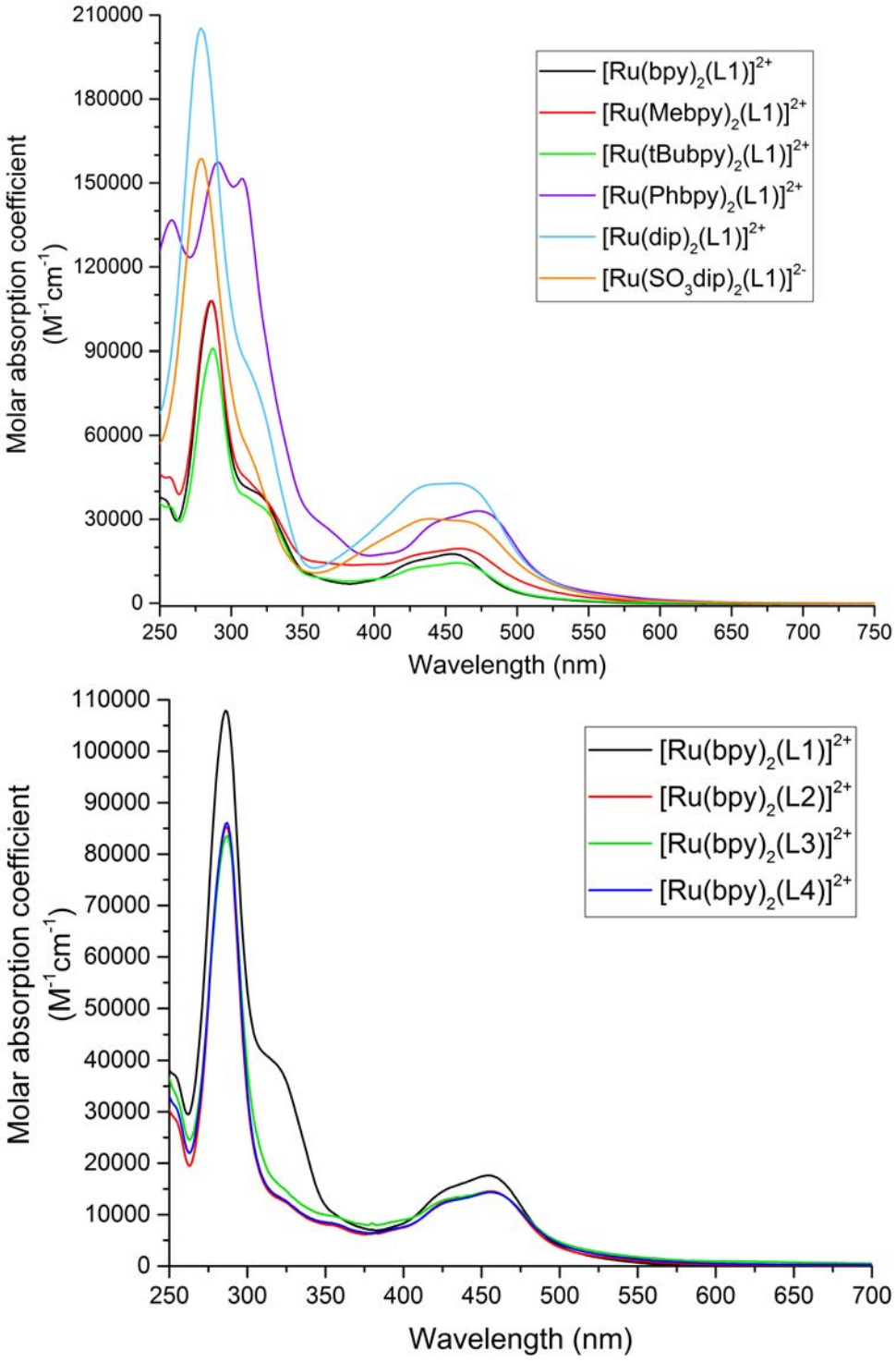

Figure 4.18: Absorbance spectra of studied ruthenium(II) complexes

air-equilibrated conditions 2.2% and under anaerobic conditions 8.1%. This is probably caused by different charge of the ruthenium complex. All other studied ruthenium complexes have the overall charge +2 while this complex has the overall charge -2.

Luminescence lifetime for all studied ruthenium complexes was measured under air-equilibrated and anaerobic conditions. Results are collected in table

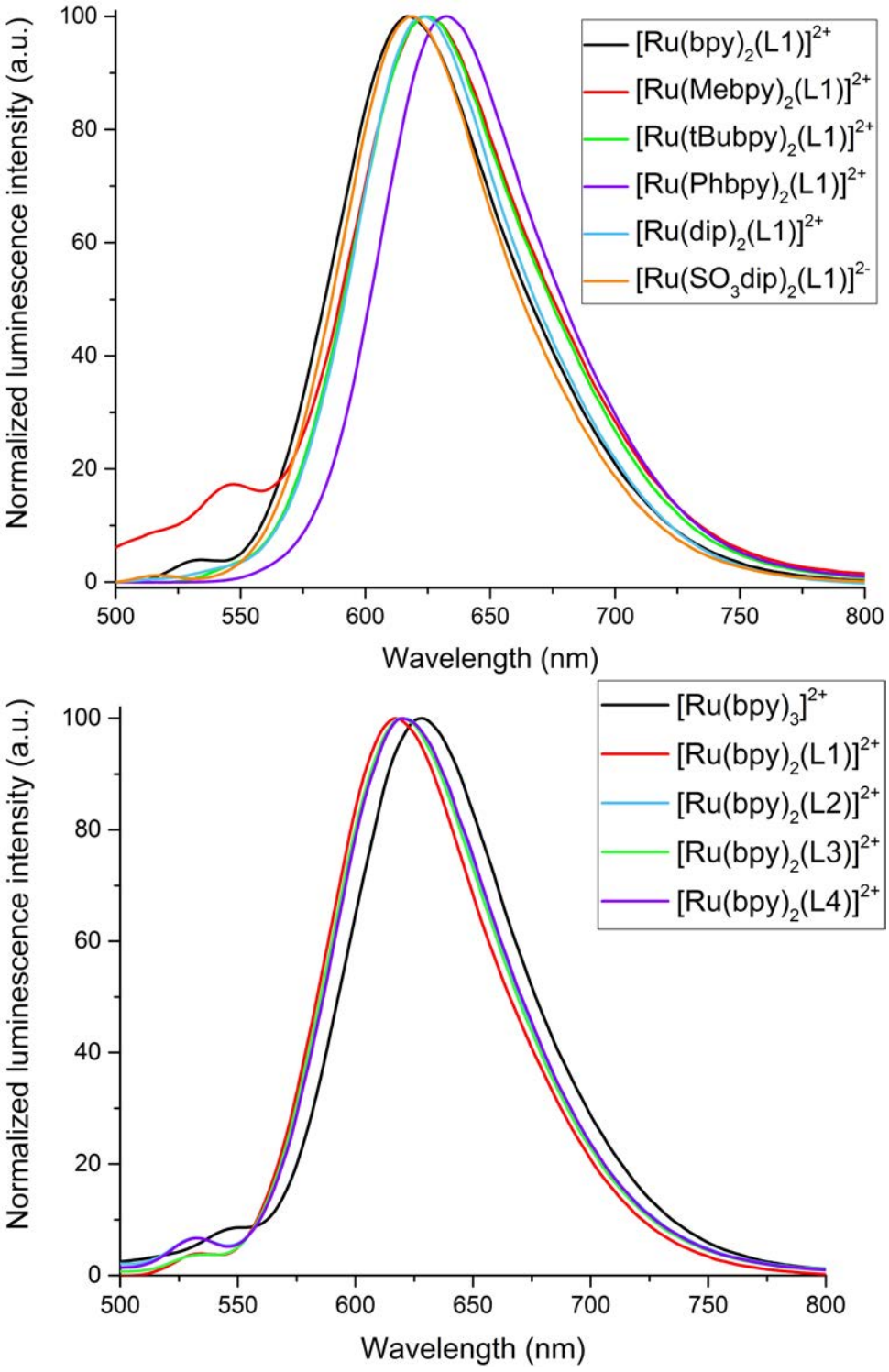

Figure 4.19: Normalized luminescence spectra of the studied ruthenium complexes

4.3. The obtained luminescence lifetimes of the studied ruthenium complexes with 2,2′-bipyridine derivatives as ligands are in the range between 0.26 and 0.37 μs under air-equilibrated conditions and in the range between 0.36 and 0.54 μs under anaerobic conditions. Those values are slightly lower than values for the homoleptic $[Ru(bpy)_3]^{2+}$

complex - 0.37 μs under air-equilibrated conditions and 0.57 μs under anaerobic conditions. The deacrease of the luminescence lifetime after introduction of the ligands which are able to form hydrogen bonds with the solvent was also observed in previously published works[149, 152]. This further confirm that formation of the hydrogen bonds between the ligand and the solvent has an impact on luminescence properties.

Additionally, negatively charged ruthenium complex $[Ru(SO_3dip)_2(L1)]^{2-}$ had the highest observed luminescence lifetime - 0.86 μs under air-equilibrated conditions and 2.90 μs under anaerobic conditions.

Table 4.3: Luminescence properties of the studied ruthenium complexes

Ruthenium complex	λ_{EM}^{MLCT} [nm]	Luminecence QY (%)		Liftime (μs)	
		Air	Anaerobic	Air	Anaerobic
$[Ru(bpy)_3]^{2+}$	628	2.80[a]	4.20[a]	0.37±0.01	0.57±0.01
$[Ru(bpy)_2(L1)]^{2+}$	617	0.92 ±0.09	1.62 ±0.02	0.27 ±0.03	0.36 ±0.06
$[Ru(Mebpy)_2(L1)]^{2+}$	626	0.68 ±0.01	1.16 ±0.03	0.26 ±0.02	0.36 ±0.04
$[Ru(tBubpy)_2(L1)]^{2+}$	624	0.74 ±0.04	1.03 ±0.02	0.29 ±0.05	0.39 ±0.02
$[Ru(Phbpy)_2(L1)]^{2+}$	632	0.88 ±0.01	1.11 ±0.06	0.37 ±0.01	0.54 ±0.01
$[Ru(dip)_2(L1)]^{2+}$	623	1.18 ±0.03	2.62 ±0.04	0.65 ±0.03	1.72 ±0.07
$[Ru(SO_3dip)_2(L1)]^{2-}$	618	2.21 ±0.13	8.10 ±0.09	0.86±0.04	2.90±0.12
$[Ru(bpy)_2(L2)]^{2+}$	620	1.12 ±0.01	2.24 ±0.02	0.35 ±0.01	0.49 ±0.01
$[Ru(bpy)_2(L3)]^{2+}$	620	0.79 ±0.01	1.73 ±0.02	0.34 ±0.01	0.49 ±0.01
$[Ru(bpy)_2(L4)]^{2+}$	620	0.96 ±0.02	1.98 ±0.03	0.33 ±0.01	0.48 ±0.01

[a] Data from[115]

4.6. Computational studies

4.6.1. Geometry calculations

For all studied ruthenium(II) complexes geometry was optimalized based on the initial crystal structure of tris(2,2′-bipyridyl)dichlororuthenium(II)hexahydrate complex[118]. Results of the calculations are summarized in two tables: table 4.4 comprises data for complexes with the structure $[Ru(bpy)_2(Lx)]^{2+}$ where Lx denotes ligand **L1** - **L4** or 2,2′-bipyridine (see fig. 4.17), while table 4.5 contains data for complexes of the type$[Ru(NN)_2(L1)]^{2+}$ where NN stands for derivative of 2,2′-bipyridine or 4,7-diphenyl-1,10-phenantroline (see fig. 4.16). The structures of all calculated complexes are presented in figure 4.20. Numbers on nitrogen atoms (blue ones) marked in figure 4.20 correspond to numbers presented in both tables.

All studied complexes with ligands **L1**, **L2**, **L3** and **L4** have geometry of ruthenium core very similar to homoleptic $[Ru(bpy)_3]^{2+}$ complex. For homoleptic complex, all Ru-N bonds have length around 2.110 Å. Substitution of one 2,2′-bipyridine ligand with Lx causes slight increase (0.001 Å) of Ru-N bonds length between this ligand and ruthenium. Simultaneously other four Ru-N bonds are slightly shorted (0.001-0.002 Å).

More distinct change can be observed for angles measurments. The presence of Lx does not change angles between Ru and nitrogen atoms of two other ligands. However for substituted ligand itself angle between N1-Ru-N2 is decreased. The smallest angle can be observed for complex with ligand **L2**: 77.5°.

The second series of calculations was made for complexes with ligand **L1** and two ligands which were either derivatives of 2,2′-bipyridine (bpy, Mebpy, tBubpy, Phbpy) or 4,7-diphenyl-1,10-phenantroline (dip). For complexes with 2,2′-bipyridine derivatives as ligands, length of both Ru-N bonds between ligand **L1** and ruthenium decreases with the increasing size of other two ligands. For 4,4′-diphenyl-2,2′-bipyridine ligands, all Ru-N bonds are the shortest (2.107 Å). The angles have a constant value of 77.7°.

For ligand dip - 4,7-diphenyl-1,10-phenantroline the Ru-N bonds of **L1** are shorter (2.106 Å) however Ru-N bonds between other ligands are much longer then in case of 2,2′-bipyridine derivatives (2.111 Å). Additionaly, angles between dip ligands and ruthenium are bigger (78.3°). This effect is probably caused by more rigid geometry of 1,10-phenantroline based ligands.

In all studied ruthenium complexes, Mulliken partial charges localized on the ruthenium core are invariable regardless of the ligands and equal 0.96 while the total charge of the complex is 2.

To summarize, the substitution of ligands **L1** - **L4** in the ruthenium complex does not have great influence on ruthenium core geometry. The increase in the size of ligands

Table 4.4: Calculated main internuclear distances (Å), bond angles(°) and Mulliken charges of ruthenium complexes bearing two 2,2′-bipyridine ligands and one of the studied ligand (**L1**-**L4**).

	$[Ru(bpy)_2(Lx)]^{2+}$				
Bonds \ Lx	bpy	L1	L2	L3	L4
$Ru\text{-}N_1$	2.110	2.111	2.111	2.111	2.111
$Ru\text{-}N_2$	2.110	2.111	2.111	2.111	2.113
$Ru\text{-}N_3$	2.109	2.107	2.108	2.108	2.108
$Ru\text{-}N_4$	2.110	2.109	2.109	2.107	2.109
$Ru\text{-}N_5$	2.110	2.107	2.108	2.108	2.108
$Ru\text{-}N_6$	2.109	2.109	2.109	2.109	2.107
Angles					
$N_1\text{-}Ru\text{-}N_2$	77.9	77.8	77.5	77.7	77.8
$N_3\text{-}Ru\text{-}N_4$	77.9	77.9	77.9	77.9	77.9
$N_5\text{-}Ru\text{-}N_6$	77.9	77.9	77.9	77.9	77.9
Mulliken charges					
Ru	0.97	0.96	0.96	0.96	0.96

Table 4.5: Calculated main internuclear distances (Å), bond angles(°) and Mulliken charges of ruthenium complexes bearing ligand **L1** and two derivatives of 2,2′-bipyridine or 1,10-phenantroline.

	$[Ru(NN)_2(L1)]^{2+}$				
Bonds \ NN	bpy	Mebpy	tBbpy	Phbpy	dip
$Ru\text{-}N_1$	2.111	2.109	2.109	2.107	2.106
$Ru\text{-}N_2$	2.111	2.110	2.108	2.107	2.106
$Ru\text{-}N_3$	2.107	2.109	2.108	2.107	2.111
$Ru\text{-}N_4$	2.109	2.109	2.106	2.107	2.111
$Ru\text{-}N_5$	2.107	2.108	2.109	2.106	2.111
$Ru\text{-}N_6$	2.109	2.108	2.106	2.107	2.111
Angles					
$N_1\text{-}Ru\text{-}N_2$	77.8	77.7	77.7	77.7	77.8
$N_3\text{-}Ru\text{-}N_4$	77.9	77.7	77.7	77.7	78.3
$N_5\text{-}Ru\text{-}N_6$	77.9	77.7	77.6	77.7	78.3
Mulliken charges					
Ru	0.96	0.96	0.96	0.97	0.96

around ruthenium core due to modification of two bpy ligands leads to the deacrese in length of Ru-N bonds unless the more rigid ligand like 4,7-diphenyl-1,10-phenantroline is used.

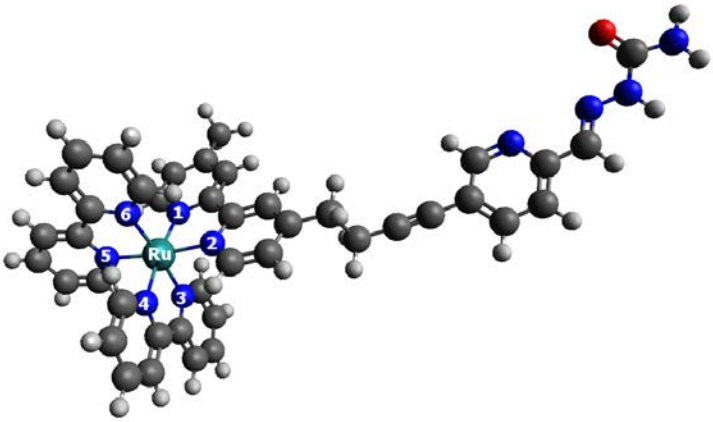

(a) $Ru(bpy)_2(L1)^{2+}$

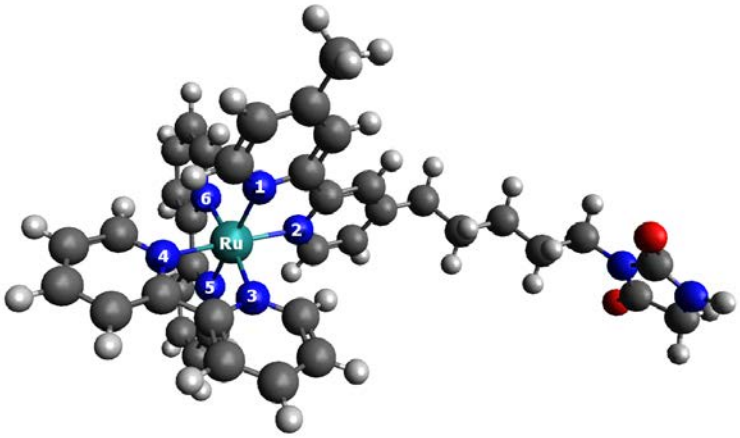

(b) $Ru(bpy)_2(L2)^{2+}$

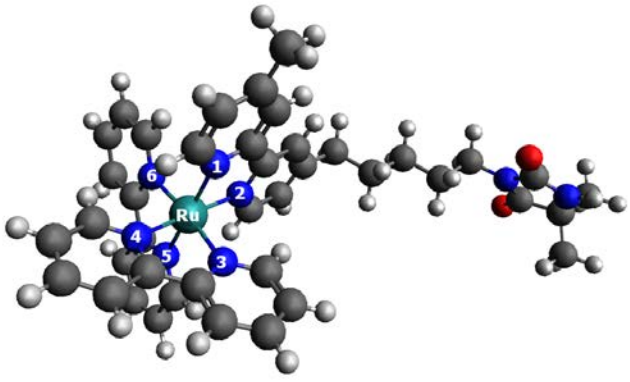

(c) $Ru(bpy)_2(L3)^{2+}$

Figure 4.20: Calculated structures of the studied ruthenium(II) complexes

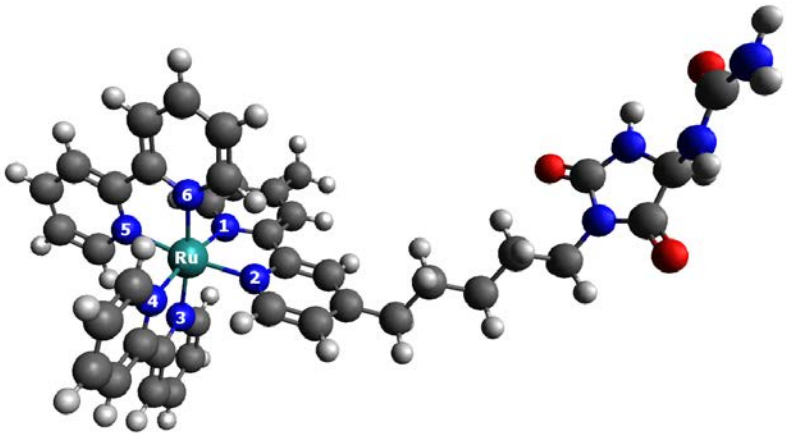

(d) $Ru(bpy)_2(L4)^{2+}$

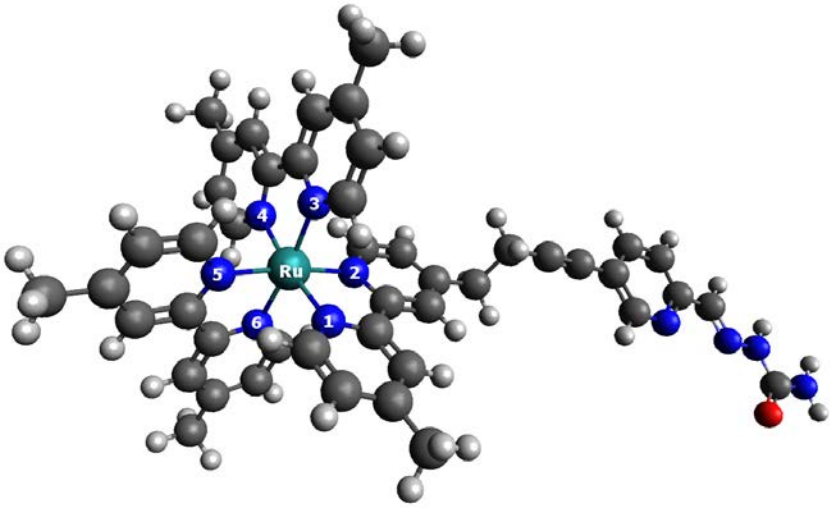

(e) $Ru(Mebpy)_2(L1)^{2+}$

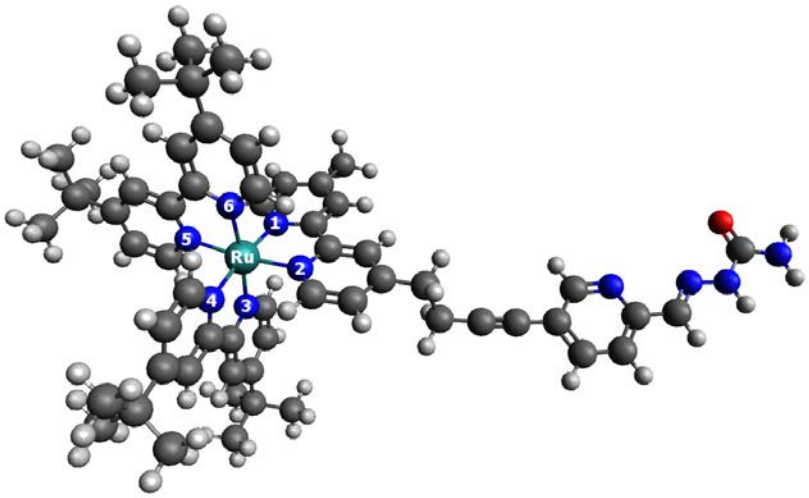

(f) $Ru(tBubpy)_2(L1)^{2+}$

Figure 4.20: Calculated structures of the studied ruthenium(II) complexes

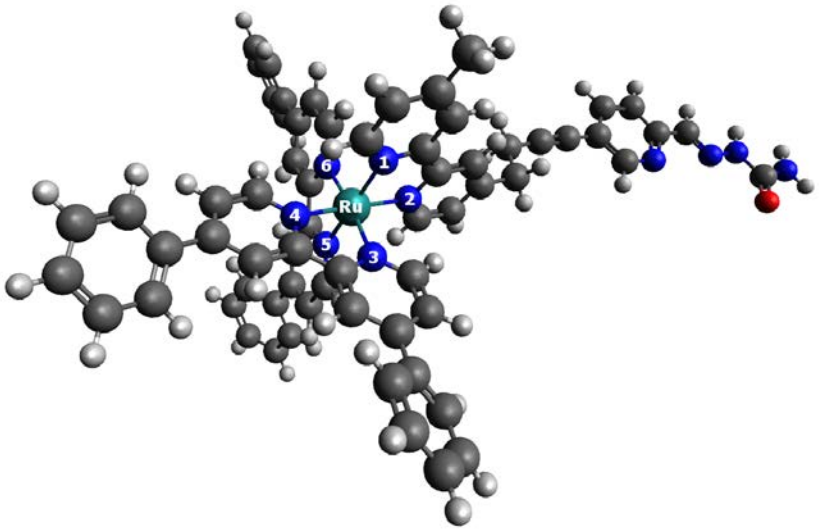

(g) $Ru(Phbpy)_2(L1)^{2+}$

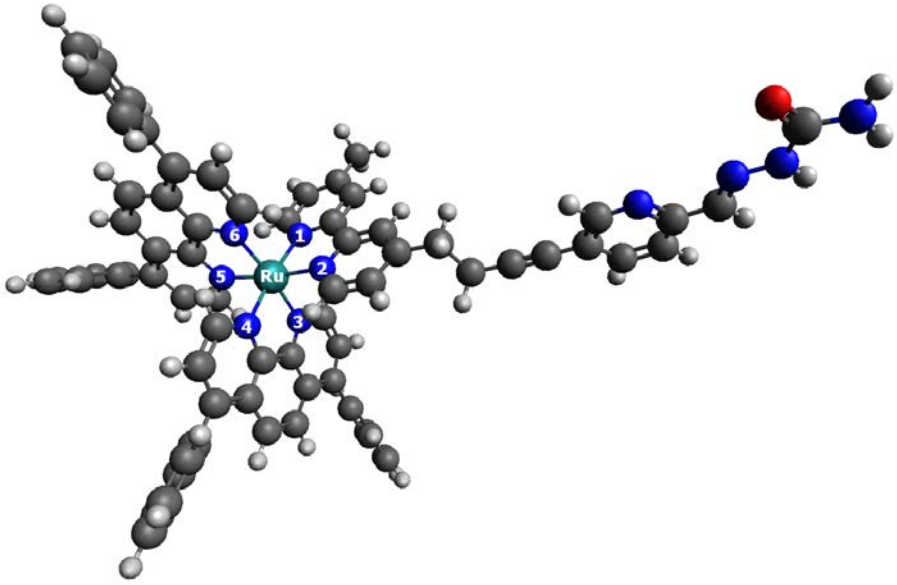

(h) $Ru(dip)_2(L1)^{2+}$

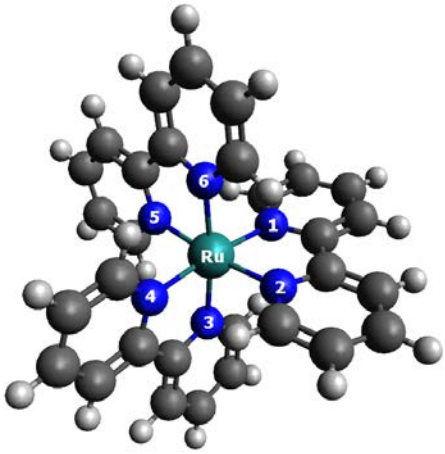

(i) $Ru(bpy)_3^{2+}$

Figure 4.20: Calculated structures of the studied ruthenium(II) complexes

4.6.2. Natural Bond Orbitals (NBO) analysis

Analysis of HOMO-LUMO energies have shown that the presence of ligand **L1** in $[Ru(bpy)_2(L1)]^{2+}$ complex drastically increases the energy of HOMO orbital in comparison to ruthenium complex with unmodified bpy ligand. As a direct result, the band gap between HOMO and LUMO is shortened. For the unmodified homoleptic ruthenium complex, the calculated energy of HOMO is around -11 eV. However, the introduction of ligand **L1** increases the HOMO energy and for complex $[Ru(bpy)_2(L1)]^{2+}$ it equals -8.32 eV. As a consequence, the HOMO-LUMO band-gap for this complex is almost 3.5 times lower than for $[Ru(bpy)_3]^{2+}$ complex (see fig. 4.21 and table 4.6). A similar effect is observed for $[Ru(dip)_2(bpy)]^{2+}$ and $[Ru(dip)_2(L1)]^{2+}$ complexes - HOMO energy is -10 eV for the unmodified complex and -8.4 eV for complex with ligand **L1**.

More detailed analysis of natural bond orbitals (NBO) has shown that for complexes with ligand **L1** the HOMO orbital is localized mostly on pyridine-2-carboxyaldehyde semicarbazone part and orbital LUMO is mostly placed on atoms close to a metallic center of the complex (see fig. 4.23). However, in case of the unmodified ruthenium complexes both HOMO and LUMO orbitals are localized at atoms close to ruthenium center.

Table 4.6: Calculated HOMO and LUMO energies with coresponding bandgap

Ruthenium complex	HOMO (eV)	LUMO (eV)	Band gap (eV)
$[Ru(bpy)_3]^{2+}$	-10.96	-7.52	3.44
$[Ru(dip)_2(bpy)]^{2+}$	-10.10	-6.88	3.22
$[Ru(bpy)_2(L1)]^{2+}$	-8.32	-7.31	1.01
$[Ru(Mebpy)_2(L1)]^{2+}$	-8.27	-6.99	1.28
$[Ru(tBubpy)_2(L1)]^{2+}$	-8.23	-6.75	1.48
$[Ru(Phbpy)_2(L1)]^{2+}$	-8.17	-6.69	1.49
$[Ru(dip)_2(L1)]^{2+}$	-8.43	-6.54	1.89
$[Ru(bpy)_2(L2)]^{2+}$	-9.76	-7.31	2.45
$[Ru(bpy)_2(L3)]^{2+}$	-9.59	-7.30	2.29
$[Ru(bpy)_2(L4)]^{2+}$	-9.54	-7.30	2.44

It was also observed that ligands **L2**, **L3** and **L4** have much weaker impact on HOMO energy than ligand **L1**. For all three complexes, HOMO energy is ca. -9.5 eV with band gap around 2.4 eV. It appeared that modification of hydantoin group does not inflict NBO energies in any significant way (see fig.4.22).

Lower energy of HOMO in those complexes may be caused by different chain structure and length of the linker. In ligands **L2**, **L3** and **L4** the linker is much longer than in case of ligand **L1**. Additionaly the simple alkane chain instead of alkyne chain

is present in **L1**. These properties probably allow to achieve a better charge separation in the final complex.

To study the influence of the other two ligands in the complex (except ligand **L1**) on NBO energies the series of complexes were analysed. It was observed that with increasing complexity of ligands, the energy of LUMO increases as well. For the simple bpy ligands, energy equals -7.31 eV, for the complex with Phbpy ligands, the energy is higher (-6.69 eV). These changes in LUMO energies lead to the increase of the band gap even though HOMO energy is almost constant.

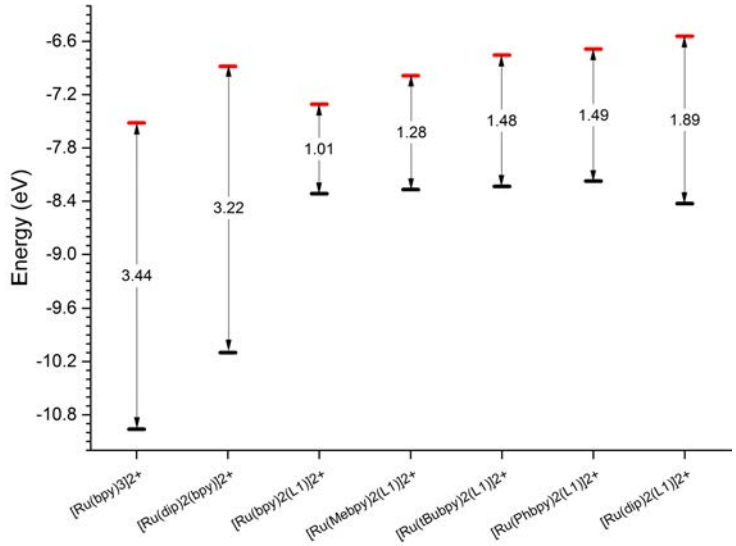

Figure 4.21: HOMO and LUMO orbitals of the studied ruthenium complexes with ligand **L1**

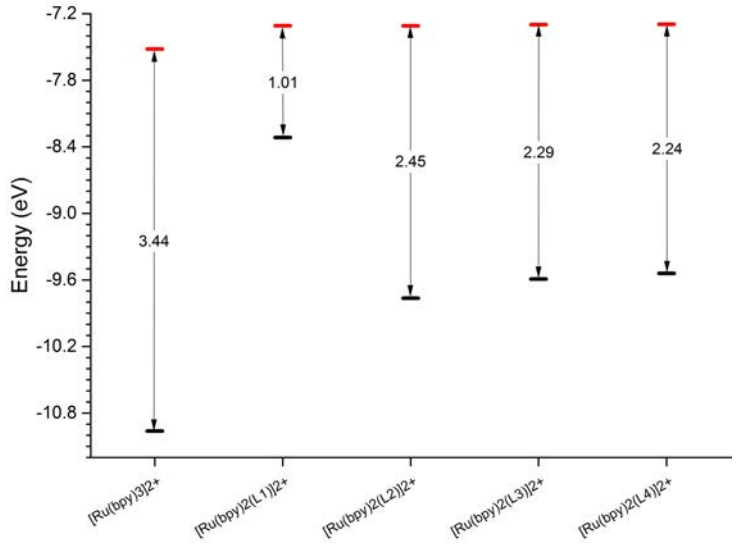

Figure 4.22: HOMO and LUMO orbitals of the studied ruthenium complexes with ligands **L1** - **L4**

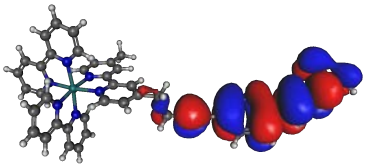

(a) $Ru(bpy)_2(L1)^{2+}$ HOMO

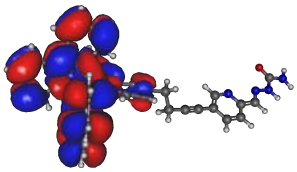

(b) $Ru(bpy)_2(L1)^{2+}$ LUMO

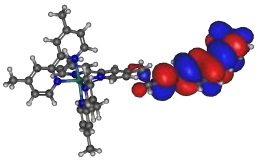

(c) $Ru(Mebpy)_2(L1)^{2+}$ HOMO

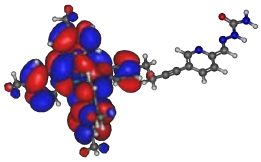

(d) $Ru(Mebpy)_2(L1)^{2+}$ LUMO

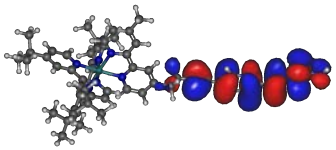

(e) $Ru(tBubpy)_2(L1)^{2+}$ HOMO

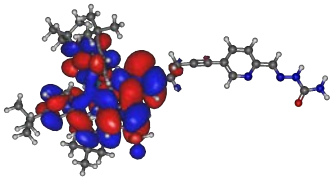

(f) $Ru(tBubpy)_2(L1)^{2+}$ LUMO

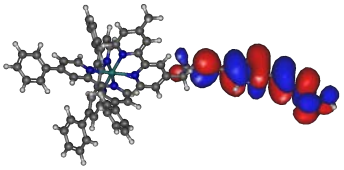

(g) $Ru(Phbpy)_2(L1)^{2+}$ HOMO

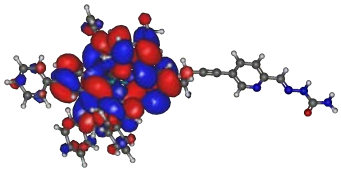

(h) $Ru(Phbpy)_2(L1)^{2+}$ LUMO

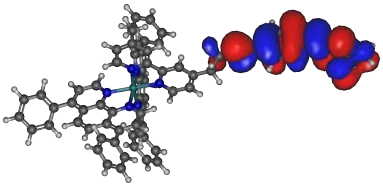

(i) $Ru(dip)_2(L1)^{2+}$ HOMO

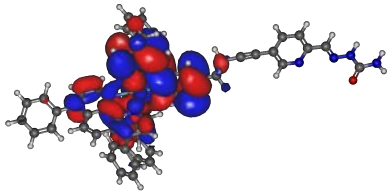

(j) $Ru(dip)_2(L1)^{2+}$ LUMO

Figure 4.23: HOMO and LUMO orbitals shapes of the studied ruthenium complexes

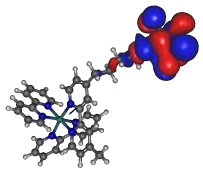

(k) $Ru(bpy)_2(L2)^{2+}$ HOMO

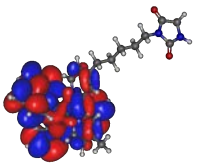

(l) $Ru(bpy)_2(L2)^{2+}$ LUMO

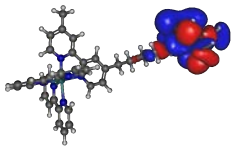

(m) $Ru(bpy)_2(L3)^{2+}$ HOMO

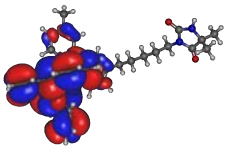

(n) $Ru(bpy)_2(L3)^{2+}$ LUMO

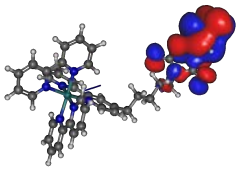

(o) $Ru(bpy)_2(L4)^{2+}$ HOMO

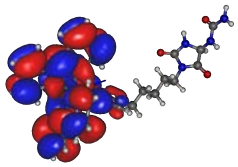

(p) $Ru(bpy)_2(L4)^{2+}$ LUMO

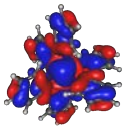

(q) $Ru(bpy)_3^{2+}$ HOMO

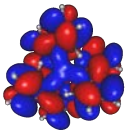

(r) $Ru(bpy)_3^{2+}$ LUMO

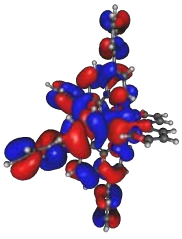

(s) $Ru(dip)_2(bpy)^{2+}$ HOMO

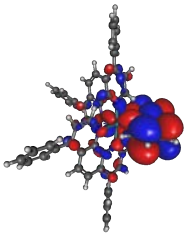

(t) $Ru(dip)_2(bpy)^{2+}$ LUMO

Figure 4.23: HOMO and LUMO orbitals shapes of the studied ruthenium complexes

4.6.3. Electronic absorption spectra

The properties of the excited states of the studied ruthenium complexes were determined using TD-DFT method. Excitation energies, oscillator strength (f) and experimental data (ΔE, ϵ) are collected in table 4.7. Experimental data were obtained for water solutions of the complexes and the calculations were done in vacuum.

Calculated spectra are in a good agreement with experimental data (compare figures 4.24 , 4.25 , 4.26 and figures 4.18). The values of excitation energies which were obtained during calculations are higher than experimental ones due to a solvent effect, however the obtained results are in a good correlation with previously reported results for different ruthenium complexes[155, 156].

Figure 4.24 shows the calculated spectra of the complexes with the general formula $[Ru(bpy)_2(Lx)]^{2+}$ where Lx is ligand **L1** - **L4** or bpy. There are slight differences in intensity of bands (oscillator strength), however the position of the main CT band is almost the same for all complexes. This corresponds to the experimental data where all complexes exhibit absorbance band with maximum near 455 nm.

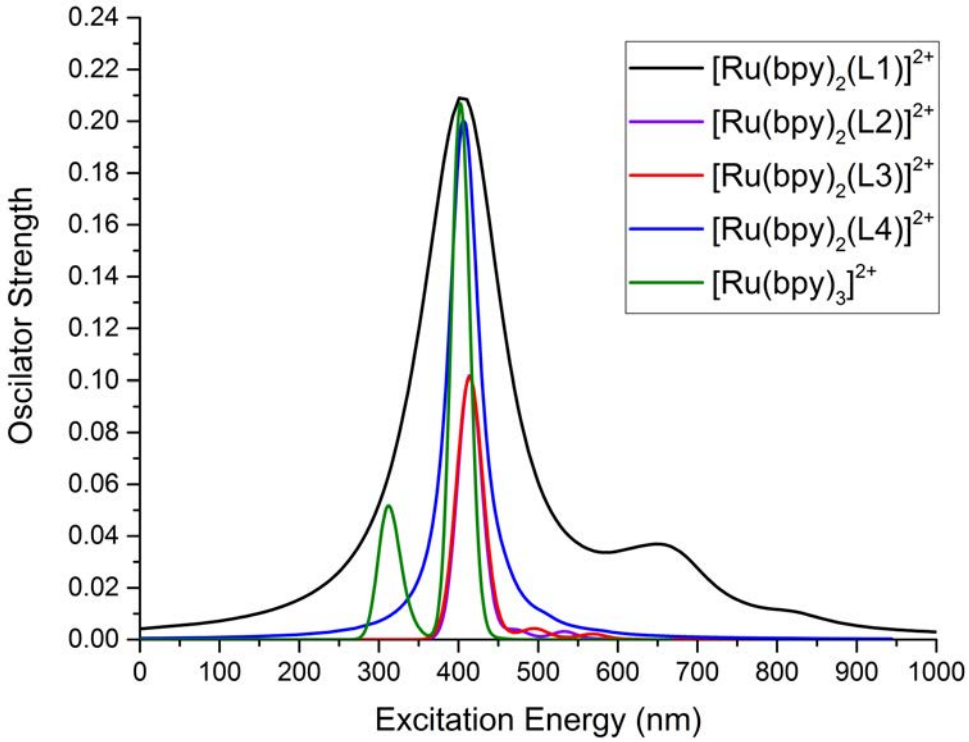

Figure 4.24: Electronic absorption spectra of ruthenium complexes with ligands **L1** - **L4**

Figure 4.25 presents spectra of the complexes having one ligand **L1** and two substituted 2,2-bipyridines as ligands. The same as in the case of experimental spectra, energy of CT band of $[Ru(Phbpy)_2(L1)]^{2+}$ complex is lower than energy of the other complexes with bpy-modified ligands. The band intensity of $[Ru(Phbpy)_2(L1)]^{2+}$

Table 4.7: Experimental and calculated energies and intensities of electronic transitions in Ru(II) complexes

Ruthenium complex	Experimental		Calculated		
	ΔE (eV)	ϵ ($M^{-1}cm^{-1}$)	ΔE (eV)	f[a]	Assignment[b]
$[Ru(bpy)_3]^{2+}$	2.743	14 000	3.082	0.207	H+3→L+1 (16%) H+3→L+2 (14%) H+3→L+3 (20%) H+2→L+1 (11%) H+2→L+2 (20%) H+2→L+3 (14%)
$[Ru(dip)_2(bpy)]^{2+}$	2.707	28 000	3.222	0.659	H+1→L+2 (80%)
$[Ru(bpy)_2(L1)]^{2+}$	2.725	18 100	3.093	0.348	H+11→L+2 (44%) H+11→L+3 (17%) H+10→L+1 (11%) H+10→L+3 (21%)
$[Ru(Mebpy)_2(L1)]^{2+}$	2.695	19 600	2.999	0.305	H+11→L+3 (16%) H+10→L+2 (21%) H+8→L+1 (15%) H+8→L+3 (19%)
$[Ru(tBubpy)_2(L1)]^{2+}$	2.707	14 600	3.006	0.341	H+11→L+3 (27%) H 10→L 2 (42%)
$[Ru(Phbpy)_2(L1)]^{2+}$	2.616	33 800	2.880	0.570	H+10→L+3 (57%) H+9→L+3 (22%)
$[Ru(dip)_2(L1)]^{2+}$	2.713	43 000	2.895	0.488	H+10→L+1 (79%)
$[Ru(bpy)_2(L2)]^{2+}$	2.719	14 600	2.999	0.102	H+7→L+1 (74%) H+6→L+2 (22%)
$[Ru(bpy)_2(L3)]^{2+}$	2.719	14 400	2.999	0.101	H+7→L+1 (74%) H+6→L+2 (22%)
$[Ru(bpy)_2(L4)]^{2+}$	2.719	14 300	3.058	0.201	H+10→L+2 (56%) H+9→L+1 (12%) H+9→L+3 (25%)

H = HOMO; L = LUMO

[a] Oscillator strength.

[b] Only the major parent one-electron excitations are reported.

complex is higher than for the others that is in agreement with the experimental molar absorbance coefficient of MLCT band - $1.8 \cdot 10^4$ $M^{-1}cm^{-1}$ for complex with simple bpy ligand and $3.4 \cdot 10^4$ $M^{-1}cm^{-1}$ for the complex bearing Phbpy ligand.

The last set of calculated spectra is presented at figure 4.26. The complexes with two 4,7-diphenyl-1,10-phenantroline ligands fit into previously presented trend. The calculated excitation energies for both complexes are higher then those obtained from experiment.

For all presented spectra assignment of the main calculated band was analyzed. Results are collected in table 4.7. Only the major one-electron excitations (with

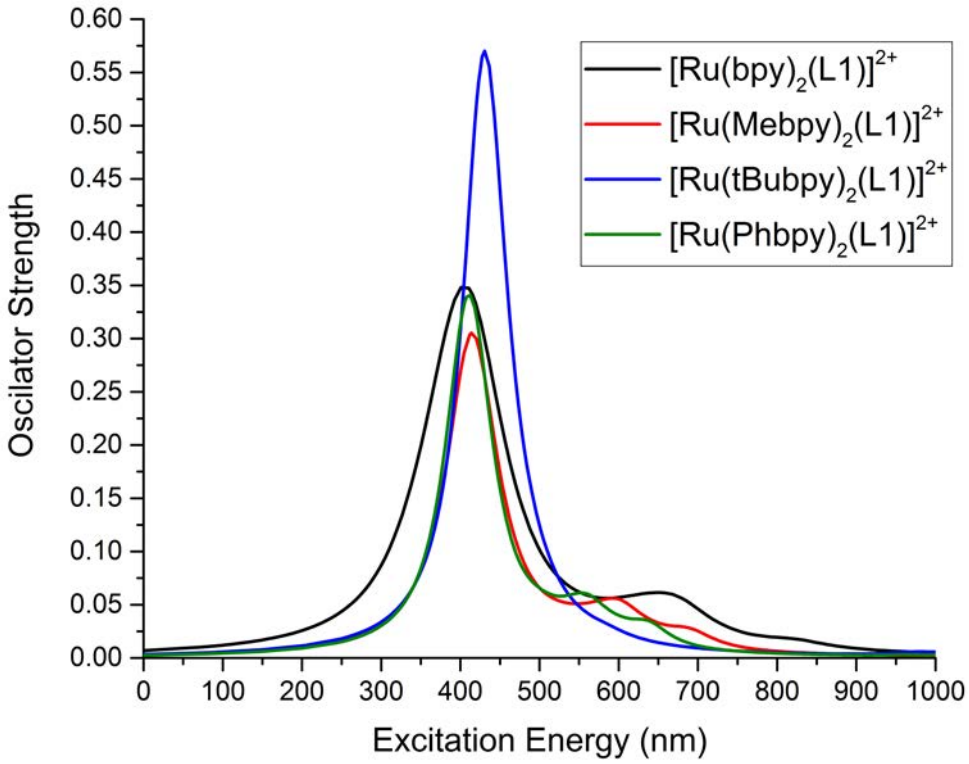

Figure 4.25: Electronic absorption spectra of ruthenium complexes with one ligand **L1** and two 2,2′-bipyridine derivatives.

percentage higher than 10%) are presented. In all complexes with ligand **L1** similar excitations from orbitals HOMO+10 and HOMO+11 onto orbitals LUMO+2 and LUMO+3 can be observed. For the complexes with ligand **L2** or **L3** the same excitations are observed - from HOMO+7 to LUMO+1 and from HOMO+6 to LUMO+2. For complex with ligand **L4** the excitations are more similar to those observed in complexes with ligand **L1** (HOMO+10 to LUMO+2, HOMO+9 to LUMO and HOMO+9 to LUMO+2) than to the complexes with ligands **L2** or **L3** which have similar structure. It is probably caused by the presence of urea group which adds additional orbitals to the molecule.

It should also be noted that transitions obtained for complex $[Ru(bpy)_3]^{2+}$ are in a good agreement with results previously reported in literature[155] which confirms the accuracy of the method.

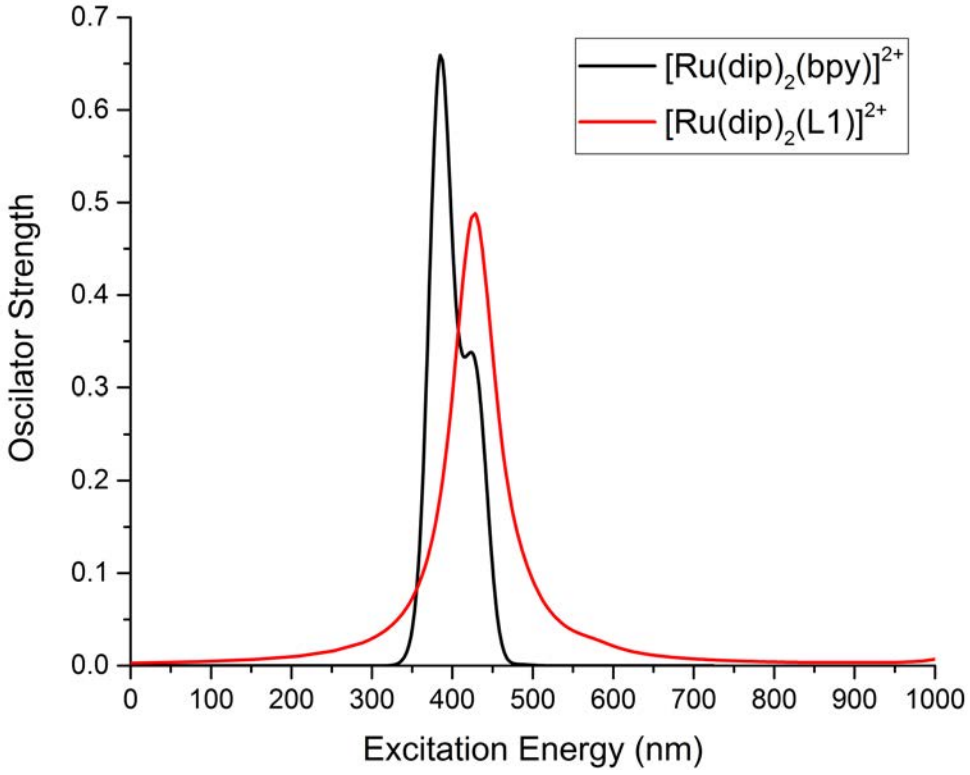

Figure 4.26: Electronic absorption spectra of ruthenium complexes with two 4,7-diphenyl-1,10-phenantroline ligands.

4.7. Ruthenium complexes intractions with Human Serum Albumin

4.7.1. Human Serum Albumin properties

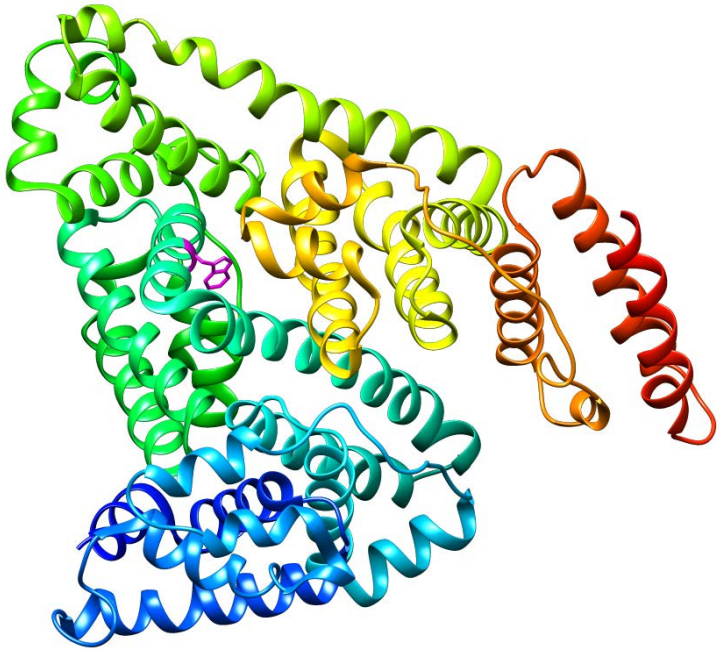

Figure 4.27: Crystal structure of Human Serum Albumin[157] with marked Tryphtophan 214 residue [PDB ID code 1e78]

Human Serum Albumin (HSA) (see fig.4.27) is the major extracellular protein of the circulatory system and its concentration is typically around 35 - 50 g/L. It is a globular serum protein with weight 65 kD and it is synthesized in the liver[158]. It serves as the major transporter of drugs as well as endogenous compounds such as fatty acids and thyroid hormones since these compounds can bind reversibly to this protein. It also plays a role in stabilizing extracellular fluid volume.

The most effective and simple method for investigating character of binding between human serum albumin and small molecules is using luminescence properties of the protein. HSA structure is composed of a single polypeptide chain which include one tryptophan residue (Trp 214). This residue is responsible for the majority of the intrinsic fluorescence of the protein[159]. Upon excitation at 295 nm, trypthophan residue in HSA exhibits strong fluorescence emission with maximum at 355 nm. This emission is sensitive to the changes in the local environment near the Trp 214 and to the changes of protein conformation. Therefore by monitoring the emission, the strength and character of binding between small molecule and protein can be determined.

4.7.2. Interactions with ruthenium complexes

In order to determine the type and the strength of interactions between the studied ruthenium complexes and human serum albumin, a series of experiments were performed. Fluorescence spectra of protein solution were recorded in the absence and the presence of various ruthenium complex concentrations (up to 5 μM). Since luminescence of tryptophan 214 is very sensitive even to small changes in local environment, measurements were carried in a constant pH 7.4 (TRIS-HCl buffer) and constant a temperature 37°C. The solution contained a high concentration (0.1 M) of sodium chloride to keep constant ionic strength. A single experiment for $[Ru(tBubpy)_2(L1)]^{2+}$ complex is presented in figure 4.28 as an example.

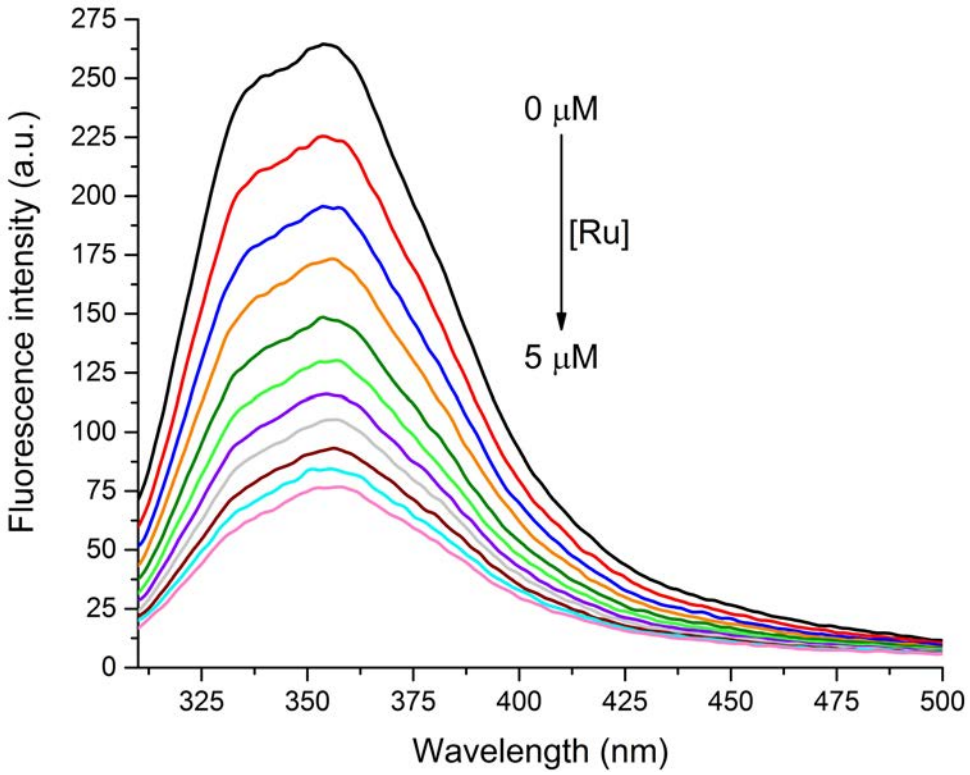

Figure 4.28: Luminescence spectra of human serum albumn solution in the presence of various concentrations of $[Ru(tBubpy)_2(L1)]^{2+}$ complex. [HSA] = 1 μM, [Ru] =0 - 5 μM, TRIS-HCl, pH = 7.4, T = 37°C, [NaCl] = 0.1 M.

Quenching constants and binding mechanism

In order to elucidate the fluorescence quenching mechanism the obtained data were firstly analyzed using the classical Stern-Volmer equation (4.1)[146]:

$$\frac{F_0}{F} = 1 + k_q\tau_0[Q] = 1 + K_{SV}[Q] \quad (4.1)$$

where F_0 and F are the fluorescence intensities in the absence and the presence of the ruthenium complex, respectively, k_q is the bimolecular quenching constant, τ_0 is the lifetime of the fluorophore in the absence of the metal complex, [Q] is concentration of the metal complex and K_{SV} is the Stern-Volmer dynamic quenching constant.

Plot F_0/F versus ruthenium complex concentration is called Stern-Volmer curve and within the studied concentration range exhibits good linear relationship (see fig.4.29 as an example). Stern-Volmer dynamic quenching constant was obtained from the slopes of the linear fit to the plot. The obtained values of K_{SV} are collected in table 4.8. For all studied ruthenium complexes, Stern-Volmer constant value is high - around 10^5 M^{-1} which may suggest that fluorescence quenching has a static character. Additionally, the obtained values are consistent with results reported for similar type of ruthenium complexes[124, 160, 161].

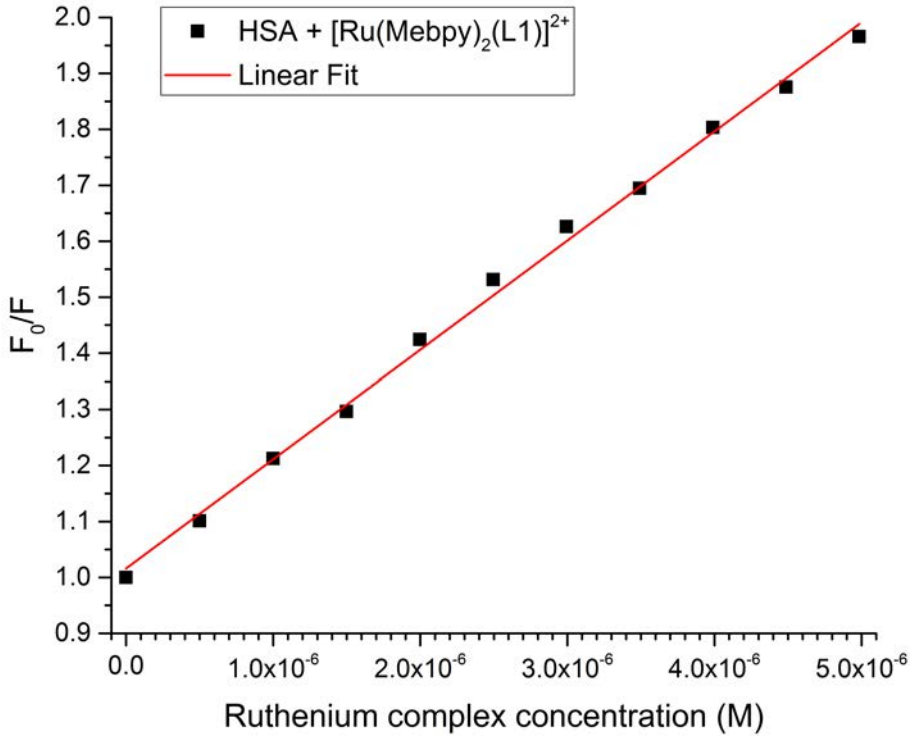

Figure 4.29: Stern-Volmer curve - F_0/F vs ruthenium complex concentration plot for complex $[Ru(tBubpy)_2(L1)]^{2+}$, [HSA]=1 μM, [Ru]= 0 - 5 μM.

The bimolecular quenching constants were calculated from K_{SV} using equation 4.1 and the assumption that τ_0 = 6 ns ([162], confirmed by experiment). The highest value of k_q resulting from collisional quenching of biopolimers is c.a. $2 \cdot 10^{10}$ $M^{-1}s^{-1}$[146]. The obtained values of k_q for the studied complexes were much higher (see table 4.8). This results strongly suggests predominance of static quenching of HSA fluorescence by the studied ruthenium complexes. It is likely that the quenching arises from formation of the ground state complex between ruthenium compound and HSA.

Table 4.8: Stern-Volmer constants of the studied ruthenium complexes with ligand **L1**

Ruthenium complex	K_{SV} x 10^5 (M^{-1})	k_q x 10^{13} ($M^{-1}s^{-1}$)
$[Ru(bpy)_3]^{2+}$	1.59 ± 0.07	2.65 ± 0.01
$[Ru(bpy)_2(L1)]^{2+}$	2.07 ± 0.12	3.45 ± 0.07
$[Ru(Mebpy)_2(L1)]^{2+}$	1.74 ± 0.25	2.90 ± 0.32
$[Ru(tBubpy)_2(L1)]^{2+}$	1.85 ± 0.14	3.08 ± 0.17
$[Ru(Phbpy)_2(L1)]^{2+}$	2.50 ± 0.32	4.16 ± 0.42
$[Ru(dip)_2(L1)]^{2+}$	3.16 ± 0.19	5.26 ± 0.08
$[Ru(SO_3dip)_2(L1)]^{2-}$	2.51 ± 0.38	4.18 ± 0.39

Binding constant and the number of binding sites

Fluorescence quenching data were analyzed to obtain various binding parameters for the interaction of the studied ruthenium complexes and human serum albumin. The apparent association constant (K_A) and the number of binding sites (n) were calculated using equation 4.2[163]:

$$log\left(\frac{F_0 - F}{F}\right) = n \cdot log(K_a) - n \cdot log\left(\frac{1}{[Q] - \frac{F_0 - F}{F} \cdot [HSA]}\right) \tag{4.2}$$

where F_0 and F are the fluorescence intensities in the absence and the presence of the ruthenium complex, respectively, [Q] is concentration of ruthenium complex and [HSA] is a total concentration of human serum albumin. The plot of log[(F_0-F)/F] versus log[1/([Q]-(F_0-F)[HSA]/F)] is linear (see fig. 4.30 for example). Number of binding sites n was obtained from a slope and an apparent association constant K_A was obtained from the intercept on the Y axis. The calculated K_A and n for the studied ruthenium complexes were collected in table 4.9. The values of n are close to 1, suggesting that only one binding site is present in HSA for most of the studied ruthenium complexes and other metal complexes[161, 164]. Ruthenium complexes most likely bind to the hydrophobic pocket of protein, located in Sudlow's site I in the subdomain II A. It is important to note that Trp 214 is located near that pocket or within it[164].

The high association constants (around 10^5 $M^{-1}s^{-1}$) suggests forming a strong Ru-HSA adducts. Additionally, the obtained values show that ligand **L1** increase the affinity of the complex to the protein two times (see table 4.9), which can arise from forming additional hydrogen bonds between HSA and ligand. The observed values of K_A are also in a good agreement with previously reported results for the metal complexes[165, 166], in particular ruthenium complexes with polypyridyl ligands[160, 161].

Table 4.9: An association constant K_a and the number of binding site n for the studied ruthenium complexes

Ruthenium complex	K_a x 10^5 ($M^{-1} \cdot s^{-1}$)	n
$[Ru(bpy)_3]^{2+}$	1.01 ± 0.10	0.91 ± 0.09
$[Ru(bpy)_2(L1)]^{2+}$	2.57 ± 0.11	0.94 ± 0.08
$[Ru(Mebpy)_2(L1)]^{2+}$	2.16 ± 0.28	0.84 ± 0.07
$[Ru(tBubpy)_2(L1)]^{2+}$	2.25 ± 0.24	0.91 ± 0.06
$[Ru(Phbpy)_2(L1)]^{2+}$	3.40 ± 0.40	0.83 ± 0.11
$[Ru(dip)_2(L1)]^{2+}$	5.24 ± 0.91	0.64 ± 0.01
$[Ru(SO_3dip)_2(L1)]^{2-}$	3.20 ± 0.69	0.70 ± 0.06

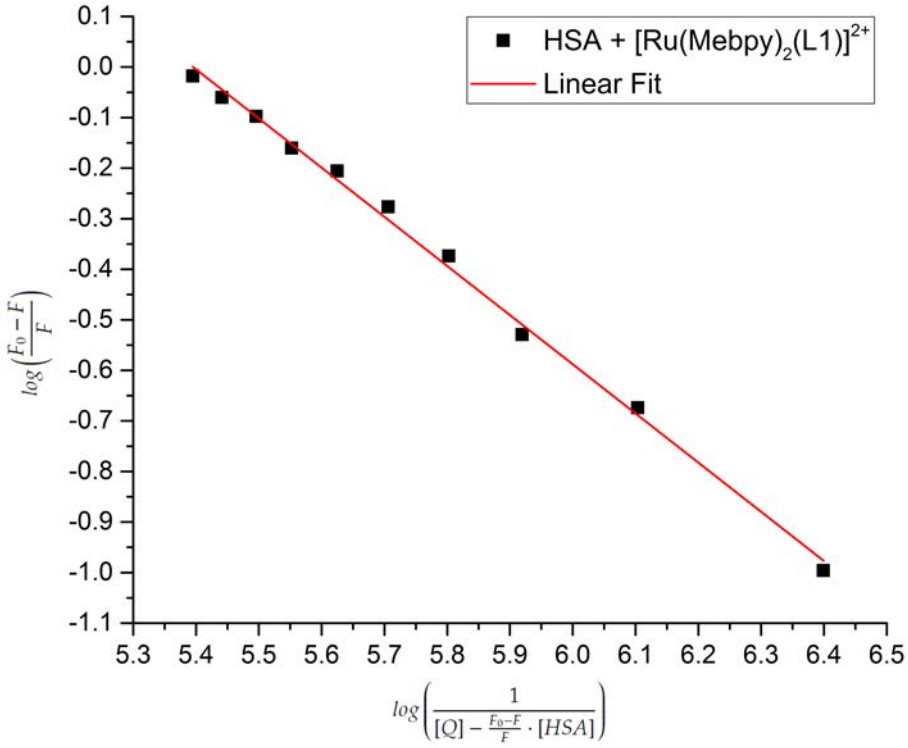

Figure 4.30: An example of log[(F_0-F)/F] vs log[1/([Q]-(F_0-F)[HSA]/F)] plot applied for determination of an association constant K_A and number of binding sites n for complex $[Ru(tBubpy)_2(L1)]^{2+}$ and HSA.

5. Summary

The main goal of this work was synthesis and characterization of novel ruthenium(II) complexes bearing biologically active moieties. As a biologically active moiety, four different molecules were chosen: pyridine-2-carboxyaldehyde semicarbazone as an example of α- heterocyclic semicarbazones and three derivatives of hydantoin: hydantoin, 5,5-dimethylhydantoin and allantoin. Those molecules have been used to obtain ruthenium(II) complexes. As the result, nine new ruthenium(II) polypyridyl complexes were synthesized.

Ligand **L1** - 5-(4-{4′-methyl-[2,2′-bipyridine]-4-yl}but-1-yn-1-yl)pyridine-2-carbaldehyde semicarbazone was synthesized with Sonogashira cross-coupling. Pyridine-2-carboxyaldehyde semicarbazone was bonded with 2,2′-bipyridine via four-carbon alkyn chain. Ligands **L2** (3-(5-{4′-methyl-[2,2′-bipyridine]-4-yl}pentyl)imidazolidine-2,4-dione), **L3** (5,5-dimethyl-3-(5-{4′-methyl-[2,2′-bipyridine]-4-yl}pentyl)imidazolidine-2,4-dione) and **L4** ([1-(5-{4′-methyl-[2,2′-bipyridine]-4-yl}pentyl)-2,5-dioxoimidazolidin-4-yl]urea) were all synthesized with the same method. The nitrogen in position 3 at the hydantoin derivative ring was selectively deprotonated with strong base under anhydrous conditions. The obtained intermediates were used without purification in reaction with 4-(5-bromopentyl)-4′-methyl-2,2′-bipyridine to get the desire products.

Cis-bis(polypyridine)dichlororuthenium(II) core complexes were synthesized with microwave irradiation method. Those complexes were used as initial molecules to obtain the final ruthenium complexes. Six various molecules: derivatives of 2,2′-bipyridine (2,2′-bipyridine, 4,4′-dimethyl-2,2-bipyridine, 4,4′-*tert*-butyl-2,2′-bipyridine, 4,4′-diphenyl-2,2-bipyridine) and 1,10-phenatroline (4,7-diphenyl-1,10-phenantroline and 4,7-di-(4-sulfonatophenyl)-1,10-phenantroline) were used as ligands for core complexes. Six various complexes bearing ligand **L1** were synthesized. The *Cis*-bis(2,2′-bipyridyne)dichlororuthenium(II) complex was used to obtain three complexes with ligands **L2**, **L3** and **L4**.

Spectroscopic and photophysical properties of those complexes were determined. Absorption spectra, luminescence quantum yield and luminescence lifetime for those complexes were measured in presence and absence of air. All studied ruthenium complexes were exhibited an emission band around 620 nm after excitation at

metal-to-ligand charge transfer band maximum. Luminescence quantum yield and luminescence lifetime for those complexes were significantly lower in comparison with the values for ruthenium homoleptic complex $[Ru(bpy)_3]^{2+}$. Those results are in a good agreement with previously published results for ruthenium(II) polypyridyl complexes with at least one ligand able to form hydrogen bonds with the solvent. The formation of hydrogen bonds between the ligand and the solvent is a plausible explanation of lower luminescence quantum yield and shorter luminescence lifetime of those complexes.

Interesting results were obtained for the negatively charged ruthenium complex with ligand **L1** - $[Ru(SO_3dip)_2(L1)]^{2-}$. The luminescence quantum yields of this complex were much higher than luminescence of the complex with similar structure ($[Ru(dip)_2(L1)]^{2+}$) but with positive charge. Under air-equilibrated conditions luminescence quantum yield was two-times higher and under anaerobic conditions was three-times higher. The luminescence lifetime of the complex $[Ru(SO_3dip)_2(L1)]^{2-}$ was almost two-times longer under anaerobic conditions then luminescence lifetime of the complex $[Ru(dip)_2(L1)]^{2+}$. Moreover, the luminescence properties of this negatively charged complex are much more sensitive for presence of oxygen. For all studied complexes, luminescence quantum yields under anaerobic conditions were two-times higher than under air-equilibrated conditions. For the negatively charged $[Ru(SO_3dip)_2(L1)]^{2-}$ complex, the luminescence quantum yield was enhanced almost four-times after removing oxygen from the system. These properties makes $[Ru(SO_3dip)_2(L1)]^{2-}$ complex a good candidate for hypoxia detection probe.

Computational calculations were performed for all studied ruthenium complexes. It was determined that the biologically active moieties have no significant impact on the geometry of the metallic center of ruthenium complex. The analysis of NBO energies have shown significant differences among complexes. In all cases, LUMO was placed mostly on ruthenium ion and atoms close to it, but HOMO was placed on biologically active molecule. This was resulting in increasing of HOMO energies and shortening band gaps. Comparing $[Ru(bpy)_3]^{2+}$ complex and $[Ru(bpy)_2(L1)]^{2+}$ complex, band gap is 3.4 times shorter for the second one. Moreover, the energies of HOMO for the complexes with hydantoins derivatives were not depended on the structure of hydantoin group and results for all three ruthenium complexes with those moieties were similar.

Time-depended computational calculations - TD-DFT were performed to simulate absorption spectra of the studied ruthenium complexes. All obtained excitation energies were in an agreement with experimental data. Calculated excitation energies were higher by ca. 0.3 eV which was expected based on previously reported results

for similar ruthenium complexes. All the major parent one-electron excitations were presented and described.

The interaction between ruthenium complexes bearing pyridine-2-carboxyaldehyde semicarbazon moiety and human serum albumin were studied. The studied complexes strongly interacted with HSA. Obtained Stern-Volmer quenching constants were around 10^5 M^{-1} and bimolecular quenching constants were around 10^{13} $M^{-1}s^{-1}$ which shown that those complexes form an adduct with human serum albumin. Further analysis of this interactions have shown that ruthenium complexes bind only to one binding site of HSA, most likely located in Sudlow's site I in the subdomain II A of the protein. The ligand **L1** had significant influence on the affinity of the studied complexes to the protein which was probably caused by forming additional hydrogen bonds between pyridine-2-carboxyaldehyde semicarbazone and HSA.

5.1. Preliminary cytotoxic studies - Future perspectives

In the future, the evaluation of the biological activity of all obtained ruthenium complexes are planned. The preliminary cytotoxicity studies for $[Ru(bpy)_2(L1)]^{2+}$ complex and $[Ru(dip)_2(L1)]^{2+}$ complex were performed in collaboration with dr. Olga Mazuryk from Jagiellonian University. The cytotoxicity of those two ruthenium complexes was determined *in vitro* on two cell lines: murine colon carcinoma (CT26) and adenocarcinomic human alveolar basal epithelial cells (A549). Both complexes had moderate cytotoxicity after 24 h incubation. The increased incubation time - up to 72 h was resulted in increased cytotoxic effect, in particular for $[Ru(bpy)_2(L1)]^{2+}$ complex towards CT26 line. The results may suggest the antiproliferate activity of the complexes bearing ligand **L1** however, further evaluation of this effect is necessary.

Moreover, the preliminary studies of cell accumulation and cellular targets revealed that the $[Ru(dip)_2(L1)]^{2+}$ complex was mostly localized in mitochondria and endoplasmatic reticulum. $[Ru(bpy)_2(L1)]^{2+}$ complex however, was mostly localized in lysosomes. The mechanism of the uptake will be further examined. It is also planned to study the mechanism of cell's death with help of flow cytometry, to explore the influence of all studied ruthenium complexes on cell's cycle and on caspase activity. The preliminary studies have shown increased numbers of cells in S-phase after treatment with $[Ru(bpy)_2(L1)]^{2+}$ complex. During mitotic cycle in S-phase, ribonucleotide reductase reduces the ribonuceotides to corresponding deoxyribonucleotides which leads to cell proliferation. To confirm that ruthenium complexes with ligand **L1** are acting as RNR inhibitors, the preliminary studies of their activity were performed in collaboration with pr. Fredric Tholander from Karolinska Institutet. All studied

ruthenium complexes with ligand **L1** exhibited an inhibition of the enzyme. Their activity was slightly higher than activity of hydroxyurea (HU) - well-known inhibitor of RNR used as standard. Those results may suggest that biologically active moiety - pyridine-2-carboxyaldehyde semicarbazon is acting as an inhibitor of ribonucleotide reductase as was planned.

The modifications of the studied complexes are also planned based on the results of the biological studies.

6. Synthetic procedures

6.1. Synthesis of Ligand L1

6.1.1. Synthesis of 4-(3-(trimethylsilyl)prop-2-yn-1-yl)-4′-methyl-2,2′-bipyridine (1)

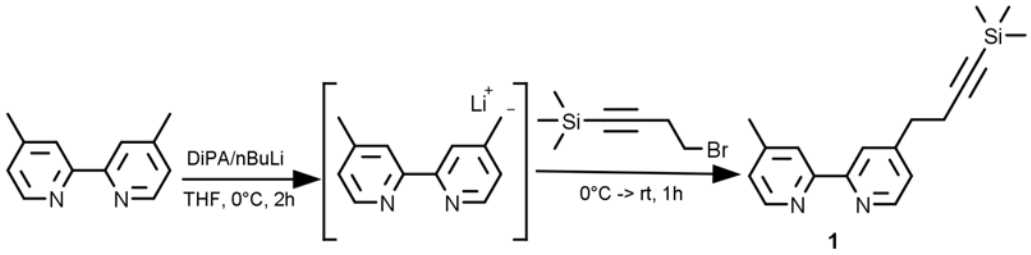

To a solution of freshly distilled diisopropylamine (0.19 mL, 1.3 mmol) in dry THF (5 mL) under argon at -78°C, a solution of n-butyllithium in hexane (0.92 mL, 1.2 mmol) was added dropwise. The solution was stirred for 30 minutes and then warmed up to 0°C. A solution of 4,4′-dimethyl-2,2′-bipyridine (0.184 g, 1 mmol) in dry THF (10 mL) was then added. After two hours 3-(trimethylsilyl)propagyl bromide (0.25 mL, 1.5 mmol) was added rapidly. After another hour, the mixture was warmed to room temperature and quenched with water (30 mL). The mixture was extracted with diethyl ether (3x20 mL). Combined organic layers were washed twice with brine and dried over magnesium sulfate. Solvent was removed under reduced pressure to give the pure product in 92% (0.276 g) yield.

^{1}H NMR (400 MHz, $CDCl_3$): (ppm): 0.11 (s, 9H); 2.44 (s, 3H); 2.58 (t, J=7.2 Hz, 2H); 2.91 (t, J=7.2 Hz, 2H); 7.12-7.14 (m, 1H), 7.18 (dd, J=4.8 Hz, 1.6 Hz, 1H); 8.22 (s, 1H); 8.28 (s, 1H); 8.52 (d, J=5.2 Hz, 1H); 8.58 (d, J=4.8 Hz, 1H).

^{13}C NMR (100 MHz, $CDCl_3$): 0.0; 21.0; 21.2; 34.4; 86.2; 105.5; 121.4; 122.0; 124.0; 124.7; 148.1; 148.9; 149.0; 150.3; 155.9; 156.3

6.1.2. Synthesis of 4-(prop-2-yn-1-yl)-4′-methyl-2,2′-bipyridine (2)

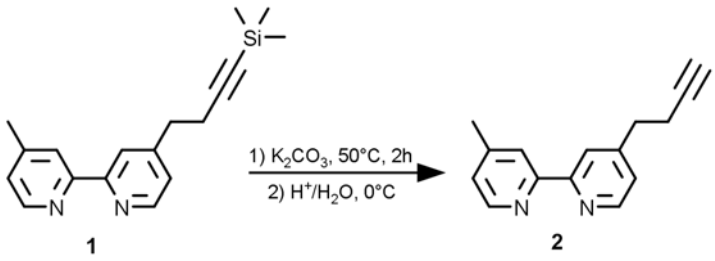

To a solution of (1) (0.276 g, 0.9 mmol) in methanol (5 mL) potassium carbonate (0.205 g, 1.5 mmol) was added. Mixture was heated under argon at 50°C for two hours. After this time, reaction was cooled down to 0°C, neutralized with 2M HCl and extracted with diethyl ether (3x30 mL). Combined organic layers were washed twice with brine and dried over magnesium sulfate. Solvent was removed under reduced pressure to give pure product as brown solid with yield 72% (0.150 g).

^{1}H NMR (200 MHz, $CDCl_3$): (ppm) 1.99 (t, J=2.6 Hz, 1H); 2.44 (s, 3H); 2.54 (td, J=7.4 Hz, 2.6 Hz, 2H); 2.94 (t, J=7.4 Hz, 2H); 7.13 (d, J=4.8 Hz, 1H); 7.20 (dd, J=5.0 Hz, 1.8 Hz, 1H); 8.23 (d, J =0.8 Hz, 1H); 8.26 (d, J=0.8 Hz, 1H); 8.52 (d, J=5 Hz, 1H); 8.58 (d, J=5 Hz, 1H).

^{13}C NMR (100 MHz, $CDCl_3$): 20.4; 21.1; 34.5; 68.9; 83.8; 120.7; 121.6; 124.0; 125.0; 148.0; 148.3; 148.9; 151.0; 155.9; 156.3

[HRMS – ESI] Calculated for $C_{15}H_{14}N_2$ m/z = 223.1230 ($M+H^+$); Found: m/z = 223.1239 ($M+H^+$).

6.1.3. Synthesis of 5-bromopyridine-2-carboxyaldehyde (3)[138]

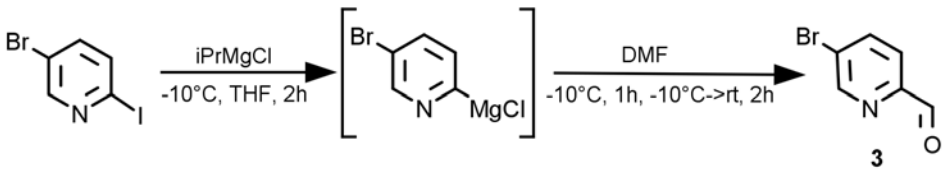

5-bromopyridine-2-carboxyaldehyde was synthesized with procedure described by Song et al[138]. To a solution of 5-bromo-2-iodopyridine (0.586 g, 2 mmol) in dry THF (10 mL) under argon at -10°C, solution of isopropylmagnesium chloride (1.5 mL, 2.17 mmol) was added dropwise. After two hours, dry DMF (0.4 mL, 5.16 mmol) was added rapidly. Mixture was kept at -10°C for another hour and then warmed

up to room temperature over two hours. Reaction was quenched with saturated solution of ammonium chloride (20 mL) and extracted with diethyl ether (3x25 mL). Combined organic layers were washed twice with brine and dried over magnesium sulfate. Solvent was removed under reduced pressure to give pure product as light yellow solid with yield 80% (0.306 g).

^{1}H NMR (200 MHz, $CDCl_3$): (ppm) 7.84 (dd, J = 8.2 Hz, 0.8 Hz, 1H); 8.02 (ddd, J = 8.2 Hz, 2.2 Hz, 0.8 Hz, 1H); 8.85 (d, J=2 Hz, 1H); 10.04 (d, J=0.8 Hz, 1H).

6.1.4. Synthesis of 5-bromopyridine-2-carboxyaldehyde semicarbazone (4)

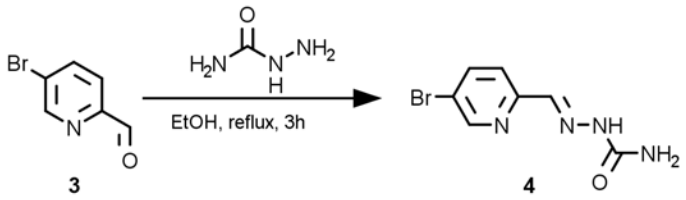

To a suspension of semicarbazide hydrochloride (0.149 g, 1.3 mmol) in anhydrous ethanol (3 mL), a solution of (3) (0.230 g, 1.2 mmol) in ethanol (9 mL) was added. Mixture was refluxed over three hours and cooled down to 0°C. Solid was filtrated, washed two times with cold, anhydrous ethanol, once with diethyl ether and dried in vacuum to give pure product as light cream powder with yield 99% (0.300 g).

^{1}H NMR (400MHz, dmso-d6) 7.02 (brs, 2H); 7.86 (s, 1H); 8.10 (dd, J=8 Hz, 1.6 Hz, 1H); 8.15 (d, J=8 Hz, 1H); 8.67 (d, J=1.6 Hz, 1H); 10.63 (s, 1H).

^{13}CNMR (100MHz, dmso-d6): (ppm) 119.7; 121.6; 137.8; 139.7; 149.3; 152.3; 156.3.

[HRMS-ESI] Calculated for $C_7H_7N_4OBr$ m/z = 264.9701 ($M+Na^+$), found m/z = 264.9692 ($M+Na^+$).

6.1.5. Synthesis of 5-(4-{4′-methyl-[2,2′-bipyridine]-4-yl}but-1-yn-1-yl)pyridine-2-carbaldehyde semicarbazone (L1)

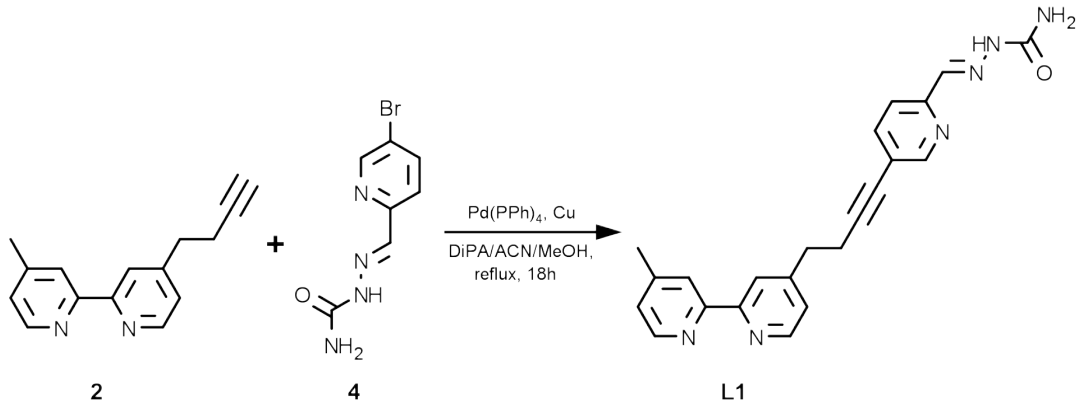

To a solution of (2) (0.170 g, 0.75 mmol) in acetonitryle (6 mL) copper(I) iodide (0.05 g, 30%mol) and tetrakis(triphenylphosphine)palladium(0) (0.045 g, 5%mol) was added under argon. Diisopropylamine (6 mL) was added and the mixture was stirred for 15 minutes. After that time, suspension of 4 (0.210 g, 0.9 mmol) in methanol (1 mL) was added and the solution was refluxed for 18 hours. Concentrated ammonia (1 mL) was added to a brown suspension and the mixture was filtrated through Celit (followed by 70 mL of acetonitryle). Solvent was removed under reduced pressure and residue was dissolved in dichloromethane/concentrated ammonia mixture. Organic phase was separated, washed two times with concentrated ammonia (till all copper was removed), once with brine and dried over magnesium sulfite. Solvent was removed under reduced pressure to give crude product which was dissolved in chloroform (15 mL) and treated with cyclohexane (60 mL). Mixture was kept at 4°C and crystals was filtrated, washed with cyclohexane and dried in vacuum to give pure product as white solid with yield 45% (0.132 g).

^{1}H NMR (200 MHz, $CDCl_3$): (ppm) 2.45 (s, 3H); 2.84 (t, J=7 Hz, 2H); 3.03 (t, J=7 Hz, 2H); 7.14 (dd, J=16.2 Hz, 4.8 Hz, 2H); 7.64-7.77 (m, 3H); 8.25 (s, 1H); 8.38 (s, 2H); 8.53-8.63 (m, 3H).

^{13}C NMR (150 MHz, $CDCl_3$): (ppm) 20.7; 21.2; 34.2; 78.7; 93.8; 119.4; 120.9; 121.4; 122.1; 123.9; 124.9; 138.9; 141.5; 148.3; 149.0; 149.2; 150.1; 151.2; 152.1; 155.8; 156.4; 156.8.

[HRMS-ESI]: calculated for $C_{22}H_{20}N_6O$ m/z = 385.1771 ($M+H^+$), found m/z = 385.1771 ($M+H^+$).

6.2. Synthesis of Ligand L2, L3 and L4

6.2.1. Synthesis of 4-(5-bromopentyl)-4′-methyl-2,2′-bipyridine (6)

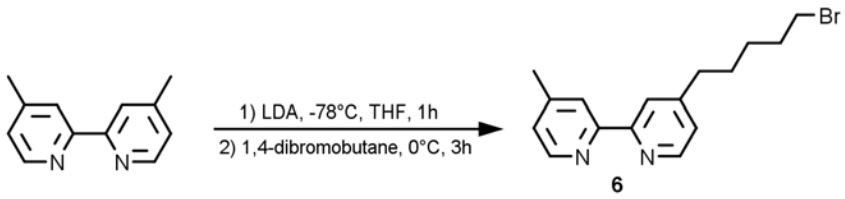

6

To a solution of diisopropylamine (0.55 mL, 3.9 mmol) in dry THF (6 mL), under argon at -78°C, solution of n-butyllithium (2.4 mL, 3.6 mmol) in n-hexane (concentration = 1.5M) was added dropwise. After 30 minutes a solution of 4,4′-dimethyl-2,2′-bipyridine (0.5532 g, 3 mmol) in dry THF (25 mL) was quickly added. Chocolate-brown solution was stirred at -78°C for 1 h and warmed to 0°C. A solution of 1,4-dibromobutan (1.8 mL, 15 mmol) in dry THF (3 mL) was added rapidly. After 3 h the solution became light yellow and reaction was quenched with water (15 mL). The mixture was neutralized with 2M HCl and extracted with dichloromethane. Combined organic layers were dried over anhydrous $MgSO_4$ and solvent was removed under reduced pressure. Crude material was purified by flash chromatography (SiO_2, dichloromethane, diethyl ether) to give pure product with yield 66% (0.6281 g).

^{1}H NMR ($CDCl_3$, 200 MHz): δ (ppm) 1.44 - 1.58 (m, 2H); 1.66 - 1.76 (m, 2H); 1.81 - 1.97 (m, 2H); 2.44 (s, 1H); 2.71 (t, J=8 Hz, 2H); 3.40 (t, J=6.8 Hz, 2H); 7.12 (d, J=4.8 Hz, 2H); 8.23 (s, 2H); 8.55 (t, J=4.8 Hz, 2H).

^{13}C NMR (150 MHz, $CDCl_3$): (ppm) 21.2; 27.8; 29.5; 32.5; 33.6; 35.3; 121.3; 122.2; 124.0; 124.8; 148.5; 148.7; 148.9; 152.5; 155.6; 155.8.

[HRMS-ESI]: Calculated for $C_{16}H_{20}N_2Br$ m/z = 319.0804 ($M+H^+$), found m/z = 319.0811 ($M+H^+$).

6.2.2. Synthesis of 3-(5-{4′-methyl-[2,2′-bipyridine]-4-yl}pentyl)--imidazolidine-2,4-dione (L2)

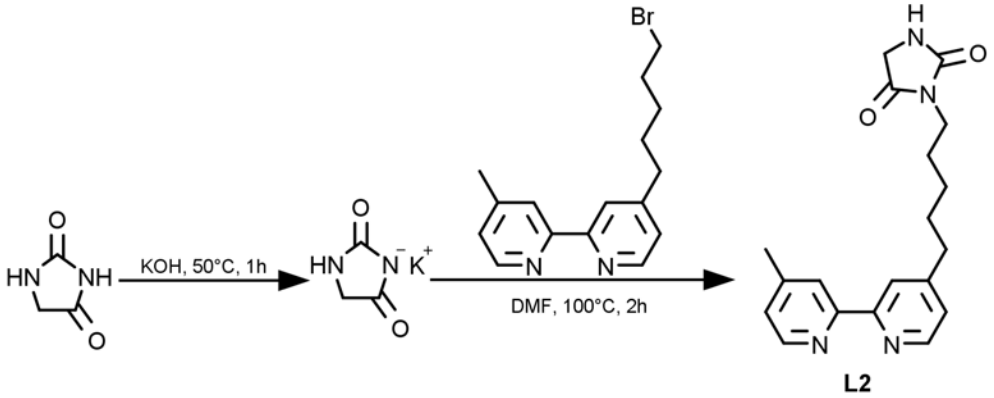

To a solution of potassium hydroxide (0.135 g, 2.4 mmol) In dry metanol (15 mL), imidazolidine-2,4-dione (hydantoin) (0.200 g, 2 mmol) was added. Suspension was heated at 50°C for 1 h under argon conditions. Clear solution was cooled down and solvent was removed under reduced pressure. White powder was dried at 65°C for 48 h and stored in desiccator over P_2O_5.

Potassium 2,4-dioxoimidazolidin-3-ide (6) (0.090 g, 0.65 mmol) was suspended in dry DMF (10 mL) and heated at 100°C for 15 minutes. Next, a solution of 4-(5-bromopentyl)-4′-methyl-2,2′-bipyridine (7) (0.125 g, 0.40 mmol) in dry DMF (5 mL) was added and brown solution was heated at 100°C for another 2h. After that solvent was removed under reduced pressure and oily mixture was partially dissolved in dichloromethane (20 mL), washed twice with water (2x20 mL), once with brine (15 mL) and dried over $CaCl_2$. Dichloromethane was removed under reduced pressure and brown residue was dissolved in small amount of ethanol. Diethyl ether was added and product was filtrated as brown powder with yield 61% (0.1 g).

^{1}H NMR (600 MHz, $CDCl_3$) 1.29-1.35 (m, 2H); 1.58-1.69 (m, 4H); 2.37 (s, 3H); 2.63 (t, J=12 Hz, 2H); 3.45 (t, J=6 Hz, 2H); 3.87 (s, 2H); 7.06 (t, J=6 Hz, 2H); 8.13 (d, J=12 Hz, 2H); 8.46 (dd, J=6 Hz, 12 Hz, 2H).

^{13}CNMR (150 MHz, $CDCl_3$): (ppm) 21.2; 26.3; 27.7; 29.8; 38.6; 46.3; 50.1; 121.3; 122.1; 123.9; 124.7; 148.9; 149.0; 170.1.

[HRMS-ESI]: Calculated for $C_{19}H_{23}N_4O_2$ m/z = 339.1816 ($M+H^+$), found m/z = 339.1821 ($M+H^+$).

6.2.3. Synthesis of 5,5-dimethyl-3-(5-{4′-methyl-[2,2′-bipyridine]-4-yl}pentyl)--imidazolidine-2,4-dione (L3)

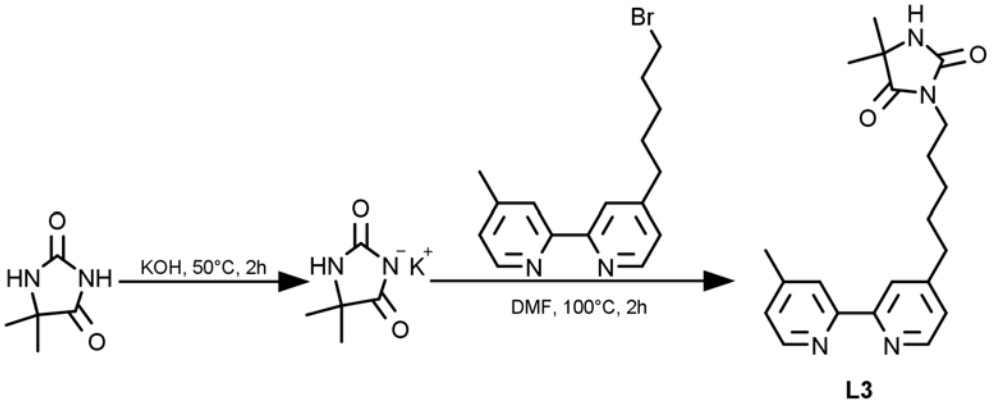

To a solution of potassium hydroxide (0.270 g, 4.8 mmol) in dry metanol (25 mL), 5,5-dimethylimidazolidine-2,4-dione (5,5-dimenthylhydantoin) (0.512 g, 4 mmol) was added. Suspension was heated at 50°C for 2 h under argon conditions. Clear solution was cooled down and solvent was removed under reduced pressure. White powder was dried at 65°C for 48 h to give product as white solid with yield 82% (0.545 g). Potassium 5,5-dimethyl-2,4-dioxoimidazolidin-3-ide (9) (0.045 g, 0.27 mmol) was suspended in dry DMF (10 mL) and heated at 100°C for 15 minutes. Next, a solution of 4-(5-bromopentyl)-4′-methyl-2,2′-bipyridine (6) (0.090 g, 0.28 mmol) in dry DMF (5 mL) was added and the brown solution was heated at 100°C for another 2 h. After that solvent was removed under reduced pressure and oily mixture was partially dissolved in dichloromethane (20 mL), washed twice with water (2x20 mL), once with brine (15 mL) and dried over $CaCl_2$. Dichloromethane was removed under reduced pressure and brown residue was dissolved in small amount of ethanol. Diethyl ether was added and product was filtrated as brown powder with yield 73% (0.072 g).

^{1}H NMR (600 MHz, $CDCl_3$) 1.18 (s, 6H); 1.28-1.36 (m, 2H); 1.57-1.68 (m, 4H); 2.36 (s, 3H); 2.63 (t, J=12 Hz, 2H); 3.45 (t, J=6 Hz, 2H); 7.06 (t, J=6 Hz, 2H); 8.13 (d, J=12 Hz, 2H); 8.47 (dd, J=12 Hz, 6 Hz, 2H).

^{13}CNMR (150 MHz, $CDCl_3$): (ppm) 20.9; 24.2; 26.4; 28.0; 29.9; 38.6; 44.9; 61.6; 121.3; 122.2; 123.5; 125.0; 148.7; 149.2; 169.7.

[HRMS-ESI]: Calculated for $C_{21}H_{27}N_4O_2$ m/z = 367.2129 ($M+H^+$), found m/z = 367.2132 ($M+H^+$).

6.2.4. Synthesis of [1-(5-{4′-methyl-[2,2′-bipyridine]-4-yl}pentyl)--2,5-dioxoimidazolidin-4-yl]urea (L4)

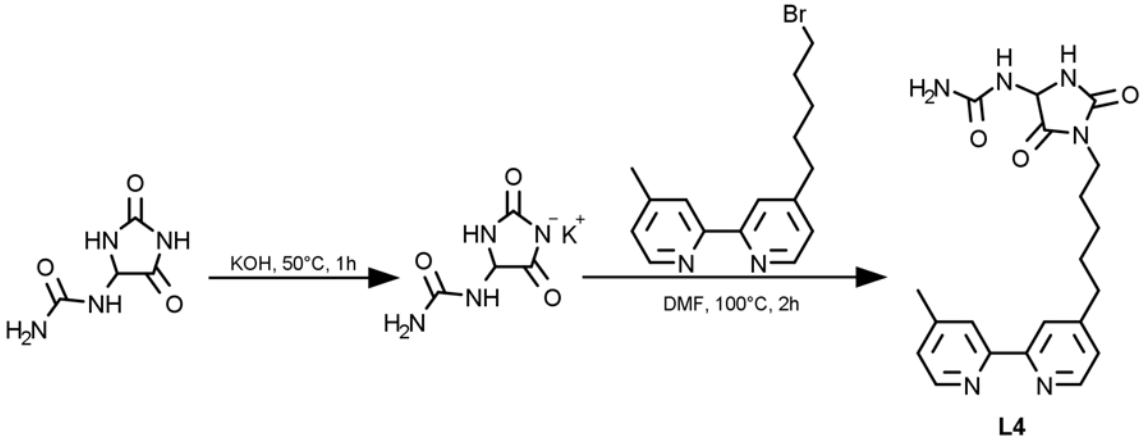

To a solution of potassium hydroxide (0.270 g, 4.8 mmol) in water (10 mL), (2,4-dioxoimidazolidin-5-yl)urea (allantoin) (0.633 g, 4 mmol) was added. Solution was heated at 50°C for 1 h under argon. Clear solution was cooled down and solvent was removed under reduced pressure. White powder was dried at 65°C for 48 h to give a product as white solid with yield 90% (0.700 g).
Potassium 5-(carbamoylamino)-2,4-dioxoimidazolidin-3-ide (0.062 g, 0.32 mmol) was suspended in dry DMF (10 mL) and heated to 100°C for 30 minutes. Next, solution of 4-(5-bromopentyl)-4′-methyl-2,2′-bipyridine (6) (0.090 g, 0.28 mmol) in dry DMF (8 mL) was added and brown solution was heated at 100°C for another 2.5 h. After that solvent was removed under reduced pressure and oily mixture was partially dissolved in dichloromethane (20 mL) and filtrated. Dichloromethane was removed under reduced pressure and brown residue was dissolved in small amount of ethanol. Diethyl ether was added and product was filtrated as brown powder with yield 27% (0.030 g).

^{1}H NMR (600 MHz, $CDCl_3$) 1.22-1.36 (m, 4H); 1.58-1.69 (m, 2H); 2.31 (s, 3H); 2.61 (t, J=12 Hz, 2H); 3.46 (t, J=6 Hz, 2H); 5.37 (s, 1H); 7.06 (d, J=6 Hz, 2H); 8.13 (s, 2H); 8.47 (t, J=6 Hz, 2H).

^{13}CNMR (150 MHz, $CDCl_3$): (ppm) 21.0; 27.7; 29.8; 38.4; 48.2; 62.0; 121.1; 121.9; 124.0; 125.1; 148.4; 149.3; 156.2; 157.4; 168.8.

[HRMS-ESI]: Calculated for $C_{20}H_{25}N_6O_3$ m/z = 419.1808 ($M+Na^+$), found m/z = 419.1814 ($M+Na^+$).

6.3. Ruthenium complexes synthesis

6.3.1. General procedure for synthesis of *cis*-Ru(NN)$_2$Cl$_2$[145, 167]

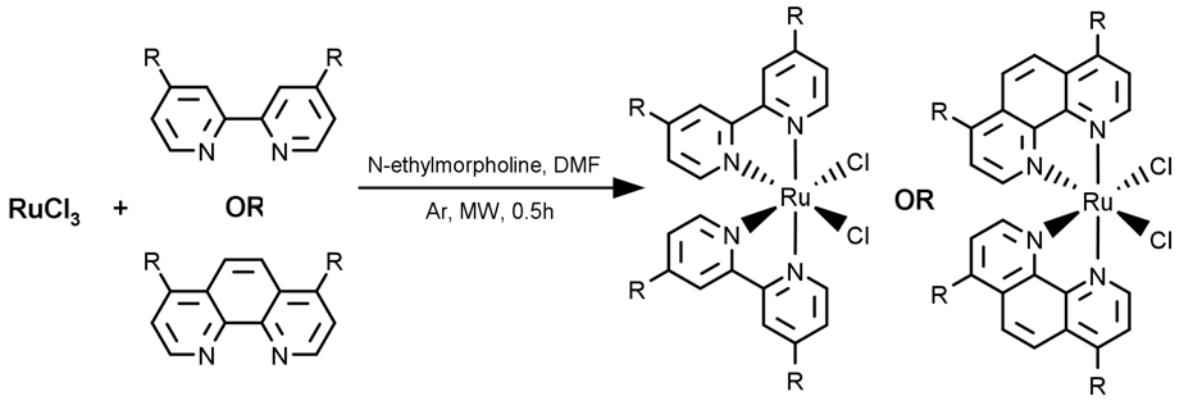

Ruthenium(III) chloride trihydrate (0.262 g, 1 mmol), NN ligand (2,2′-bipyridine or 1,10-phenantroline drivative) (0.308 g, 2 mmol) and 2 drops of N-ethylmorpholine were dissolved in degassed N,N-dimethylformamide (10 mL) under argon. The mixture was heated into microwave reactor for 30 minutes (power 250 W, temperature 160°C). Solvent was removed under reduced pressure to c.a. 1 mL and acetone (20 mL) was added. After 24 h at -20°C dark solid was filtrated, and washed with cold acetone, twice with diethyl ether and dried by suction. Crude product was purified by flash chromatography (Al_2O_3 neutral, dichloromethane/methanol (5%)) to give pure product.

Synthesis of *cis*-Ru(bpy)$_2$Cl$_2$ (10)[168]

Ligand: 2,2′-bipyridine. Yield 38% (0.181 g).

^{1}H NMR (600 MHz, d6-dmso): (ppm) 7.08 (t, J=6 Hz, 2H); 7.49 (d, J=6.6 Hz, 2H); 7.67 (t, J=7.2 Hz, 2H); 7.75 (t, J=7.2 Hz, 2H); 8.04 (td, J=7.8 Hz, 1.2 Hz, 2H); 8.46 (d, J=7.8 Hz, 2H); 8.61 (d, J=8.4 Hz, 2H); 9.95 (d, J=7.2 Hz, 2H).

[HRMS-ESI]: Calculated for $C_{20}H_{16}Cl_2N_4Ru$ m/z = 483.9784, found m/z = 483.9791.

Synthesis of *cis*-Ru(Mebpy)$_2$Cl$_2$ (11)[169]

Ligand: 4,4′-dimethyl-2,2′-bipyridine. Yield 42% (0.280 g).

[HRMS-ESI]: Calculated for $C_{24}H_{24}ClN_4Ru$ m/z = 505.0722, found m/z = 505.0736.

Synthesis of *cis*-Ru(tBbpy)$_2$Cl$_2$ (12)[170]

Ligand: 4,4′-di-*tert*-butyl-2,2′-bipyridine. Yield 39% (0.274 g).

[HRMS-ESI]: Calculated for $C_{36}H_{48}ClN_4Ru$ m/z = 673.2600, found m/z = 673.2594.

Synthesis of *cis*-Ru(Phbpy)$_2$Cl$_2$ (13)[171]

Ligand: 4,4′-diphenyl-2,2′-bipyridine. Yield 47% (0.370 g).

[HRMS-ESI]: Calculated for $C_{44}H_{32}Cl_2N_4Ru$ m/z = 788.1036, found m/z = 788.1022.

Synthesis of *cis*-Ru(dip)$_2$Cl$_2$ (14)[172]

Ligand: 4,7-diphenyl-1,10-phenantroline. Yield: 55% (0.460 g)

[HRMS-ESI]: Calculated for $C_{48}H_{32}Cl_2N_4Ru$ m/z = 859.0929 ($M+Na^+$), found m/z = 859.0949 ($M+Na^+$).

Synthesis of *cis*-Na$_4$Ru(SO$_3$dip)$_2$Cl$_2$(15)[173]

Yield 58% (0.033 g).

[HRMS-ESI]: Calculated for $C_{48}H_{28}Cl_2N_4O_{12}Na_2S_4Ru$ m/z = 598.9401 (M^{2-}), found m/z = 598.9364 (M^{2-}).

6.3.2. Synthesis of $[Ru(bpy)_2(L1)]Cl_2$ (16)

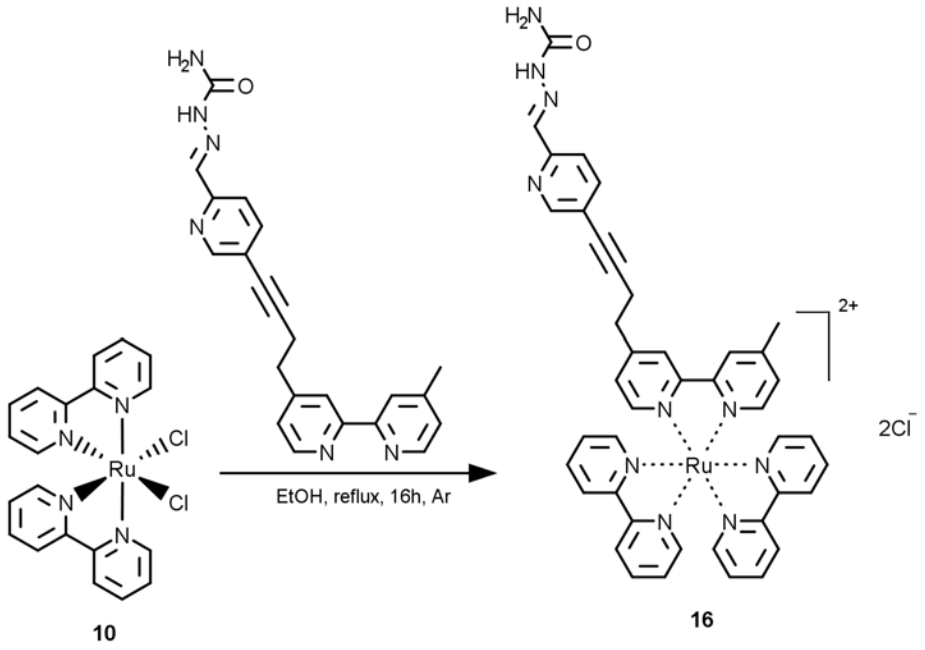

10 16

Ligand 1 (5) (0.023 g, 0.060 mmol) was dissolved in absolute ethanol (5 mL) under argon. A solution of cis-$Ru(bpy)_2Cl_2$(10) (0.023 g, 0.048 mmol) in absolute ethanol (5 mL) was added. Dark violet mixture was refluxed under argon for 16 hours. After that, solvent was removed under reduced pressure, residue was dissolved in water (1 mL) and filtrated. The pure product was obtained after crystallization as dark red crystals with yield 80% (0.033 g)

^{1}H NMR (600 MHz, CD_3CN): (ppm) 2.51 (s, 3H); 2.91 (t, J=6 Hz, 2H); 2.95 (t, J=6 Hz, 2H); 7.19 (s, 1H); 7.33-7.40 (m, 6H); 7.46 (d, J=7.8 Hz, 1H); 7.51 (d, J=6 Hz, 1H); 7.61 (d, J=6 Hz, 1H); 7.71-7.74 (m, 6H); 7.80 (t, J=7.8 Hz, 1H); 8.03-8.07 (m, 4H); 8.13 (s, 1H); 8.25 (d, J=6 Hz, 1H); 8.54-8.66 (m, 8H).

[HRMS]: Calculated for $C_{42}H_{36}N_{10}ORu$ 399.1052 m/z; Found 399.1058 m/z.

6.3.3. Synthesis of $[Ru(Mebpy)_2(L1)]Cl_2$ (17)

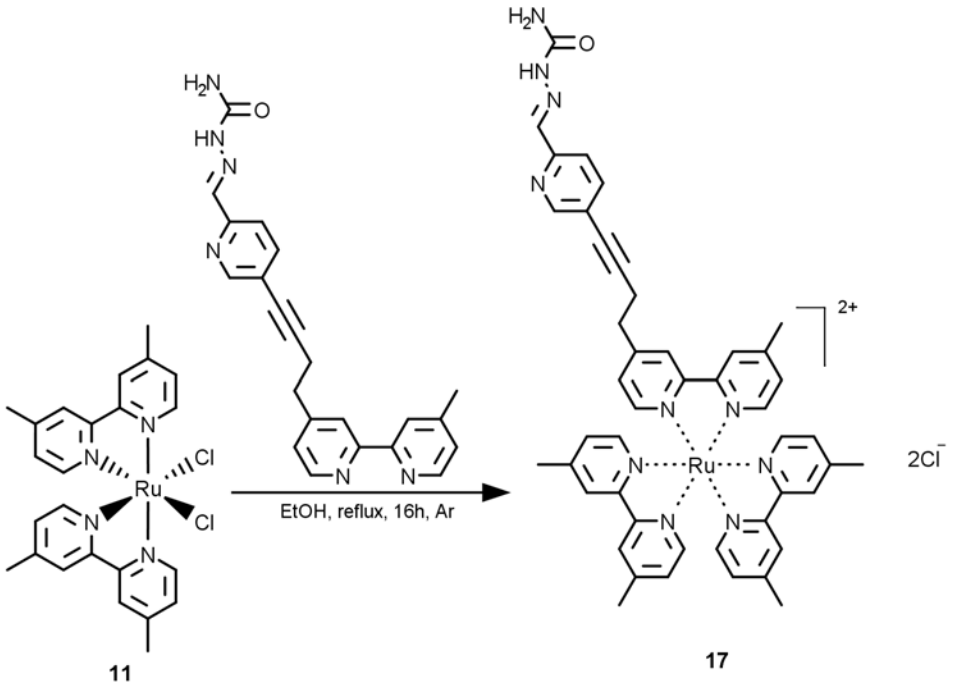

To a solution of cis-$Ru(mebpy)_2Cl_2$(11) (0.027 g, 0.05 mmol) in absolute ethanol (5 mL) under argon conditions, solution of ligand1 (5) (0.022 g, 0.06 mmol) in absolute ethanol (3 mL) was added. Mixture was refluxed for 16 hours. After that time solvent was removed under reduced pressure. Residue was dissolved in water (10 mL) and filtrated. Filtrate was evaporated to dryness, dissolved in small amount of dichloromethane with few drops of methanol and precipiteted with diethyl ether to give pure product with yield 79% (0.036 g).

^{1}H NMR (600 MHz, dmso-d6) 2.94 (t, J=7.2 Hz, 2H); 3.07 (t, J=7.2 Hz, 2H); 6.64 (s, wide, 2H); 7.19-7.24 (m, 1H); 7.27-7.30 (m, 1H); 7.32-7.34 (m, 4H); 7.43 (d, J=11.4 Hz, 1H); 7.46 (d, J=6.6 Hz, 1H); 7.50-7.52 (m, 3H); 7.65 (dd, J=8.4 Hz, 1.8 Hz, 1H); 8.09 (d, J=8.4 Hz, 1H); 8.31 (s, 1H); 8.68-8.73 (m, 6H); 10.59 (s, 1H).

[HRMS]: Calculated for $C_{46}H_{44}N_{10}ORu$ m/z = 427.1366, Found m/z = 427.1370.

6.3.4. Synthesis of $[Ru(tBbpy)_2(L1)]Cl_2$ (18)

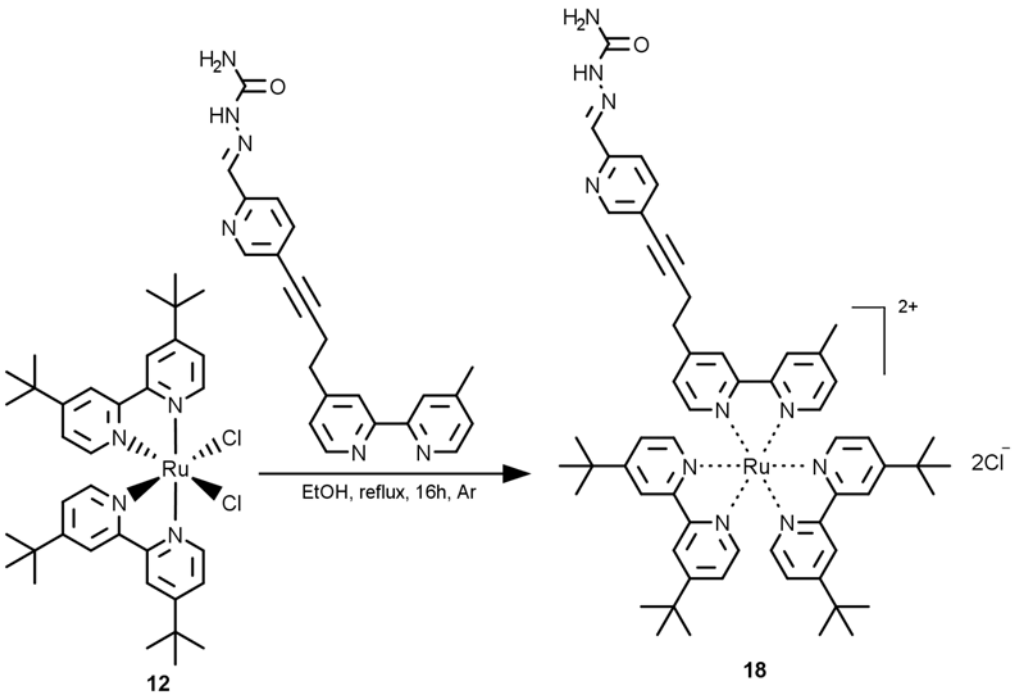

To a solution of cis-Ru(tbbpy)$_2$Cl$_2$(12) (0.028 g, 0.04 mmol) in absolute ethanol (5 mL) under argon conditions, solution of ligand1 (5) (0.019 g, 0.05 mmol) in absolute ethanol (3 mL) was added. Mixture was refluxed for 16 hours. After that time solvent was removed under reduced pressure. Residue was dissolved in water (1 mL) and filtrated. Filtrate was evaporated to dryness, dissolved in small amount of dichloromethane with few drops of methanol and precipitated with diethyl ether to give pure product with yield 76% (0.033 g).

^{1}H NMR (600 MHz, dmso-d6) 1.32 - 1.37 (m, 36H); 2.51 (s, 3̃H superimposed with solvent signal); 2.69 (t, J=6.0 Hz, 2H); 3.09 (t, J=6.0 Hz, 2H); 7.38 (dd, J=6 Hz, 2.4 Hz, 2H); 7.46-7.58 (m, 10H); 7.63 (d, J=24 Hz, 1H); 7.90 (dd, J=8.4 Hz, 1.8 Hz, 1H); 8.48 (s, 1H); 8.78-8.89 (m, 6H); 10.61 (s, 1H); 12.73 (s, 1H).

[HRMS]: Calculated for $C_{58}H_{68}N_{10}ORu$ m/z = 1021.4537 (M-H+), Found m/z = 1021.4468 (M-H+).

6.3.5. Synthesis of $[Ru(Phbpy)_2(L1)]Cl_2$ (19)

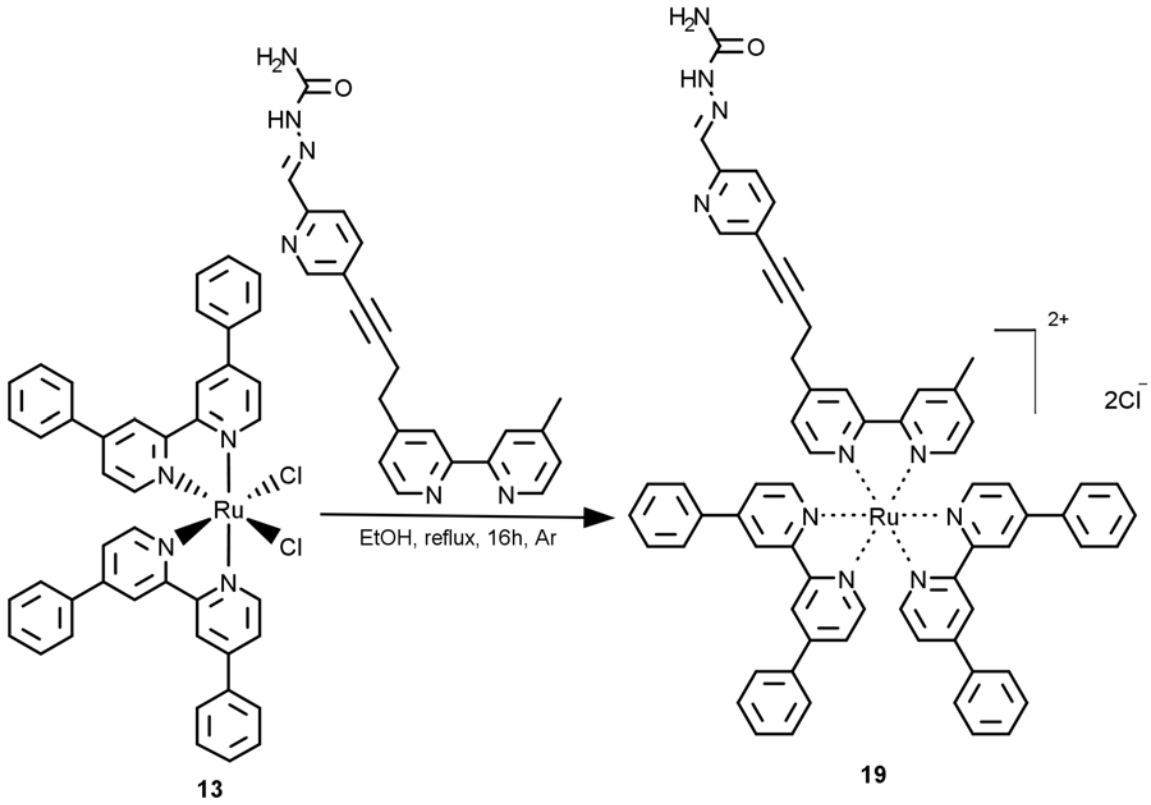

To a solution of cis-$Ru(phbpy)_2Cl_2$(13) (0.04 g, 0.05 mmol) in absolute ethanol (5 mL) under argon conditions, solution of ligand1 (5) (0.024 g, 0.06 mmol) in absolute ethanol (5 mL) was added. Mixture was refluxed for 16 hours. After that time solvent was removed under reduced pressure. Crude product was dissolved in dichloromethane and purified by flash chromatography (Al_2O_3 neutral, dichloromethane/Methanol(5->20%)) to give pure product with yield 56% (0.033 g).

^{1}H NMR (600 MHz, dmso-d6) 2.53 (s, 3H superimposed with solvent signal); 2.84 (t, J=6.6 Hz, 2H); 3.11 (t, J=6.6 Hz, 2H); 6.73 (s, 1H); 7.16 (s, 1H); 7.27 (d, J=4.8 Hz, 1H); 7.39-7.42 (m, 2H); 7.52-7.63 (m, 12H); 7.71-7.91 (m, 12H); 7.97 (d, J=6.6 Hz, 2H); 8.01-8.06 (m, 6H); 8.09 (d, J=3.6 Hz, 1H); 8.22 (s, 1H); 8.46 (dd, J=8.4 Hz, 1.8 Hz, 2H); 8.53 (t, J=4.8 Hz, 1H); 8.59 (t, J=4.8 Hz, 1H); 8.82 (s, 1H); 8.92 (d, J=10.2 Hz, 1H).

[HRMS]: Calculated for $C_{66}H_{52}N_{10}ORu$ m/z = 551.1679, Found: m/z = 551.1688.

6.3.6. Synthesis of $[Ru(dip)_2(L1)]Cl_2$ (20)

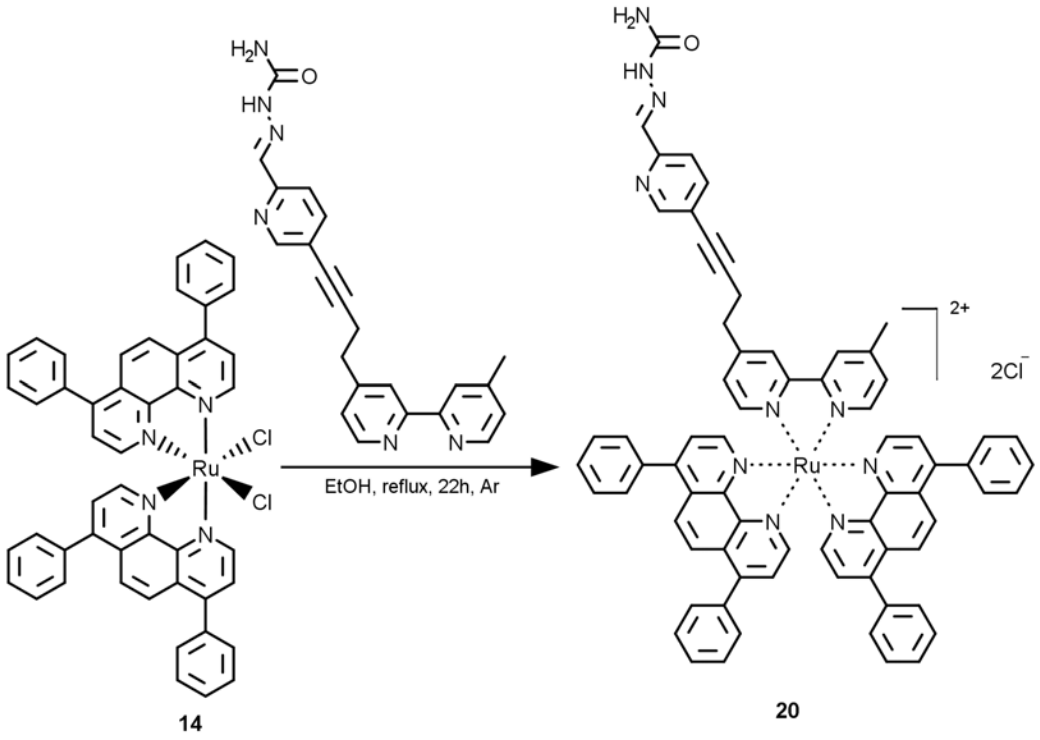

14 20

To a solution of cis-$Ru(dip)_2Cl_2$(14) (0.019 g, 0.023 mmol) in absolute ethanol (10 mL) under argon conditions, solution of ligand1 (5) (0.010 g, 0.026 mmol) in absolute ethanol (5 mL) was added. Mixture was refluxed for 22 hours. After that time solvent was removed under reduced pressure. Crude product was dissolved in dichloromethane and purified by flash chromatography (Al_2O_3 neutral, dichloromethane/Methanol(5->10%)) to give pure product with yield 47% (0.013 g).

^{1}H NMR (600 MHz, CD_3CN) (ppm) 2.55 (s, 3H); 2.95 (t, J=6 Hz, 2H); 3.13 (t, J=6 Hz, 2H); 7.04 (s, 1H); 7.22 (d, J=6 Hz, 1H); 7.37 (dd, J=15.6 Hz, 6 Hz, 2H); 7.57-7.63 (m, 20H); 7.67 (d, J=5.4 Hz, 2H); 7.73 (dd, J=5.4 Hz, 2.4 Hz, 2H); 7.79 (t, J=5.4 Hz, 1H); 8.13-8.20 (m, 6H); 8.23 (d, J=5.4 Hz, 1H); 8.26 (d, J=5.4 Hz, 1H); 8.33 (d, J=5.4 Hz, 3.6 Hz, 1H); 8.80 (d, J=12.6 Hz, 1H); 8.90 (d, J=12.6 Hz, 1H).

[HRMS]: Calculated for $C_{70}H_{52}N_{10}ORu$ m/z = 575.1679, Found: m/z = 575.1683.

6.3.7. Synthesis of $[Ru(SO_3dip)_2(L1)]Cl_2$ (21)

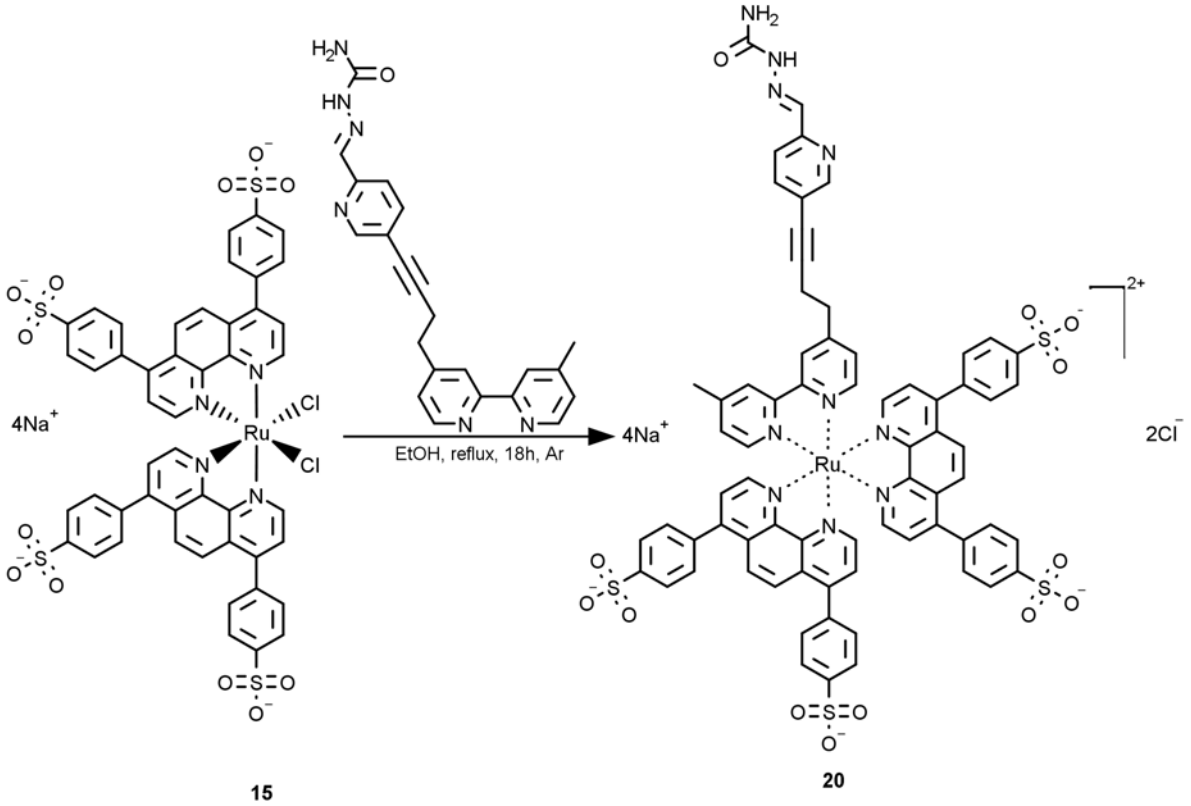

To a solution of cis-$Ru((NaSO_3)_2dip)_2Cl_2$(15) (0.020 g, 0.016 mmol) in absolute ethanol (5 mL) under argon conditions, ligand 1 (5) (0.008 g, 0.019 mmol) was added. Mixture was refluxed for 18 hours. After that time mixture was filtrated and black solid was dissolved in water (2 mL). New solution was filtrated again and water was removed from filtrat. Black solid was dissolved in methanol (1 mL) and crude product was precipitated with diethyl ether. Product was purified by flash chromatography (Al_2O_3 neutral, dichloromethane/Methanol(5->10%)) to give pure product with yield 42% (0.011 g).

^{1}H NMR (600 MHz, dmso-d6): (ppm) 2.52 (s, superimposed with solvent signal); 2.93-2.99 (m, 2H); 3.06-3.11 (m, 2H); 7.58-7.69 (m, 16H); 7.78-7.83 (m, 10H); 7.89 (s, 4H); 8.18 (s, 2H); 8.23-8.31 (m, 3H); 8.35 (s, 1H); 8.37 (s, 2H).

[HRMS]: Calculated for $C_{70}H_{48}N_{10}O_{13}S_4RuNa_4$ m/z = 779.0454, found m/z = 779.0450.

6.3.8. Synthesis of $[Ru(bpy)_2(L2)](PF_6)_2$ (22)

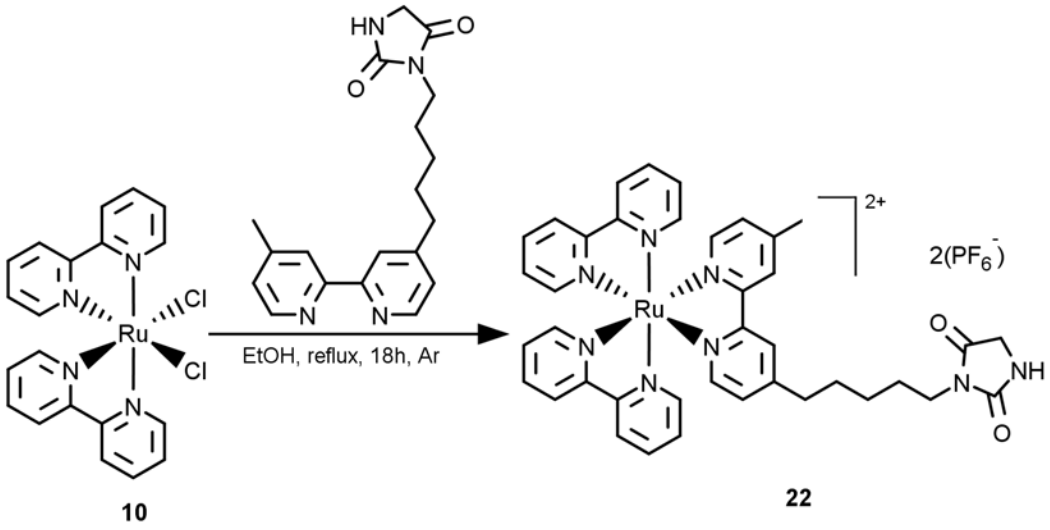

Ligand 2 (7) (0.020 g, 0.06 mmol) was dissolved in absolute ethanol (5 mL) under argon conditions. Solution of cis-$Ru(bpy)_2Cl_2$(10) (0.030 g, 0.062 mmol) in absolute ethanol (5 mL) was added. Dark violet mixture was refluxed under argon conditions for 18 hours. After that solvent was removed under reduced pressure, residue was dissolved in acetonitryl (1 mL) and saturated solution of KPF_6 was added (5 mL). Crude product was filtrated and washed with cold water. Pure product was obtained after flash chromatography (Al_2O_3 neutral, dichloromethane/methanol 9/1) with yield 43% (0.0278 g)

^{1}H NMR (600 MHz, dmso-d6): (ppm) 1.28 (qw, J=7.2 Hz, 2H); 1.52 (qw, J=7.2 Hz, 2H); 1.66 (qw, J=7.2 Hz, 2H); 2.51 (s, 3H); 2.74 (t, J=7.8 Hz, 2H); 3.86 (s, 2H); 7.34 (t, J=6.6 Hz, 2H); 7.48-7.54 (m, 6H); 7.68-7.74 (m, 4H); 7.98 (s, 1H); 8.12-8.15 (m, 4H); 8.68 (s, 1H); 8.74 (s, 1H); 8.79 (d, J=8.4 Hz, 4H).

[HRMS]: Calculated for $C_{39}H_{38}N_8O_2Ru$ m/z = 376.1075, Found m/z = 376.1068.

6.3.9. Synthesis of $[Ru(bpy)_2(L3)](PF_6)_2$ (23)

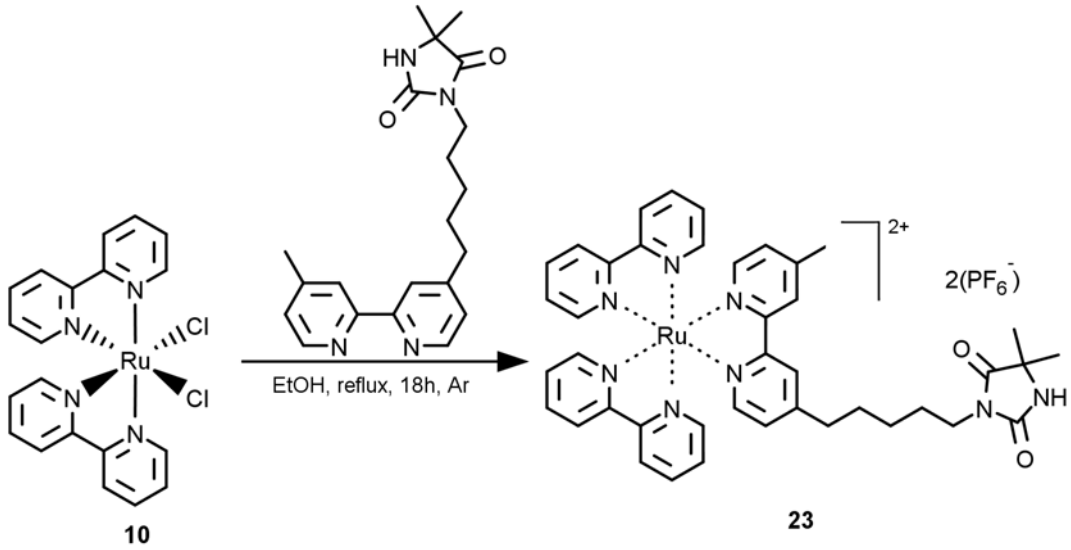

Ligand 3 (8) (0.006 g, 0.016 mmol) was dissolved in absolute ethanol (3 mL) under argon conditions. Solution of cis-$Ru(bpy)_2Cl_2$(10) (0.0045 g, 0.01 mmol) in absolute ethanol (4 mL) was added. Dark violet mixture was refluxed under argon conditions for 18 hours. After that solvent was removed under reduced pressure, residue was dissolved in acetonitryl (1 mL) and saturated solution of KPF_6 was added (6 mL). Crude product was filtrated and washed with cold water. Pure product was obtained after flash chromatography (Al_2O_3 neutral, dichloromethane/methanol 9/1) with yield 84% (0.009 g)

^{1}H NMR (600 MHz, dmso-d6): (ppm) 1.21 (s, 6H); 1.30-1.36 (m, 2H); 1.44-1.51 (m, 2H); 1.65-1.70 (m, 2H); 2.74 (t, J=7.8 Hz, 2H); 7.34 (d, J=4.8 Hz, 2H); 7.48-7.52 (m, 6H); 7.68-7.73 (m, 4H); 8.12-8.14 (m, 4H); 8.60-8.67 (m, 3H); 8.79 (d, J=7.8 Hz, 4H).

[HRMS]: Calculated for $C_{41}H_{42}N_8O_2Ru$ m/z = 390.1232, Found m/z = 390.1237.

6.3.10. Synthesis of $[Ru(bpy)_2(L4)](PF_6)_2$ (24)

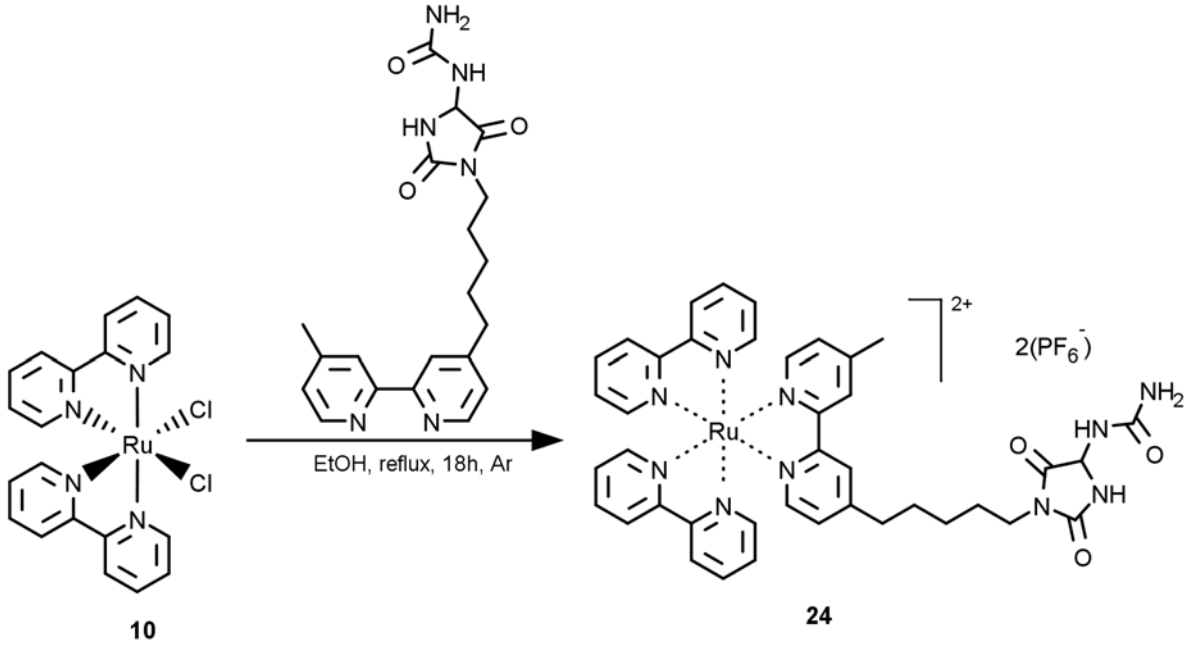

Ligand 4 (9) (0.011 g, 0.028 mmol) was dissolved in chloroform/ethanol mixture (v/v 1/1) (5 mL) under argon conditions. Solution of cis-$Ru(bpy)_2Cl_2$(10) (0.011 g, 0.023 mmol) in absolute ethanol (10 mL) was added. Dark violet mixture was refluxed under argon conditions for 18 hours. After that solvent was removed under reduced pressure, residue was dissolved in acetonitryl (1 mL) and saturated solution of KPF_6 was added (3 mL). Crude product was filtrated and washed with cold water. Pure product was obtained after flash chromatography (Al_2O_3 neutral, dichloromethane/methanol 9/1) with yield 44% (0.0112 g)

^{1}H NMR (600 MHz, dmso-d6): (ppm) 1.33-1.69 (m, 6H); 2.75 (t, J=7.8 Hz, 2H); 5.78 (s, 1H); 7.35 (s, 2H); 7.49-7.53 (m, 6H); 7.68-7.73 (m, 4H); 7.93 (s, 1H); 8.12-8.16 (m, 4H); 8.68-8.71 (m, 2H); 8.74 (s, 1H); 8.80 (d, J=8.4 Hz, 4H).

[HRMS]: Calculated for $C_{40}H_{40}N_{10}O_3Ru$ m/z = 405.1159, Found m/z = 405.1167.

6.4. Other synthesis

6.4.1. Synthesis of 2-bromo-4-methylpyridine (25)[174]

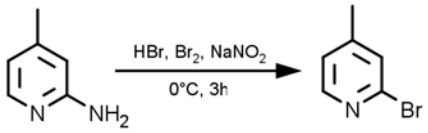

The 48% solution of hydrobromic acid (120 mL) was added dropwise to 2-amino-4-methylpyridine (15.0066 g, 0.14 mol) at 0°C. Then, bromine (21 mL) and solution of $NaNO_2$ (25.3 g) in water (50 mL) was successively added dropwise to the mixture. Solution was stirred at 0°C for 3 h. After that time, water solution of potassium hydroxide (200 mL, concentration 50%) and solution of sodium sulfite (18 g) in water (50 mL) was added. Mixture was extracted with dichloromethane. Combined organic layers were washed with water, dried over anhydrous $MgSO_4$ and solvent was removed under reduced pressure. Crude product was purified by flash chromatography (SiO_2, dichloromethane) to give pure product with yield 77% (18.3329 g).

^{1}H NMR ($CDCl_3$, 200 MHz): δ (ppm) 2.30 (s, 3H); 7.02 (d, J=5 Hz, 1H); 7.28 (s, 1H); 8.16 (d, J=5 Hz, 1H).

6.4.2. Synthesis of 4-methylpyridine-2-carboxyaldehyde (26)

Methode A[129]

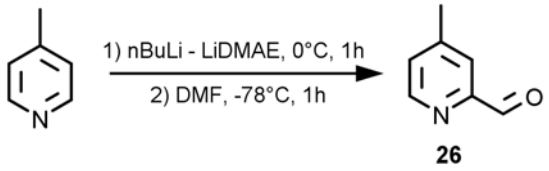

26

To a solution of 2-dimethylaminoethanol (0.8 mL, 8 mmol) in dry n-hexane (25 mL), solution of n-butyllithium (11 mL, 16 mmol) in n-hexane (concentration 1.45 M) was added dropwise at -5°C, under argon. Mixture was stirred in that temperature for 20 minutes and then, solution of 4-methylpyridine (0.39 mL, 4 mmol) in dry n-hexane (5 mL) was added dropwise. Orange mixture was stirred at 0°C for 1 h. After that time, the solution was cooled down to -78°Cand solution of N,N-dimethylformamide (0.8 mL, 10 mmol) in dry THF (10 mL) was added rapidly. Mixture was kept at -78°C for 1 h, warmed to room temperature and quenched with 20 mL ice-water. The mixture was extracted twice with diethyl ether. Combined organic layers was dried

over anhydrous $MgSO_4$ and concentrated under reduced pressure. Crude product was purified by flash chromatography (SiO_2, cyclohexane: ethyl acetate 50:50) to give pure product with yield 28% (138 mg).

^{1}H NMR ($CDCl_3$, 200 MHz): δ (ppm) 2.44 (s, 3H); 7.32 (d, J=5 Hz, 1H); 7.78 (s, 1H); 8.61 (d, J=5 Hz, 1H); 10.05 (s, 1H).

Methode B[175]

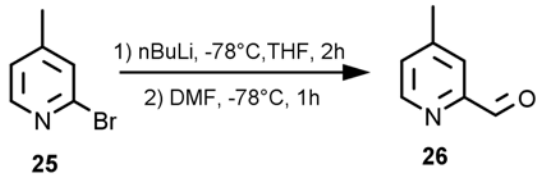

25 **26**

To a solution of 2-bromo-4-methylpyridine (25) (1 mL, 9.0 mmol) in dry THF (20 mL), under argon at -78°C, solution of n-butyllithium (9 mL, 10.8 mmol, 1.2 eq) in n-hexane (concentration 1.2 M) was added dropwise. Mixture was stirred in that temperature for 2 h and then, N,N-dimethylformamide (1.4 mL, 18 mmol) was added rapidly. Mixture was kept at -78°C for 1 h and slowly warmed to room temperature. Reaction was quenched with saturated solution of ammonium chloride (10 mL) and extracted with dichloromethane. Combined organic layers was dried over anhydrous $MgSO_4$ and concentrated under reduced pressure. Crude product was purified by flash chromatography (SiO_2, cyclohexane: ethyl acetate 50:50) to give pure product with yield 20% (198 mg).

^{1}H NMR ($CDCl_3$, 200 MHz): δ (ppm) 2.44 (s, 3H); 7.32 (d, J=5 Hz, 1H); 7.78 (s, 1H); 8.61 (d, J=5 Hz, 1H); 10.05 (s, 1H).

Methode C[176]

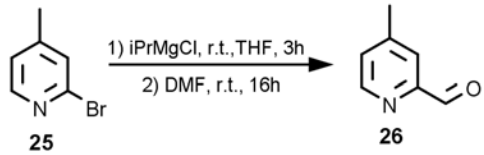

25 **26**

To a solution of 2-bromo-4-methylpyridine (25) (2 mL, 18 mmol) in dry THF (17 mL), under argon at room temperature, solution of isopropylmagnesium chloride (13.5 mL, 21.6 mmol) in THF (concentration 1.6 M) was added dropwise. Mixture was stirred in that temperature for 3 h and then, anhydrous N,N-dimethylformamide (2 mL,

25.8 mmol) was added rapidly. Mixture was cooled down to room temperature and stirred for 16 h. Reaction was quenched with ice-water (50 mL), neutralizated with 2M HCl and extracted with dichloromethane. Combined organic layers were washed with brine, dried over anhydrous $MgSO_4$ and concentrated under reduced pressure to give pure product with yield 94% (2.0264 g).

^{1}H NMR ($CDCl_3$, 200 MHz): δ (ppm) 2.42 (s, 3H); 7.32 (d, J=5 Hz, 1H); 7.75 (s, 1H); 8.60 (d, J=5 Hz, 1H); 10.03 (s, 1H).

6.4.3. Synthesis of 2-[1,3]-dioxolan-2-yl-4-methylpyridine (27)[177]

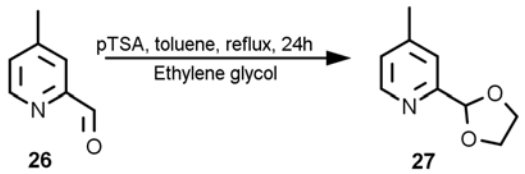

4-methylpyridine-2-carboxyaldehyde (26) (0.4850 g, 4 mmol), ethylene glycol (0.45 mL, 8 mmol), p-toluenesulfonic acid monohydrate (0.2267 g, 1.2 mmol) and anhydrous toluene (30 mL) were refluxed in Dean-Stark apparatus for 24 h. Solution was cooled down, neutralized with saturated solution of sodium hydrogen carbonate and separated. Water layer was extracted twice with toluene. Combined organic layers was washed with brine, dried over anhydrous $MgSO_4$ and concentrated in vacuum. Pure product was obtained without further purification with quantitative yield.

^{1}H NMR ($CDCl_3$, 200 MHz): δ (ppm) 2.37 (s, 3H); 4.06 - 4.19 (m, 4H); 5.82 (s, 1H); 7.08 (d, J=5 Hz, 1H); 7.36 (s, 1H); 8.46 (d, J=5 Hz, 1H).

6.4.4. Synthesis of 4-(7-bromoheptyl)-4′-methyl-2,2′-bipyridine (28)

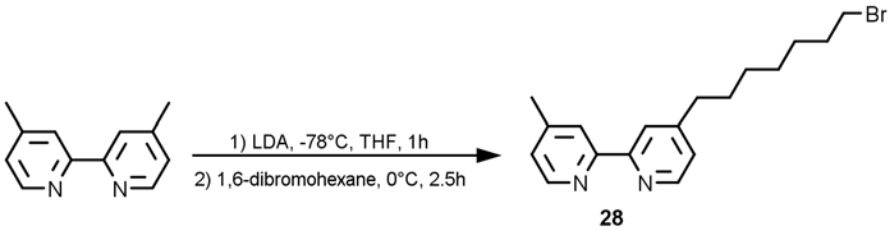

To a solution of diisopropylamine (0.24 mL, 1.7 mmol) in dry THF (6 mL), under argon at -78°C, solution of n-butyllithium (1.05 mL, 1.6 mmol) in n-hexane (concentration =

1.5M) was added dropwise. After 20 minutes a solution of 4,4′-dimethyl-2,2′-bipyridine (0.2459 g, 1.3 mmol) in dry THF (17 mL) was added rapidly. Chocolate-brown solution was stirred at -78°C for 1 h and warmed to 0°C. A solution of 1,6-dibromohexane (1 mL, 6.5 mmol) in dry THF (3 mL) was added rapidly. After 2.5 h the solution became light yellow and reaction was quenched with water (10 mL). Mixture was neutralized with 2M HCl and extracted with dichloromethane. Combined organic layers were dried over anhydrous $MgSO_4$ and solvent was removed under reduced pressure. Crude material was purified by flash chromatography (SiO_2, dichloromethane, diethyl ether) to give pure product with yield 82% (382 mg).

^{1}H NMR ($CDCl_3$, 200 MHz): δ (ppm) 1.35 - 1.45 (m, 6H); 1.61 - 1.69 (m, 2H); 1.76 - 1.89 (m, 2H); 2.42 (s, 1H); 2.68 (t, J=8 Hz, 2H); 3.38 (t, J=6.8 Hz, 2H); 7.10 (d, J=5 Hz, 2H); 8.22 (s, 2H); 8.53 (t, J=4.4 Hz, 2H).

6.4.5. Synthesis of 2-bromo-4-[6-(2-bromopyridin-4-yl)hexyl]pyridine (29)

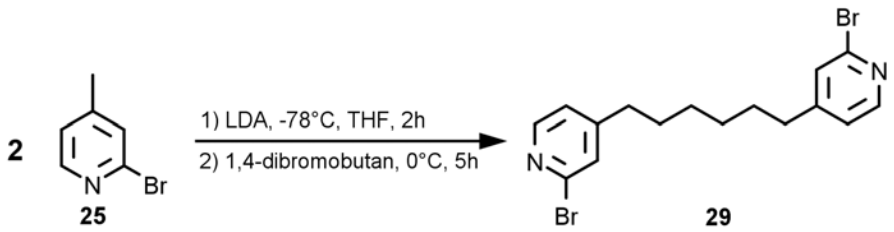

To a solution of diisopropylamine (0.91 mL, 6.5 mmol) in dry THF (6 mL), under argon at -78°C, a solution of n-butyllithium (4.3 mL, 6 mmol) in n-hexane (concentration = 1.4M) was added dropwise. After 30 minutes a solution of 2-bromo-4-methylpyridine (25) (0.867 g, 5 mmol) in dry THF (4 mL) was added dropwise. Mixture was kept in this temperature for 2 h and solution of 1,4-dibronobutane (0.554 g, 2.5 mmol) in dry THF (5 mL) was added slowly. Mixture was warmed up to 0°C over 1 h and kept in this temperature for another 5 h. After that, the reaction was quenched with water (25 mL) and extracted with ethyl acetate (3x30 mL). Combined organic layers were dried over $MgSO_4$, filtrated and evaporate under reduced pressure to give pure product as orange solid with yield 64% (0.643 g).

^{1}H NMR (400 MHz, $CDCl_3$): (ppm) 1.29-1.37 (m, 4H); 1.56-1.64 (m, 4H); 2.55 (t, J=8 Hz, 4H); 7.02 (d, J=4 Hz, 2H); 7.31 (s, 2H); 8.21 (d, J=4 Hz, 2H).

^{13}C NMR (100 MHz, $CDCl_3$): 28.8; 29.9; 34.8; 123.0; 127.9; 142.3; 149.8; 154.6.

[HRMS-ESI]: Calculated for $C_{16}H_{18}N_2Br_2$ m/z = 396.9910 ($M+H^+$), found m/z = 396.9903 ($M+H^+$).

6.4.6. Synthesis of 2-bromopyridine-5-carboxyaldehyde (30)[178]

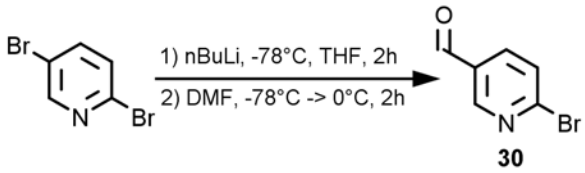

30

To a solution of 2,5-dibromopyridine (0.2370 g, 1 mmol) in dry THF (7 mL), under argon at -78°C, a solution of n-butyllithium (0.85 mL, 1.2 mmol) in n-hexane (concentration = 1.4 M) was added dropwise. After 2 h, N,N-dimethylformamide (0.40 mL, 5 mmol, 5 eq) was added rapidly. After 1 h, mixture was warmed up to 0°C and kept in this temperature for 1 h. After that time, reaction was quenched with saturated solution of ammonium chloride (10 mL) and extracted three times with ethyl acetate. Combined organic layers were dried over anhydrous $MgSO_4$ and concentrated to give pure product with yield 63% (0.117 g).

^{1}H NMR (200 MHz, $CDCl_3$): (ppm) 7.69 (d, J=8 Hz, 1H); 8.03 (dd, J=8 Hz, 2 Hz, 2H); 8.86 (d, J=2 Hz, 2H); 10.12 (s, 1H).

6.4.7. Synthesis of (2-bromopyridin-5-yl)methanol (31)[179]

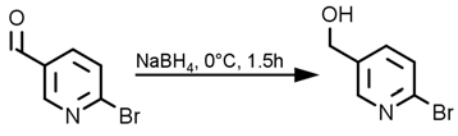

30 31

To a solution of 2-bromopyridine-5-carboxyaldehyde (30) (0.815 g, 4.4 mmol) in methanol (25 mL), sodium borohydride (0.1 g, 2.2 mmol) was added at 0°C. After 1.5 h concentrated hydrochloric acid was added to reach pH 2 and mixture was neutralized with potassium biscarbonate saturated solution. Mixture was extracted with ethyl acetate (3x30mL). Combined organic layers were dried over $MgSO_4$ and solvent was removed under reduced pressure to give product as yellow oil with yield 84% (0.689 g)

^{1}H NMR (200 MHz, $CDCl_3$): (ppm) 4.74 (s, 2H); 7.49 (d, J=8 Hz, 1H); 7.60 (dd, J=8 Hz, 2 Hz, 1H); 8.37 (d, J=2 Hz, 1H).

6.4.8. Synthesis of ({4′-methyl-[2,2′-bipyridine]-4-yl}pentyl)triphenylphosphonium bromide (32)

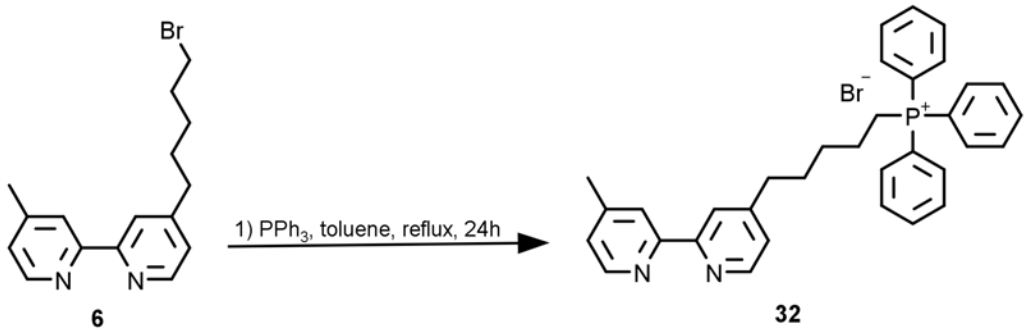

To a solution of 4-(5-bromopentyl)-4′-methyl-2,2′-bipyridine (6) (0.390 g, 1.2 mmol) in dry toluene (12 mL) under argon, triphenylphosphine (0.641 g, 2.4 mmol) was added. Mixture was refluxed for 24 h and cooled down to room temperature. Most of the solvent was removed under reduced pressure. Crude brown oil was mixed with diethyl ether and kept at 4°C for few hours. White-brown crystals were filtrated of and dried to give pure product.

^{1}H NMR (200 MHz, $CDCl_3$): (ppm) 1.30-1.60 (m, 8H); 2.37 (s, 3H); 2.59 (t, J=6 Hz, 2H); 3.77-3.84 (m, 2H); 7.05-7.15 (m, 2H); 7.59-7.83 (m, 15H); 8.07 (s, 1H); 8.16 (s, 1H); 8.46 (t, J=4 Hz, 2H).

6.4.9. Synthesis of diethyl ({4′-methyl-[2,2′-bipyridine]-4-yl}pentyl)phosphonate (33)

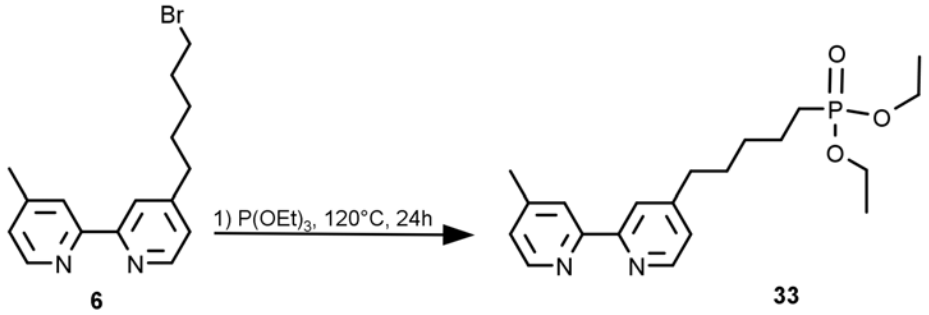

4-(5-bromopentyl)-4′-methyl-2,2′-bipyridine (6) (0.313 g, 1 mmol) was dissolved in triethyl phosphate (6.6 mL, 40 mmol) and heated at 120°C for 24 h. Residue mixture was evaporated under reduced pressure and dried in vaccum desicator over P_2O_5 for

48 h. Residue brown oil was relatively pure compound and was used without further purification. Yield 92% (0.341 g).

^{1}H NMR (200 MHz, $CDCl_3$): (ppm) 1.24 (t, J=6 Hz, 6H); 1.31-1.62 (m, 8H); 2.37 (s, 3H); 2.63 (t, J=6 Hz, 2H); 4.01 (qw, J=2 Hz, 4H); 7.06 (d, J=2 Hz, 2H); 8.15 (s, 2H); 8.47 (t, J=2 Hz, 2H).

References

[1] S. J. Lippard, *Bioinorganic chemistry: Metals in medicine*. 1994.

[2] L. N. Magner, *A History of Medicine*. Taylor & Francis Group, 2005.

[3] P. J. Sadler, Inorganic Chemistry and Drug Design *Advances in Inorganic Chemistry*, vol. 36, pp. 1 – 48, 1991.

[4] K. H. Antman, Introduction: The History of Arsenic Trioxide in Cancer Therapy *The Oncologist*, vol. 6, no. suppl 2, pp. 1–2, 2001.

[5] S. Waxman and K. C. Anderson, History of the Development of Arsenic Derivatives in Cancer Therapy *The Oncologist*, vol. 6, no. suppl 2, pp. 3–10, 2001.

[6] B. Rosenberg, L. van Camp, and T. Krigas, Inhibition of Cell Division in Escherichia coli by Electrolysis Products from a Platinum Electrode *Nature*, vol. 205, pp. 698–699, 1965.

[7] C. Orvig and M. J. Abrams, Medicinal Inorganic Chemistry: Introduction *Chemical Reviews*, vol. 99, no. 9, pp. 2201–2204, 1999.

[8] G. T. S. Darleane C. Hoffman, Albert Ghiorso, *The Transuranium People*, ch. Chapter 1.2: Early Days at the Berkeley Radiation Laboratory, pp. 6–20. Singapore: Imperial College Press, 2000.

[9] M. Peyrone, Ueber die Einwirkung des Ammoniaks auf Platinchlorür *Justus Liebigs Annalen der Chemie*, vol. 51, no. 1, pp. 1–29, 1844.

[10] S. Trzaska, Top pharmaceuticals: Cisplatin *Chemical and engineering news*, vol. 83, no. 25, pp. 28–42, 2005.

[11] P. Pfeiffer, Alfred Werner *Journal of Chemical Education*, vol. 5, no. 9, p. 1090, 1928.

[12] B. Rosenberg, L. van Camp, J. E. Trosko, and V. H. Mansour, Platinum compounds: a new class of potent antitumour agents. *Nature*, vol. 222, pp. 385–286, 1969.

[13] L. Kelland, The resurgence of platinum-based cancer chemotherapy *Nat Rev Cancer*, vol. 7, pp. 573–584, Aug 2007.

[14] M. A. Jakupec, M. Galanski, and B. K. Keppler, Tumour-inhibiting platinum complexes—state of the art and future perspectives *Reviews of Physiology, Biochemistry and Pharmacology*, vol. 146, pp. 1–53, 2003.

[15] S. Kim, L. Ma, J. Unruh, S. McKinney, and C. R. Yu, Intracellular chloride concentration of the mouse vomeronasal neuron *BMC Neuroscience*, vol. 16, p. 90,

2015.

[16] E. R. Jamieson, , and S. J. Lippard, Structure, Recognition, and Processing of Cisplatin-DNA Adducts *Chemical Reviews*, vol. 99, no. 9, pp. 2467–2498, 1999.

[17] A. Eastman, M. M. Jennerwein, and D. L. Nagel, Characterization of bifunctional adducts produced in DNA by trans-diamminedichloroplatinum(II) *Chemico-Biological Interactions*, vol. 67, no. 1, pp. 71 – 80, 1988.

[18] K.-B. Lee, D. Wang, S. J. Lippard, and P. A. Sharp, Transcription-coupled and DNA damage-dependent ubiquitination of RNA polymerase II in vitro *Proceedings of the National Academy of Sciences*, vol. 99, no. 7, pp. 4239–4244, 2002.

[19] N. Poklar, D. S. Pilch, S. J. Lippard, E. A. Redding, S. U. Dunham, and K. J. Breslauer, Influence of cisplatin intrastrand crosslinking on the conformation, thermal stability, and energetics of a 20-mer DNA duplex. *Proc Natl Acad Sci U S A*, vol. 93, pp. 7606–7611, Jul 1996.

[20] F. Herman, J. Kozelka, V. Stoven, E. Guittet, J.-P. Girault, T. Huynh-Dinh, J. Igolen, J.-Y. Lallemand, and J.-C. Chottard, A d(GpG)-platinated decanucleotide duplex is kinked *European Journal of Biochemistry*, vol. 194, no. 1, pp. 119–133, 1990.

[21] U.-M. Ohndorf, M. A. Rould, Q. He, C. O. Pabo, and S. J. Lippard, Basis for recognition of cisplatin-modified DNA by high-mobility-group proteins *Nature*, vol. 399, pp. 708–712, Jun 1999.

[22] M. J. McKeage, *Platinum-Based Drugs in Cancer Therapy*, ch. Clinical Toxicology of Platinum-Based Cancer Chemotherapeutic Agents, pp. 251–276. New York: Humana Press, 2000.

[23] A. Bergamo and G. Sava, Linking the future of anticancer metal-complexes to the therapy of tumour metastases *Chem. Soc. Rev.*, vol. 44, pp. 8818–8835, 2015.

[24] M. S. Highley and A. H. Calvert, *Platinum-Based Drugs in Cancer Therapy*, ch. Clinical Experience with Cisplatin and Carboplatin, pp. 171–194. New York: Humana Press, 2000.

[25] P. A. Andrews, *Platinum-Based Drugs in Cancer Therapy*, ch. Cisplatin Accumulation, pp. 89–114. New York: Humana Press, 2000.

[26] E. Van Cutsem, F. Rivera, S. Berry, A. Kretzschmar, M. Michael, M. DiBartolomeo, M.-A. Mazier, J.-L. Canon, V. Georgoulias, M. Peeters, J. Bridgewater, D. Cunningham, and on behalf of the First BEAT investigators, Safety and efficacy of first-line bevacizumab with FOLFOX, XELOX, FOLFIRI and fluoropyrimidines in metastatic colorectal cancer: the BEAT study *Annals of Oncology*, vol. 20, no. 11, pp. 1842–1847, 2009.

[27] C. Garufi, C. Nistico, A. Vaccaro, A. D'Ottavio, A. R. Zappala, A. M. Aschelter, and E. Terzoli, Single-agent oxaliplatin in pretreated advanced breast cancer patients:

A phase II study *Annals of Oncology*, vol. 12, no. 2, pp. 179–182, 2001.

[28] M. J. Piccart, J. A. Green, A. J. Lacave, N. Reed, I. Vergote, P. Benedetti-Panici, A. Bonetti, V. Kristeller-Tome, C. M. Fernandez, D. Curran, M. Van Glabbeke, D. Lacombe, M.-C. Pinel, and S. Pecorelli, Oxaliplatin or Paclitaxel in Patients With Platinum-Pretreated Advanced Ovarian Cancer: A Randomized Phase II Study of the European Organization for Research and Treatment of Cancer Gynecology Group *Journal of Clinical Oncology*, vol. 18, no. 6, pp. 1193–1202, 2000.

[29] P. J. O'Dwyer, J. P. Stevenson, and S. W. Johnson, *Platinum-Based Drugs in Cancer Therapy*, ch. Clinical Experience: DACH-Based Platinum Drugs, pp. 231–250. New York: Humana Press, 2000.

[30] N. J. Wheate, S. Walker, G. E. Craig, and R. Oun, The status of platinum anticancer drugs in the clinic and in clinical trials *Dalton Trans.*, vol. 39, pp. 8113–8127, 2010.

[31] H. Choy, C. Park, and M. Yao, Current Status and Future Prospects for Satraplatin, an Oral Platinum Analogue *Clinical Cancer Research*, vol. 14, no. 6, pp. 1633–1638, 2008.

[32] Drugbank: Satraplatin. Retrieved June 2016 from http://www.drugbank.ca/drugs/DB04996

[33] M. Clarke, S. Bitler, D. Rennert, M. Buchbinder, and A. Kelman, Reduction and Subsequent Binding of Ruthenium Ions Catalyzed by Subcellular Components *Journal of Inorganic Biochemistry*, vol. 12, no. 1, pp. 79 – 87, 1980.

[34] M. J. Clarke, Ruthenium metallopharmaceuticals *Coordination Chemistry Reviews*, vol. 236, no. 1–2, pp. 209 – 233, 2003.

[35] D. Frasca, J. Ciampa, J. Emerson, R. S. Umans, and M. J. Clarke, Effects of Hypoxia and Transferrin on Toxicity and DNA Binding of Ruthenium Antitumor Agents in Hela Cells *Met Based Drugs*, vol. 3, no. 4, pp. 197–209, 1996.

[36] M. J. Clarke, F. Zhu, and D. R. Frasca, Non-Platinum Chemotherapeutic Metallopharmaceuticals *Chemical Reviews*, vol. 99, no. 9, pp. 2511–2534, 1999.

[37] B. M. Blunden and M. H. Stenzel, Incorporating ruthenium into advanced drug delivery carriers – an innovative generation of chemotherapeutics *Journal of Chemical Technology & Biotechnology*, vol. 90, no. 7, pp. 1177–1195, 2015.

[38] M. Brindell, S. Elmroth, and G. Stochel, Mechanistic information on the reaction of cis- and trans-[RuCl2(DMSO)4] with d(T2GGT2) derived from MALDI-TOF and {HPLC} studies *Journal of Inorganic Biochemistry*, vol. 98, no. 8, pp. 1367 – 1377, 2004.

[39] E. Alessio, G. Mestroni, G. Nardin, W. M. Attia, M. Calligaris, G. Sava, and S. Zorzet, Cis- and trans-dihalotetrakis(dimethyl sulfoxide)ruthenium(II) complexes (RuX2(DMSO)4; X = Cl, Br): synthesis, structure, and antitumor

activity *Inorganic Chemistry*, vol. 27, no. 23, pp. 4099–4106, 1988.

[40] M. Brindell, E. Kulis, S. K. C. Elmroth, K. Urbańska, and G. Stochel, Light-Induced Anticancer Activity of [RuCl2(DMSO)4] Complexes *Journal of Medicinal Chemistry*, vol. 48, no. 23, pp. 7298–7304, 2005.

[41] A. Levina, A. Mitra, and P. A. Lay, Recent developments in ruthenium anticancer drugs *Metallomics*, vol. 1, pp. 458–470, 2009.

[42] R. Hudej, D. Miklavcic, M. Cemazar, V. Todorovic, G. Sersa, A. Bergamo, G. Sava, A. Martincic, J. Scancar, B. K. Keppler, and I. Turel, Modulation of Activity of Known Cytotoxic Ruthenium(III) Compound (KP418) with Hampered Transmembrane Transport in Electrochemotherapy In Vitro and In Vivo *The Journal of Membrane Biology*, vol. 247, no. 12, pp. 1239–1251, 2014.

[43] R. Trondl, P. Heffeter, C. R. Kowol, M. A. Jakupec, W. Berger, and B. K. Keppler, NKP-1339 the first ruthenium-based anticancer drug on the edge to clinical application *Chem. Sci.*, vol. 5, pp. 2925–2932, 2014.

[44] G. Sava, S. Pacor, G. Mestroni, and E. Alessio, Na[trans-RuCl4(DMSO)Im], a metal complex of ruthenium with antimetastatic properties *Clinical & Experimental Metastasis*, vol. 10, no. 4, pp. 273–280, 1992.

[45] G. Sava, F. Frausin, M. Cocchietto, F. Vita, E. Podda, P. Spessotto, A. Furlani, V. Scarcia, and G. Zabucchi, Actin-dependent tumour cell adhesion after short-term exposure to the antimetastasis ruthenium complex NAMI-A *European Journal of Cancer*, vol. 40, no. 9, pp. 1383–1396, 2004.

[46] A. Vacca, M. Bruno, A. Boccarelli, M. Coluccia, D. Ribatti, A. Bergamo, S. Garbisa, L. Sartor, and G. Sava, Inhibition of endothelial cell functions and of angiogenesis by the metastasis inhibitor NAMI-A *Br J Cancer*, vol. 86, no. 6, pp. 993–998, 2002.

[47] B. Gava, S. Zorzet, P. Spessotto, M. Cocchietto, and G. Sava, Inhibition of B16 Melanoma Metastases with the Ruthenium Complex Imidazolium trans-Imidazoledimethylsulfoxide-tetrachlororuthenate and Down-Regulation of Tumor Cell Invasion *Journal of Pharmacology and Experimental Therapeutics*, vol. 317, no. 1, pp. 284–291, 2006.

[48] G. Sava, I. Capozzi, K. Clerici, G. Gagliardi, E. Alessio, and G. Mestroni, Pharmacological control of lung metastases of solid tumours by a novel ruthenium complex *Clinical & Experimental Metastasis*, vol. 16, no. 4, pp. 371–379, 1998.

[49] B. K. Keppler, M. Hennl, M. Juhll, M. R. Berger, R. Niebl, and F. E. Wagner, *Ruthenium and Other Non-Platinum Metal Complexes in Cancer Chemotherapy*, ch. New Ruthenium Complexes for the Treatment of Cancer, pp. 41–69. Berlin Heidelberg: Springer-Verlag, 1989.

[50] A. Bergamo, C. Gaiddon, J. Schellens, J. Beijnen, and G. Sava, Approaching tumour therapy beyond platinum drugs: Status of the art and perspectives of ruthenium drug candidates *Journal of Inorganic Biochemistry*, vol. 106, no. 1, pp. 90 – 99, 2012.

[51] C. G. Hartinger, S. Zorbas-Seifried, M. A. Jakupec, B. Kynast, H. Zorbas, and B. K. Keppler, From bench to bedside – preclinical and early clinical development of the anticancer agent indazolium trans-[tetrachlorobis(1H-indazole)ruthenate(III)] (KP1019 or FFC14A) *Journal of Inorganic Biochemistry*, vol. 100, no. 5–6, pp. 891 – 904, 2006.

[52] O. Mazuryk, K. Kurpiewska, K. Lewiński, G. Stochel, and M. Brindell, Interaction of apo-transferrin with anticancer ruthenium complexes NAMI-A and its reduced form *Journal of Inorganic Biochemistry*, vol. 116, pp. 11 – 18, 2012.

[53] M. Sulyok, S. Hann, C. G. Hartinger, B. K. Keppler, G. Stingeder, and G. Koellensperger, Two dimensional separation schemes for investigation of the interaction of an anticancer ruthenium(iii) compound with plasma proteins *J. Anal. At. Spectrom.*, vol. 20, pp. 856–863, 2005.

[54] R. Trondl, L. S. Flocke, C. R. Kowol, P. Heffeter, U. Jungwirth, G. E. Mair, R. Steinborn, v. A. Enyedy, M. A. Jakupec, W. Berger, and B. K. Keppler, Triapine and a More Potent Dimethyl Derivative Induce Endoplasmic Reticulum Stress in Cancer Cells *Molecular Pharmacology*, vol. 85, no. 3, pp. 451–459, 2014.

[55] M. Groessl, C. G. Hartinger, P. J. Dyson, and B. K. Keppler, CZE–ICP-MS as a tool for studying the hydrolysis of ruthenium anticancer drug candidates and their reactivity towards the {DNA} model compound dGMP *Journal of Inorganic Biochemistry*, vol. 102, no. 5–6, pp. 1060 – 1065, 2008.

[56] N. Graf and S. J. Lippard, Redox activation of metal-based prodrugs as a strategy for drug delivery *Adv Drug Deliv Rev*, vol. 64, pp. 993–1004, Aug 2012.

[57] M. Brindell, I. Stawoska, J. Supel, A. Skoczowski, G. Stochel, and R. van Eldik, The reduction of (ImH)[trans-RuIIICl4(dmso)(Im)] under physiological conditions: preferential reaction of the reduced complex with human serum albumin *JBIC Journal of Biological Inorganic Chemistry*, vol. 13, no. 6, pp. 909–918, 2008.

[58] J. M. Rademaker-Lakhai, D. van den Bongard, D. Pluim, J. H. Beijnen, and J. H. M. Schellens, A Phase I and Pharmacological Study with Imidazolium-trans-DMSO-imidazole-tetrachlororuthenate, a Novel Ruthenium Anticancer Agent *Clinical Cancer Research*, vol. 10, no. 11, pp. 3717–3727, 2004.

[59] Ruthenium Complexes as Anticancer Agents *Current Medicinal Chemistry*, vol. 13, no. 9, pp. 1085–1107, 2006.

[60] C. G. Hartinger, M. A. Jakupec, S. Zorbas-Seifried, M. Groessl, A. Egger, W. Berger, H. Zorbas, P. J. Dyson, and B. K. Keppler, KP1019, A New Redox-Active Anticancer Agent – Preclinical Development and Results of a Clinical Phase I Study in Tumor Patients *Chemistry & Biodiversity*, vol. 5, no. 10, pp. 2140–2155, 2008.

[61] S. Leijen, S. A. Burgers, P. Baas, D. Pluim, M. Tibben, E. van Werkhoven, E. Alessio, G. Sava, J. H. Beijnen, and J. H. M. Schellens, Phase I/II study with ruthenium compound NAMI-A and gemcitabine in patients with non-small cell lung cancer after first line therapy *Investigational New Drugs*, vol. 33, no. 1, pp. 201–214, 2015.

[62] H. von der Maase, S. Hansen, J. Roberts, L. Dogliotti, T. Oliver, M. Moore, I. Bodrogi, P. Albers, A. Knuth, C. Lippert, P. Kerbrat, P. Sanchez Rovira, P. Wersall, S. Cleall, D. Roychowdhury, I. Tomlin, C. Visseren-Grul, and P. Conte, Gemcitabine and Cisplatin Versus Methotrexate, Vinblastine, Doxorubicin, and Cisplatin in Advanced or Metastatic Bladder Cancer: Results of a Large, Randomized, Multinational, Multicenter, Phase III Study *Journal of Clinical Oncology*, vol. 18, no. 17, pp. 3068–3077, 2000.

[63] D. S. Thompson, G. J. Weiss, S. F. Jones, H. A. Burris, R. K. Ramanathan, J. R. Infante, J. C. Bendell, A. Ogden, and D. D. Von Hoff, NKP-1339: Maximum tolerated dose defined for first-in-human GRP78 targeted agent. *ASCO Meeting Abstracts*, vol. 30, no. 15 suppl, p. 3033, 2012.

[64] C. S. Allardyce, A. Dorcier, C. Scolaro, and P. J. Dyson, Development of organometallic (organo-transition metal) pharmaceuticals *Applied Organometallic Chemistry*, vol. 19, no. 1, pp. 1–10, 2005.

[65] R. E. Morris, R. E. Aird, P. del Socorro Murdoch, H. Chen, J. Cummings, N. D. Hughes, S. Parsons, A. Parkin, G. Boyd, D. I. Jodrell, and P. J. Sadler, Inhibition of Cancer Cell Growth by Ruthenium(II) Arene Complexes *Journal of Medicinal Chemistry*, vol. 44, no. 22, pp. 3616–3621, 2001.

[66] A. K. Renfrew, L. Juillerat-Jeanneret, and P. J. Dyson, Adding diversity to ruthenium(II)–arene anticancer (RAPTA) compounds via click chemistry: The influence of hydrophobic chains *Journal of Organometallic Chemistry*, vol. 696, no. 3, pp. 772 – 779, 2011.

[67] H. Chen, J. A. Parkinson, R. E. Morris, and P. J. Sadler, Highly Selective Binding of Organometallic Ruthenium Ethylenediamine Complexes to Nucleic Acids: Novel Recognition Mechanisms *Journal of the American Chemical Society*, vol. 125, no. 1, pp. 173–186, 2003.

[68] R. E. Aird, J. Cummings, A. A. Ritchie, M. Muir, R. E. Morris, H. Chen, P. J. Sadler, and D. I. Jodrell, In vitro and in vivo activity and cross resistance profiles

of novel ruthenium (II) organometallic arene complexes in human ovarian cancer *Br J Cancer*, vol. 86, no. 10, pp. 1652–1657, 2002.

[69] C. Scolaro, A. Bergamo, L. Brescacin, R. Delfino, M. Cocchietto, G. Laurenczy, T. J. Geldbach, G. Sava, and P. J. Dyson, In Vitro and in Vivo Evaluation of Ruthenium(II)-Arene PTA Complexes *Journal of Medicinal Chemistry*, vol. 48, no. 12, pp. 4161–4171, 2005.

[70] P. J. Dyson and G. Sava, Metal-based antitumour drugs in the post genomic era *Dalton Trans.*, pp. 1929–1933, 2006.

[71] J. G. Vos and J. M. Kelly, Ruthenium polypyridyl chemistry; from basic research to applications and back again *Dalton Trans.*, pp. 4869–4883, 2006.

[72] A. W. McKinley, P. Lincoln, and E. M. Tuite, Sensitivity of [Ru(phen)2dppz]2+ light switch emission to ionic strength, temperature, and DNA sequence and conformation *Dalton Trans.*, vol. 42, pp. 4081–4090, 2013.

[73] A. E. Friedman, J. C. Chambron, J. P. Sauvage, N. J. Turro, and J. K. Barton, A molecular light switch for DNA: Ru(bpy)2(dppz)2+ *Journal of the American Chemical Society*, vol. 112, no. 12, pp. 4960–4962, 1990.

[74] K. Ishii, M. Shiine, Y. Shimizu, S. ichi Hoshino, H. Abe, K. Sogawa, and N. Kobayashi, Control of Photobleaching in Photodynamic Therapy Using the Photodecarbonylation Reaction of Ruthenium Phthalocyanine Complexes via Stepwise Two-Photon Excitation *The Journal of Physical Chemistry B*, vol. 112, no. 10, pp. 3138–3143, 2008.

[75] M. Dickerson, Y. Sun, B. Howerton, and E. C. Glazer, Modifying Charge and Hydrophilicity of Simple Ru(II) Polypyridyl Complexes Radically Alters Biological Activities: Old Complexes, Surprising New Tricks *Inorganic Chemistry*, vol. 53, no. 19, pp. 10370–10377, 2014.

[76] C. Mari, V. Pierroz, S. Ferrari, and G. Gasser, Combination of Ru(ii) complexes and light: new frontiers in cancer therapy *Chem. Sci.*, vol. 6, pp. 2660–2686, 2015.

[77] A. N. Hidayatullah, E. Wachter, D. K. Heidary, S. Parkin, and E. C. Glazer, Photoactive Ru(II) Complexes With Dioxinophenanthroline Ligands Are Potent Cytotoxic Agents *Inorganic Chemistry*, vol. 53, no. 19, pp. 10030–10032, 2014.

[78] H. Komatsu, K. Yoshihara, H. Yamada, Y. Kimura, A. Son, S.-i. Nishimoto, and K. Tanabe, Ruthenium Complexes with Hydrophobic Ligands That Are Key Factors for the Optical Imaging of Physiological Hypoxia *Chemistry – A European Journal*, vol. 19, no. 6, pp. 1971–1977, 2013.

[79] K. K.-W. Lo, T. K.-M. Lee, J. S.-Y. Lau, W.-L. Poon, and S.-H. Cheng, Luminescent Biological Probes Derived from Ruthenium(II) Estradiol Polypyridine Complexes *Inorganic Chemistry*, vol. 47, no. 1, pp. 200–208, 2008.

[80] M.-J. Li, K. M.-C. Wong, C. Yi, and V. W.-W. Yam, New Ruthenium(II) Complexes Functionalized with Coumarin Derivatives: Synthesis, Energy-Transfer-Based Sensing of Esterase, Cytotoxicity, and Imaging Studies *Chemistry – A European Journal*, vol. 18, no. 28, pp. 8724–8730, 2012.

[81] C. A. Puckett and J. K. Barton, Targeting a ruthenium complex to the nucleus with short peptides *Bioorganic & Medicinal Chemistry*, vol. 18, no. 10, pp. 3564 – 3569, 2010.

[82] J.-X. Zhang, J.-W. Zhou, C.-F. Chan, T. C.-K. Lau, D. W. J. Kwong, H.-L. Tam, N.-K. Mak, K.-L. Wong, and W.-K. Wong, Comparative Studies of the Cellular Uptake, Subcellular Localization, and Cytotoxic and Phototoxic Antitumor Properties of Ruthenium(II)–Porphyrin Conjugates with Different Linkers *Bioconjugate Chemistry*, vol. 23, no. 8, pp. 1623–1638, 2012.

[83] O. Mazuryk, M. Maciuszek, G. Stochel, F. Suzenet, and M. Brindell, 2-Nitroimidazole-ruthenium polypyridyl complex as a new conjugate for cancer treatment and visualization. *Journal of inorganic biochemistry*, vol. 134, pp. 83–91, may 2014.

[84] O. Mazuryk, F. Suzenet, C. Kieda, and M. Brindell, The biological effect of the nitroimidazole derivative of a polypyridyl ruthenium complex on cancer and endothelial cells. *Metallomics*, vol. 7, pp. 553–66, mar 2015.

[85] A. Byrne, C. Dolan, R. D. Moriarty, A. Martin, U. Neugebauer, R. J. Forster, A. Davies, Y. Volkov, and T. E. Keyes, Osmium(ii) polypyridyl polyarginine conjugate as a probe for live cell imaging; a comparison of uptake, localization and cytotoxicity with its ruthenium(ii) analogue *Dalton Trans.*, vol. 44, pp. 14323–14332, 2015.

[86] C.-T. Poon, P.-S. Chan, C. Man, F.-L. Jiang, R. N. S. Wong, N.-K. Mak, D. W. Kwong, S.-W. Tsao, and W.-K. Wong, An amphiphilic ruthenium(II)–polypyridyl appended porphyrin as potential bifunctional two-photon tumor-imaging and photodynamic therapeutic agent *Journal of Inorganic Biochemistry*, vol. 104, no. 1, pp. 62 – 70, 2010.

[87] J. Zhang, K.-L. Wong, W.-K. Wong, N.-K. Mak, D. W. J. Kwong, and H.-L. Tam, Two-photon induced luminescence, singlet oxygen generation, cellular uptake and photocytotoxic properties of amphiphilic Ru(ii) polypyridyl-porphyrin conjugates as potential bifunctional photodynamic therapeutic agents *Org. Biomol. Chem.*, vol. 9, pp. 6004–6010, 2011.

[88] C. Truillet, F. Lux, J. Moreau, M. Four, L. Sancey, S. Chevreux, G. Boeuf, P. Perriat, C. Frochot, R. Antoine, P. Dugourd, C. Portefaix, C. Hoeffel, M. Barberi-Heyob, C. Terryn, L. van Gulick, G. Lemercier, and O. Tillement, Bifunctional

polypyridyl-Ru(ii) complex grafted onto gadolinium-based nanoparticles for MR-imaging and photodynamic therapy *Dalton Trans.*, vol. 42, pp. 12410–12420, 2013.

[89] K. Mori, M. Kawashima, M. Che, and H. Yamashita, Enhancement of the Photoinduced Oxidation Activity of a Ruthenium(II) Complex Anchored on Silica-Coated Silver Nanoparticles by Localized Surface Plasmon Resonance *Angewandte Chemie International Edition*, vol. 49, no. 46, pp. 8598–8601, 2010.

[90] J. R. Mohrig, C. N. Hammond, P. F. Schatz, and T. C. Morrill, *Organic Qualitative Analysis*, pp. 341–342. W.H. Freeman, 2003.

[91] A. E. Liberta and D. X. West, Antifungal and antitumor activity of heterocyclic thiosemicarbazones and their metal complexes: current status *Biometals*, vol. 5, no. 2, pp. 121–126, 1992.

[92] R. B. de Oliveira, E. M. de Souza-Fagundes, R. P. Soares, A. A. Andrade, A. U. Krettli, and C. L. Zani, Synthesis and antimalarial activity of semicarbazone and thiosemicarbazone derivatives *European Journal of Medicinal Chemistry*, vol. 43, no. 9, pp. 1983 – 1988, 2008.

[93] M. J. Ahsana, J. G. Samy, H. Khalilullah, and M. Nomani, Semicarbazone analogues: A mini review *Der Pharmacia Sinica*, vol. 2, no. 6, pp. 107–113, 2011.

[94] M. Kamal and T. Jawaid, A Systematic Review of Semicarbazones as an Anticonvulsant Agent. *American Journal of PharmTech Research*, vol. 3, no. 5, pp. 162–184, 2013.

[95] W. E. Antholine, J. M. Knight, and D. H. Petering, Some properties of copper and zinc complexes of 2-formylpyridine thiosemicarbazone *Inorganic Chemistry*, vol. 16, no. 3, pp. 569–574, 1977.

[96] J. Ma, G. Hu, L. Xie, L. Chen, B. Xu, and P. Gong, Design, synthesis and biological evaluation of novel benzothiazole derivatives bearing semicarbazone moiety as antitumor agents *Chemical Research in Chinese Universities*, vol. 31, no. 6, pp. 958–963, 2015.

[97] K. Islam, S. M. M. Ali, M. Jesmin, and J. A. Khanam, In vivo Anticancer Activities of Benzophenone Semicarbazone against Ehrlich Ascites Carcinoma Cells in Swiss Albino Mice *Cancer biology and chemistry*, vol. 9, pp. 242–247, 2012.

[98] D. Lundin, E. Torrents, A. M. Poole, and B.-M. Sjöberg, RNRdb, a curated database of the universal enzyme family ribonucleotide reductase, reveals a high level of misannotation in sequences deposited to Genbank *BMC Genomics*, vol. 10, no. 1, pp. 1–8, 2009.

[99] T. W. Traut, *Ribonucleotide Reductase*, pp. 161–178. Boston, MA: Springer US, 2008.

[100] N. M. F. S. A. Cerqueira, P. A. Fernandes, L. A. Eriksson, and M. J. Ramos, Dehydration of Ribonucleotides Catalyzed by Ribonucleotide Reductase: The Role of the Enzyme *Biophysical Journal*, vol. 90, no. 6, pp. 2109–2119, 2006.

[101] Y. Aye, M. Li, M. J. C. Long, and R. S. Weiss, Ribonucleotide reductase and cancer: biological mechanisms and targeted therapies *Oncogene*, vol. 34, pp. 2011–2021, Apr 2015.

[102] E. C. Minnihan, D. G. Nocera, and J. Stubbe, Reversible, Long-Range Radical Transfer in E. coli Class Ia Ribonucleotide Reductase *Accounts of Chemical Research*, vol. 46, no. 11, pp. 2524–2535, 2013.

[103] A. Popović-Bijelić, C. R. Kowol, M. E. Lind, J. Luo, F. Himo, Éva A. Enyedy, V. B. Arion, and A. Gräslund, Ribonucleotide reductase inhibition by metal complexes of Triapine (3-aminopyridine-2-carboxaldehyde thiosemicarbazone): A combined experimental and theoretical study *Journal of Inorganic Biochemistry*, vol. 105, no. 11, pp. 1422 – 1431, 2011.

[104] Y. Aye, M. J. C. Long, and J. Stubbe, Mechanistic Studies of Semicarbazone Triapine Targeting Human Ribonucleotide Reductase in Vitro and in Mammalian Cells *Journal of Biological Chemistry*, vol. 287, no. 42, pp. 35768–35778, 2012.

[105] K. E. Tiedje and D. F. Weaver, Deducing the bioactive face of hydantoin anticonvulsant drugs using NMR spectroscopy. *Can J Neurol Sci*, vol. 35, no. 2, pp. 232–236, 2008.

[106] M. L. Scheuer and T. A. Pedley, The Evaluation and Treatment of Seizures *New England Journal of Medicine*, vol. 323, no. 21, pp. 1468–1474, 1990.

[107] G. Singh, J. H. Rees, and J. W. Sander, Seizures and epilepsy in oncological practice: causes, course, mechanisms and treatment *Journal of Neurology, Neurosurgery & Psychiatry*, vol. 78, no. 4, pp. 342–349, 2007.

[108] M. V. Relling, C.-H. Pui, J. T. Sandlund, G. K. Rivera, M. L. Hancock, J. M. Boyett, E. G. Schuetz, and W. E. Evans, Adverse effect of anticonvulsants on efficacy of chemotherapy for acute lymphoblastic leukaemia *The Lancet*, vol. 356, no. 9226, pp. 285–290, 2000.

[109] F. Olimpieri, M. C. Bellucci, A. Volonterio, and M. Zanda, A Mild, Efficient Approach for the Synthesis of 1,5-Disubstituted Hydantoins *European Journal of Organic Chemistry*, vol. 2009, no. 35, pp. 6179–6188, 2009.

[110] G. Spengler, M. Evaristo, J. Handzlik, J. Serly, J. Molnár, M. Viveiros, K. Kieć-Kononowicz, and L. Amaral, Biological Activity of Hydantoin Derivatives on P-Glycoprotein (ABCB1) of Mouse Lymphoma Cells *Anticancer Research*, vol. 30, no. 12, pp. 4867–4871, 2010.

[111] A. W. Roszak and D. F. Weaver, 5,5-Diphenyl-2-thiohydantoin *Acta Crystallographica Section C*, vol. 54, pp. 1168–1170, Aug 1998.

[112] N. Shankaraiah, S. Nekkanti, K. J. Chudasama, K. R. Senwar, P. Sharma, M. K. Jeengar, V. Naidu, V. Srinivasulu, G. Srinivasulu, and A. Kamal, Design, synthesis and anticancer evaluation of tetrahydro-ß-carboline-hydantoin hybrids *Bioorganic & Medicinal Chemistry Letters*, vol. 24, no. 23, pp. 5413 – 5417, 2014.

[113] Y. A. Ivanenkov, M. S. Veselov, I. G. Rezekin, D. A. Skvortsov, Y. B. Sandulenko, M. V. Polyakova, D. S. Bezrukov, S. V. Vasilevsky, M. E. Kukushkin, A. A. Moiseeva, A. V. Finko, V. E. Koteliansky, N. L. Klyachko, L. A. Filatova, E. K. Beloglazkina, N. V. Zyk, and A. G. Majouga, Synthesis, isomerization and biological activity of novel 2-selenohydantoin derivatives *Bioorganic & Medicinal Chemistry*, vol. 24, no. 4, pp. 802 – 811, 2016.

[114] P. Majumdar, C. Bathula, S. M. Basu, S. K. Das, R. Agarwal, S. Hati, A. Singh, S. Sen, and B. B. Das, Design, synthesis and evaluation of thiohydantoin derivatives as potent topoisomerase I (Top1) inhibitors with anticancer activity *European Journal of Medicinal Chemistry*, vol. 102, pp. 540 – 551, 2015.

[115] K. Nakamaru, Synthesis, luminescence quantum yields, and lifetimes of trischelated ruthenium(II) mixed-ligand complexes including 3,3′-dimethyl-2,2′-bipyridyl. *Bulletin of the Chemical Society of Japan*, vol. 55, no. 9, pp. 2697–2705, 1982.

[116] P. J. Hay and W. R. Wadt, Ab initio effective core potentials for molecular calculations. Potentials for the transition metal atoms Sc to Hg *The Journal of Chemical Physics*, vol. 82, no. 1, pp. 270–283, 1985.

[117] W. R. Wadt and P. J. Hay, Ab initio effective core potentials for molecular calculations. Potentials for main group elements Na to Bi *The Journal of Chemical Physics*, vol. 82, no. 1, pp. 284–298, 1985.

[118] K. S. Low, J. M. Cole, X. Zhou, and N. Yufa, Rationalizing the molecular origins of Ru- and Fe-based dyes for dye-sensitized solar cells *Acta Crystallographica Section B*, vol. 68, pp. 137–149, Apr 2012.

[119] M. J. Frisch, G. W. Trucks, H. B. Schlegel, G. E. Scuseria, M. A. Robb, J. R. Cheeseman, G. Scalmani, V. Barone, B. Mennucci, G. A. Petersson, H. Nakatsuji, M. Caricato, X. Li, H. P. Hratchian, A. F. Izmaylov, J. Bloino, G. Zheng, J. L. Sonnenberg, M. Hada, M. Ehara, K. Toyota, R. Fukuda, J. Hasegawa, M. Ishida, T. Nakajima, Y. Honda, O. Kitao, H. Nakai, T. Vreven, J. A. Montgomery, Jr., J. E. Peralta, F. Ogliaro, M. Bearpark, J. J. Heyd, E. Brothers, K. N. Kudin, V. N. Staroverov, R. Kobayashi, J. Normand, K. Raghavachari, A. Rendell, J. C. Burant, S. S. Iyengar, J. Tomasi, M. Cossi, N. Rega, J. M. Millam, M. Klene, J. E. Knox,

J. B. Cross, V. Bakken, C. Adamo, J. Jaramillo, R. Gomperts, R. E. Stratmann, O. Yazyev, A. J. Austin, R. Cammi, C. Pomelli, J. W. Ochterski, R. L. Martin, K. Morokuma, V. G. Zakrzewski, G. A. Voth, P. Salvador, J. J. Dannenberg, S. Dapprich, A. D. Daniels, . Farkas, J. B. Foresman, J. V. Ortiz, J. Cioslowski, and D. J. Fox, Gaussian 09 Revision E.01

[120] A. Allouche, Gabedit—A graphical user interface for computational chemistry softwares *Journal of Computational Chemistry*, vol. 32, no. 1, pp. 174–182, 2011.

[121] M. D. Hanwell, D. E. Curtis, D. C. Lonie, T. Vandermeersch, E. Zurek, and G. R. Hutchison, Avogadro: an advanced semantic chemical editor, visualization, and analysis platform *Journal of Cheminformatics*, vol. 4, no. 1, pp. 1–17, 2012.

[122] W. L. E. . Armarego and C. L. L. Chai, *Purification of Laboratory Chemicals, 5th ed.* Elsevier Science, 2003.

[123] M. C. Pirrung, *The Synthetic Organic Chemist's Companion*. New Jersey: Wiley, 2007.

[124] O. Mazuryk, M. Łomzik, D. Martineau, M. Beley, M. Brindell, G. Stochel, and P. C. Gros, Anticancer activity of ruthenium(II) polypyridine complexes bearing pyrrolidine substituents *Inorganica Chimica Acta*, vol. 443, pp. 86 – 90, 2016.

[125] E. A. Enyedy, M. F. Primik, C. R. Kowol, V. B. Arion, T. Kiss, and B. K. Keppler, Interaction of Triapine and related thiosemicarbazones with iron(iii)/(ii) and gallium(iii): a comparative solution equilibrium study *Dalton Trans.*, vol. 40, pp. 5895–5905, 2011.

[126] Radiation Therapy and Cisplatin With or Without Triapine in Treating Patients With Newly Diagnosed Stage IB2, II, or IIIB-IVA Cervical Cancer or Stage II-IVA Vaginal Cancer. Retrieved May 2016 from https://clinicaltrials.gov/ct2/show/NCT02466971

[127] Triapine With Chemotherapy and Radiation Therapy in Treating Patients With IB2-IVA Cervical or Vulvar Cancer. Retrieved May 2016 from https://clinicaltrials.gov/ct2/show/NCT02595879

[128] P. C. Gros, S. Choppin, J. Mathieu, and Y. Fort, Lithiation of 2-Heterosubstituted Pyridines with BuLi-LiDMAE: Evidence for Regiospecificity at C-6 *The Journal of Organic Chemistry*, vol. 67, no. 1, pp. 234–237, 2002.

[129] T. Kaminski, P. Gros, and Y. Fort, Side-Chain Retention During Lithiation of 4-Picoline and 3,4-Lutidine: Easy Access to Molecular Diversity in Pyridine Series *European Journal of Organic Chemistry*, vol. 2003, no. 19, pp. 3855–3860, 2003.

[130] D. Cai, D. L. Hughes, and T. R. Verhoeven, A study of the lithiation of 2,6-dibromopyridine with butyllithium, and its application to synthesis of

L-739,010 *Tetrahedron Letters*, vol. 37, no. 15, pp. 2537 – 2540, 1996.

[131] A. Krasovskiy and P. Knochel, A LiCl-Mediated Br/Mg Exchange Reaction for the Preparation of Functionalized Aryl- and Heteroarylmagnesium Compounds from Organic Bromides *Angewandte Chemie International Edition*, vol. 43, no. 25, pp. 3333–3336, 2004.

[132] A. Shariff and S. McLean, The synthesis of Nauclea indole-pyridine alkaloids. 3,4-Disubstituted and 3,4,5-trisubstituted pyridines as synthetic intermediates; a total synthesis of decarbomethoxy-3- and -3-nauclechine *Canadian Journal of Chemistry*, vol. 61, no. 12, pp. 2813–2820, 1983.

[133] D. Chen, R. De, and D. L. Mohler, A Facile Synthesis of Thioalkyl- and Di(thioalkyl)-Substituted Bipyridines *Synthesis*, vol. 2, pp. 0211–0216, 2009.

[134] S. Sun, Y. He, Z. Yang, Y. Pang, F. Liu, and J. Fan, Synthesis and DNA photocleavage study of $Ru(bpy)_3^{2+}$-$(CH_2)_n$-MV^{2+} complexes *Dalton Trans.*, vol. 39, pp. 4411–4416, 2010.

[135] L. Hanuš, S. Abu-Lafi, E. Fride, A. Breuer, Z. Vogel, D. E. Shalev, I. Kustanovich, and R. Mechoulam, 2-Arachidonyl glyceryl ether, an endogenous agonist of the cannabinoid CB1 receptor *Proceedings of the National Academy of Sciences*, vol. 98, no. 7, pp. 3662–3665, 2001.

[136] W. E. Parham and R. M. Piccirilli, Selective halogen-lithium exchange in 2,5-dibromobenzenes and 2,5-dibromopyridine *The Journal of Organic Chemistry*, vol. 42, no. 2, pp. 257–260, 1977.

[137] X. Li, C. L. Gibb, M. E. Kuebel, and B. C. Gibb, Two new ligands for carbonic anhydrase mimicry *Tetrahedron*, vol. 57, no. 7, pp. 1175 – 1182, 2001.

[138] J. J. Song, N. K. Yee, Z. Tan, J. Xu, S. R. Kapadia, and C. H. Senanayake, Synthesis of 5-bromopyridyl-2-magnesium chloride and its application in the synthesis of functionalized pyridines *Organic Letters*, vol. 6, no. 2, pp. 4905–4907, 2004.

[139] A. M. Alanazi, A. S. El-Azab, I. A. Al-Swaidan, A. R. Maarouf, E. R. El-Bendary, M. A. A. El-Enin, and A. A. M. Abdel-Aziz, CHEMISTRY Synthesis , single-crystal , in vitro antitumor evaluation and molecular docking of 3-substitued 5 , 5-diphenylimidazolidine- *Medical Chemistry Reaserch*, vol. 22, pp. 6129–6142, 2013.

[140] N. Trišović, B. Božić, A. Obradović, O. Stefanović, S. Marković, L. Čomić, B. Božić, and G. Uščumlić, Structure – activity relationships of 3-substituted-5 , 5- -diphenylhydantoins as potential antiproliferative and antimicrobial agents *Journal of Serbian Chemical Society*, vol. 76, no. 12, pp. 1597–1606, 2011.

[141] J. Shreeve, *Inorganic Syntheses vol. 24*. Inorganic Syntheses, Wiley, 2009.

[142] E. Seddon, K. Seddon, and R. Clark, *The Chemistry of Ruthenium*. Topics in Inorganic and General Chemistry, Elsevier Science, 2013.

[143] S. Cotton, *Chemistry of Precious Metals*. Springer Netherlands, 2012.

[144] G. Sprintschnik, H. W. Sprintschnik, P. P. Kirsch, and D. G. Whitten, Photochemical reactions in organized monolayer assemblies. 6. Preparation and photochemical reactivity of surfactant ruthenium(II) complexes in monolayer assemblies and at water-solid interfaces *Journal of the American Chemical Society*, vol. 99, no. 15, pp. 4947–4954, 1977.

[145] D. Martineau, M. Beley, P. C. Gros, S. Cazzanti, S. Caramori, and C. a. Bignozzi, Tuning of ruthenium complex properties using pyrrole- and pyrrolidine-containing polypyridine ligands *Inorganic Chemistry*, vol. 46, no. 6, pp. 2272–2277, 2007.

[146] J. R. Lakowicz, *Principles of Fluorescence Spectroscopy*. Springer, 2006.

[147] A. O. Adeloye, Synthesis, Photophysical and Electrochemical Properties of a Mixed Bipyridyl-Phenanthrolyl Ligand Ru(II) Heteroleptic Complex Having trans-2-Methyl-2-butenoic Acid Functionalities *Molecules*, vol. 16, no. 10, p. 8353, 2011.

[148] R. C. Kerber, If It's Resonance, What Is Resonating? *Journal of Chemical Education*, vol. 83, no. 2, p. 223, 2006.

[149] S. Verma, P. Kar, A. Das, and H. N. Ghosh, Photophysical properties of ligand localized excited state in ruthenium(ii) polypyridyl complexes: a combined effect of electron donor-acceptor ligand *Dalton Trans.*, vol. 40, pp. 9765–9773, 2011.

[150] J.-G. Liu, B.-H. Ye, H. Li, Q.-X. Zhen, L.-N. Ji, and Y.-H. Fu, Polypyridyl ruthenium(II) complexes containing intramolecular hydrogen-bond ligand: syntheses, characterization, and DNA-binding properties *Journal of Inorganic Biochemistry*, vol. 76, no. 3–4, pp. 265 – 271, 1999.

[151] A. Juris, S. Campagna, V. Balzani, G. Gremaud, and A. Von Zelewsky, Absorption spectra, luminescence properties, and electrochemical behavior of tris-heteroleptic ruthenium(II) polypyridine complexes *Inorganic Chemistry*, vol. 27, no. 20, pp. 3652–3655, 1988.

[152] P.-H. Xie, Y.-J. Hou, B.-W. Zhang, Y. Cao, F. Wu, W.-J. Tian, and J.-C. Shen, Spectroscopic and electrochemical properties of ruthenium(II) polypyridyl complexes *J. Chem. Soc., Dalton Trans.*, pp. 4217–4221, 1999.

[153] A. E. Friedman, C. V. Kumar, N. J. Turro, and J. K. Barton, Luminescence of ruthenium(II) polypyridyls: evidence for intercalative binding to Z-DNA. *Nucleic Acids Res*, vol. 19, pp. 2595–2602, May 1991.

[154] A. M. Pyle, J. P. Rehmann, R. Meshoyrer, C. V. Kumar, N. J. Turro, and J. K. Barton, Mixed-ligand complexes of ruthenium(II): factors governing binding to DNA *Journal of the American Chemical Society*, vol. 111, no. 8, pp. 3051–3058, 1989.

[155] S. Gorelsky and A. Lever, Electronic structure and spectra of ruthenium diimine complexes by density functional theory and INDO/S. Comparison of the two methods *Journal of Organometallic Chemistry*, vol. 635, no. 1–2, pp. 187 – 196, 2001.

[156] O. V. Sizova, V. I. Baranovski, N. V. Ivanova, and A. I. Panin, Semiempirical calculations of electronic spectra of Ru (II) and Ru (III) compounds in restricted active space CI approximation *International Journal of Quantum Chemistry*, vol. 63, no. 4, pp. 853–860, 1997.

[157] A. A. Bhattacharya, S. Curry, and N. P. Franks, Binding of the General Anesthetics Propofol and Halothane to Human Serum Albumin *The Journal of biological chemistry*, vol. 275, no. 49, pp. 38731–38738, 2000.

[158] N. Sharma, V. Sivalingam, S. Maurya, A. Prasad, P. Khandelwal, S. Chandra, and B. K. Patel, New insights into in vitro amyloidogenic properties of human serum albumin suggest considerations for therapeutic precautions *FEBS Letters*, vol. 589, no. 24, pp. 4033–4038, 2015.

[159] Y. Moriyama, D. Ohta, K. Hachiya, Y. Mitsui, and K. Takeda, Fluorescence behavior of tryptophan residues of bovine and human serum albumins in ionic surfactant solutions: A comparative study of the two and one tryptophan(s) of bovine and human albumins *Journal of Protein Chemistry*, vol. 15, no. 3, pp. 265–272, 1996.

[160] M. Nišavić, M. Stoiljković, I. Crnolatac, M. Milošević, A. Rilak, and R. Masnikosa, Highly water-soluble ruthenium(II) terpyridine coordination compounds form stable adducts with blood-borne metal transporting proteins *Arabian Journal of Chemistry*, pp. –, 2016.

[161] J. Sun, Y. Huang, C. Zheng, Y. Zhou, Y. Liu, and J. Liu, Ruthenium (II) Complexes Interact with Human Serum Albumin and Induce Apoptosis of Tumor Cells *Biological Trace Element Research*, vol. 163, no. 1, pp. 266–274, 2015.

[162] J. R. Lakowicz, G. Freshwater, and G. Weber, Nanosecond segmental mobilities of tryptophan residues in proteins observed by lifetime-resolved fluorescence anisotropies *Biophysical Journal*, vol. 32, no. 1, pp. 591–601, 1980.

[163] S. Bi, D. Song, Y. Tian, X. Zhou, Z. Liu, and H. Zhang, Molecular spectroscopic study on the interaction of tetracyclines with serum albumins *Spectrochimica Acta Part A: Molecular and Biomolecular Spectroscopy*, vol. 61, no. 4, pp. 629 – 636, 2005.

[164] P. Ascenzi, A. Bocedi, S. Notari, E. Menegatti, and M. Fasano, Heme impairs allosterically drug binding to human serum albumin Sudlow's site I *Biochemical and Biophysical Research Communications*, vol. 334, no. 2, pp. 481 – 486, 2005.

[165] L. Yan, X. Wang, Y. Wang, Y. Zhang, Y. Li, and Z. Guo, Cytotoxic palladium(II) complexes of 8-aminoquinoline derivatives and the interaction with human

serum albumin *Journal of Inorganic Biochemistry*, vol. 106, no. 1, pp. 46 – 51, 2012.

[166] J. Yellol, S. A. Pérez, A. Buceta, G. Yellol, A. Donaire, P. Szumlas, P. J. Bednarski, G. Makhloufi, C. Janiak, A. Espinosa, and J. Ruiz, Novel C,N-Cyclometalated Benzimidazole Ruthenium(II) and Iridium(III) Complexes as Antitumor and Antiangiogenic Agents: A Structure–Activity Relationship Study *Journal of Medicinal Chemistry*, vol. 58, no. 18, pp. 7310–7327, 2015.

[167] O. V. Kharissova, B. I. Kharisov, and U. O. Méndez, *Advances in Induction and Microwave Heating of Mineral and Organic Materials*, ch. Microwave-assisted Synthesis of Coordination and Organometallic Compounds, pp. 345–390. InTech, 2011.

[168] K. Neuthe, F. Bittner, F. Stiemke, B. Ziem, J. Du, M. Zellner, M. Wark, T. Schubert, and R. Haag, Phosphonic acid anchored ruthenium complexes for ZnO-based dye-sensitized solar cells *Dyes and Pigments*, vol. 104, pp. 24 – 33, 2014.

[169] W. K. Seok, M. Ran Jo, N. Kim, and H. Yun, Comparative Study of Ruthenium(II) and Ruthenium(III) Complexes with the Ligand dmbpy (dmbpy = 4, 4'-Dimethyl-2, 2'-bipyridine) *Zeitschrift für anorganische und allgemeine Chemie*, vol. 638, no. 5, pp. 754–757, 2012.

[170] S. Ardo, Y. Sun, A. Staniszewski, F. N. Castellano, and G. J. Meyer, Stark Effects after Excited-State Interfacial Electron Transfer at Sensitized TiO2 Nanocrystallites *Journal of the American Chemical Society*, vol. 132, no. 19, pp. 6696–6709, 2010.

[171] A. P. Halverson, T. A. Elmaaty, and L. W. Castle, Complexes of (bpy)2Ru(II) and (Ph2bpy)2Ru(II) with a series of thienophenanthroline ligands: synthesis, characterization, and electronic spectra. *Journal of Coordination Chemistry*, vol. 64, no. 21, pp. 3693 – 3699, 2011.

[172] A. Frei, R. Rubbiani, S. Tubafard, O. Blacque, P. Anstaett, A. Felgenträger, T. Maisch, L. Spiccia, and G. Gasser, Synthesis, Characterization, and Biological Evaluation of New Ru(II) Polypyridyl Photosensitizers for Photodynamic Therapy *Journal of Medicinal Chemistry*, vol. 57, no. 17, pp. 7280–7292, 2014.

[173] W. Bannwarth, R. Knorr, F. Mueller, and D. Schmidt, Ruthenium-containing DNA and RNA for use in nucleic acid sequencing and hydridization *Patent*, vol. EP0340605, 11 1989.

[174] A. B. Mandal, J. K. Augustine, A. Quattropani, and A. Bombrun, The expedient access to bromo-pyridine carbaldehyde scaffolds using gem-dibromomethyl intermediates *Tetrahedron Letters*, vol. 46, no. 36, pp. 6033 – 6036, 2005.

[175] D. Ma, F. Lu, T. Overstreet, D. E. Milenic, and M. W. Brechbiel, Novel chelating agents for potential clinical applications of copper *Nuclear Medicine and Biology*, vol. 29, no. 1, pp. 91 – 105, 2002.

[176] F. Thaler, A. Colombo, A. Mai, R. Amici, C. Bigogno, R. Boggio, A. Cappa, S. Carrara, T. Cataudella, F. Fusar, E. Gianti, S. J. di Ventimiglia, M. Moroni, D. Munari, G. Pain, N. Regalia, L. Sartori, S. Vultaggio, G. Dondio, S. Gagliardi, S. Minucci, C. Mercurio, and M. Varasi, Synthesis and Biological Evaluation of N-Hydroxyphenylacrylamides and N-Hydroxypyridin-2-ylacrylamides as Novel Histone Deacetylase Inhibitors *Journal of Medicinal Chemistry*, vol. 53, no. 2, pp. 822–839, 2010.

[177] R. H. Dodd, C. Ouannes, M. Robert-Gero, and P. Potier, Hybrid molecules: growth inhibition of Leishmania donovani promastigotes by thiosemicarbazones of 3- carboxy-.beta.-carbolines *Journal of Medicinal Chemistry*, vol. 32, no. 6, pp. 1272–1276, 1989.

[178] B. H. Lipshutz, S. S. Pfeiffer, and W. Chrisman, Formylations of anions with a 'Weinreb' formamide: N-methoxy-N-methylformamide *Tetrahedron Letters*, vol. 40, no. 45, pp. 7889 – 7892, 1999.

[179] M. van den Heuvel, T. A. van den Berg, R. M. Kellogg, C. T. Choma, and B. L. Feringa, Synthesis of a Non-Heme Template for Attaching Four Peptides: An Approach to Artificial Iron(II)-Containing Peroxidases *The Journal of Organic Chemistry*, vol. 69, no. 2, pp. 250–262, 2004.

List of publications

Mazuryk, O., Łomzik, M., Martineau, D., Beley, M., Brindell, M., Stochel, G., Gros, P. C., "Anticancer activity of ruthenium(II) polypyridine complexes bearing pyrrolidine substituents." *Inorganica Chimica Acta*, vol. 443, pp. 86-90, 2016.

Łomzik M., Brindell M., "Synthesis and interaction with albumin of N,N-dimethylaminbenzyl derivative of thiosemicarbazone and its ruthenium(II) complex", *CHEMIK*, vol. 67, no. 2, pp. 91-98, 2013.

List of conferences

"Synthesis and characteryzation of novel Ruthenium(II) complexes with pyridine-2-carboxyaldehyde semicarbazone moiety", *3rd European Colloquium on Inorganic Reaction Mechanisms*, Kraków 21-25.06.2016 **(Poster)**

"Luminescence and bioactivity of ruthenium(II) complexes", 21st International *Symposium on the Photochemistry and Photophysics of Coordination Compounds*, Kraków 05-09.07.2015 **(Poster)**

"Synthesis and characterization of hybrid drugs based on ruthenium complex moiety and biologically active organic compounds", *Ecole Doctorale de Chimie et Physique Moléculaires Journée Scientifique de rentrée*, Metz, 24.11.2014 **(Lecture)**

"Photophysical and biological evaluation of series of homoleptic polypyridyl ruthenium(II) complexes, *7th Central Europe Conference Chemistry Towards Biology*, Katowice, 09-12.09.2014 **(Poster)**

"Novel bifunctional compounds as potential antitumor agents", *Ecole Doctorale de Chimie et Physique Moléculaires Journée Scientifique de rentrée*, Metz, 22.11.2013 **(Poster)**

"Novel ruthenium(II) complexes as potential antitumor agents", *XII International Symphosium on Inorganic Biochemistry - Collaboration and Beyond*, Wrocław, 28.08 - 01.09.2013 **(Poster)**

"Tiosemikarbazony jako ligandy dla kompleksów Ru(II) - synteza i badania fizykochemiczne", *55 Zjazd PTChem i SITPChem*, Białystok 16-20.09.2012 **(Poster)**

"Synteza kompleksów rutenu(II) z ligandami tiosemikarbazonowymi jako potencjalnych związków o aktywności antynowotworowej", *54 Zjazd PTChem i SITPChem*, Lublin 18-22.09.2011 **(Poster)**